# Contributions to the Analysis of Random Wireless Networks in Non-full Interference

Mohammadreza Mardani Varmazyar

# THESE DE DOCTORAT DE

L'INSTITUT NATIONAL DES SCIENCES APPLIQUEES RENNES

ECOLE DOCTORALE N° 601
*Mathématiques et Sciences et Technologies de l'Information et de la Communication*
Spécialité : *Télécommunications*

Par

**Mohammadreza MARDANI VARMAZYAR**

## Contributions to the Analysis of Random Wireless Networks in Non-full Interference

**Thèse présentée et soutenue à « Rennes », le « 24/03/2022 »**
**Unité de recherche : Institut d'Électronique et de Télécommunications de Rennes (IETR), INSA-Rennes**
**Thèse N° : 22ISAR 06 / D22 - 06**

**Rapporteurs avant soutenance** :

Jean-Marie GORCE Professeur, INSA de Lyon
Marios KOUNTOURIS Professeur, Eurecom, Sophia Antipolis

**Composition du Jury :**

| | | |
|---|---|---|
| Président : | Ghaya REKAYA-BEN OTHMAN | Professeur, Telecom Paris Tech |
| Examinateurs : | Jean-Marie GORCE | Professeur, INSA de Lyon |
| | Marios KOUNTOURIS | Professeur, Eurecom, Sophia Antipolis |
| | Ghaya REKAYA-BEN OTHMAN | Professeur, Telecom Paris Tech |
| | Didier LE RUYET | Professeur, CNAM Paris |
| Dir. de thèse : | Philippe MARY | Maître de conférences, HDR, INSA de Rennes |
| Co-dir. de thèse : | Jean-Yves BAUDAIS | Chargé de recherche, HDR, CNRS |

# Contents

# List of Figures

# List of Tables

# List of acronyms

| | |
|---|---|
| **AWGN** | Additive white Gaussian noise |
| **BPP** | Binomial point process |
| **BS** | Base station |
| **BW** | Bandwidth |
| **BWP** | Bandwidth partitioning |
| **CB** | Coordination beamforming |
| **CCDF** | Complementary cumulative distribution function |
| **CCU** | Cell center user |
| **CDF** | Cumulative distribution function |
| **CEU** | Cell edge user |
| **CoMP** | Coordinated multipoint |
| **CRE** | Cell range expansion |
| **CS** | Coordination scheduling |
| **D2D** | Device-to-device |
| **DPP** | Determinantal point process |
| **FFR** | Fractional frequency reuse |
| **FR** | Frequency Reuse |
| **GPP** | Ginibre point process |
| **HD** | Half-duplex |
| **HetNet** | Heterogeneous network |
| **HPPP** | Homogeneous Poisson point process |
| **IETR** | *Institut d'électronique et des technologies du numérique* |
| **ICIC** | Intercell interference coordination |
| **IPPP** | Inhomogeneous Poisson point process |
| **i.i.d.** | Independent and identically distributed |
| **JT** | Joint transmission |
| **KKT** | Karush–Kuhn–Tucker |
| **KPI** | Key performance indicator |
| **LOS** | Line-of-sight |
| **LTE** | Long Term Evolution |
| **MAC** | Medium access control |

| | |
|---|---|
| **MCP** | Matern cluster process |
| **MGF** | Moment generating function |
| **MHPP** | Matern hard-core point process |
| **MIMO** | Multiple input multiple output |
| **MPT** | Modern portfolio theory |
| **mmWave** | Millimeter wave |
| **NLOS** | Non-line-of-sight |
| **NOMA** | Non-orthogonal multiple access |
| **OFDMA** | Orthogonal frequency division multiplexing access |
| **OPS** | Optimal point selection |
| **PCP** | Poisson cluster process |
| **PDF** | Probability density function |
| **PGFL** | Probability generating functional |
| **PMF** | Probability mass function |
| **PP** | Point process |
| **PPP** | Poisson point process |
| **RAT** | radio access technology |
| **QoS** | Quality of service |
| **RDP** | Relative distance process |
| **RRM** | Radio resource management |
| **r.v.** | Random variable |
| **SE** | Spectral efficiency |
| **SFR** | Soft frequency reuse |
| **SG** | Stochastic geometry |
| **SIC** | Successive interference cancellation |
| **SINR** | Signal-to-interference-plus-noise ratio |
| **SIR** | Signal-to-interference ratio |
| **TCP** | Thomas cluster process |
| **UDN** | Ultra-dense network |

# Mathematical notation and variables

| | |
|---|---|
| $B \setminus A$ | In $B$ but not in $A$ |
| $B \subset \mathbb{R}^d$ | $B$ is a subset of $\mathbb{R}^d$ |
| $\mathbb{E}[X]$ | Expectation of r.v. $X$ |
| $\mathbb{E}_Y[X]$ | Expectation of r.v. $X$ over r.v. $Y$ |
| $f(x)$ | function of $x$ |
| ${}_2F_1(a,b;c;z)$ | Gauss hyper-geometric function |
| $\forall$ | For all |
| $M_k$ | $k$-th order moment |
| $\left( \begin{array}{c} n \\ k \end{array} \right)$ | $n$ choose $k$, the binomial coefficient |
| $n!$ | Factorial of $n$ |
| $\Phi$ | Point process |
| $P_x^!$ | Reduced Palm measure of the point process $\Phi$ |
| $\Phi(B)$ | Number of points of $\Phi$ in $B$ |
| $P(A)$ | Probability of event $A$ |
| $\prod_{x \in \Phi} f(x)$ | Product of function $f$ evaluated at a point $x$ of the point process $\Phi$ |
| $Q(x)$ | Marcuum function that provides the CCDF of a standard normal r.v. |
| $\mathbb{R}^d$ | Real $d$-dimensional Euclidean space |
| $\sum_{x \in \Phi} f(x)$ | Sum of function $f$ evaluated at a point $x$ of $\Phi$ |
| $Var[X]$ | Variance of r.v. $X$ |
| $\mathbf{1}(\mathscr{P}) \in \{0,1\}$ | Indicator function, which is one when the proposition $\mathscr{P}$ is true and is null otherwise |
| $\|\|.\|\|$ | $L_2$ vector norm |
| $\lim_{x \to \infty} f(x) = q$ | $f(x)$ approaches the limit $q$ as $x$ approaches $\infty$ |

# Résumé en français

Cette thèse se place dans le contexte général de l'analyse de performance des réseaux sans-fil à large échelle et à géométrie aléatoire. De ce fait, nous faisons une grande utilisation de l'outil de géométrie stochastique (GS). Cet outil mathématique a été introduit dans le domaine des télécommunications sans fil il y a quelques décennies afin de dépasser le modèle de déploiement régulier hexagonale qui ne rend pas compte de la diversité des géométries de déploiement des stations de base et qui ne permet donc pas de prédire les performances moyennes d'un utilisateur sur l'ensemble des déploiements possibles. La GS permet donc de moyenner un critère de performance, par exemple la probabilité de couverture, sur l'ensemble des déploiements possibles en supposant que la configuration des stations de base résulte d'un tirage d'une distribution de probabilité particulière. Parmi ces distributions, celle du processus ponctuel de Poisson (PPP) est la plus utilisée de part sa simplicité et ses propriétés qui permettent de calculer les métriques d'intérêt pour n'importe quel point dans le réseau, e.g. la probabilité de couverture, l'efficacité spectrale moyenne. Cette approche est notamment basée sur la transformée de Laplace de l'interférence. Ainsi les hypothèses prisent pour la caractérisation de cette dernière sont primordiales.

La majorité des travaux de la littérature suppose que l'ensemble des stations de base transmettent tout le temps. C'est ce que l'on appelle le modèle d'interférence totale sur lequel sont notamment basés les travaux de Andrews *et al.* dans [2]. Cependant, une cellule qui n'aurait pas d'utilisateur couvert ne transmettrait pas et ne provoquerait pas d'interférence sur l'utilisateur d'intérêt, dit utilisateur typique. Cette thèse s'intéresse à l'analyse de performance des réseaux large échelle précisément dans ce cas de figure. Nous reprenons notamment la notion de classification des utilisateurs en fonction de la qualité de leur rapport signal à interférence plus bruit (RSIB) pour lequel nous associons un bloc de ressource fixe. Ainsi, une station de base ne couvrant pas d'utilisateurs sur ce bloc de ressources ne transmet pas dans cette bande est donc ne créée pas d'interférence pour les autres cellules dans ce bloc de ressource. La difficulté de l'analyse tient au fait que la probabilité d'activité des stations de bases dans un bloc de ressource dépend donc de la probabilité de couverture que l'on cherche à calculer, liant créant ainsi une dépendence dans le processus ponctuel. Cette thèse s'attache à la dérivation d'un cadre théorique permettant de traiter ce cas

de figure. Dans la suite, nous donnons un résumé du contenu des différents chapitres.

# Chapitre 1. Introduction

Ce chapitre expose le contexte de la thèse et le problème étudié et se termine par les publications issues de ces travaux. Le contexte de l'étude est celui de la densification toujours plus massive des réseaux de communication et de la prédiction de performance moyenne de ces systèmes. L'optimisation de la ressource radio conduit à une réutilisation importante des fréquences d'une cellule à l'autre afin d'augmenter le débit global du réseau, mais peut conduire à une forte dégradation de performance pour les utilisateurs en bord de cellule qui souffrent de beaucoup d'interférence et d'un lien radio assez faible.

Les contributions de cette thèse sont les suivantes :

- Un nouveau modèle de réseau à interférence partielle est proposé. En classifiant les utilisateurs selon leur RSIB et en leur allouant une sous-bande fixe, que la cellule s'interdit de réutiliser si aucun utilisateur n'est affecté à la sous-bande, on montre que la probabilité de couverture d'un utilisateur typique dépend de la probabilité d'activation de la transmission dans cette sous-bande. Elle-même dépend de la probabilité de couverture que l'on cherche à calculer. En traitant d'abord le cas à 2 types d'utilisateurs, utilisateurs de centre et utilisateurs de bord de cellule, nous montrons que la probabilité de couverture de l'utilisteur de bord de cellule est largement améliorée dans ce cas. Nous étendons ensuite l'étude à $N$ classes d'utilisateur. Nous étudions en particulier le compromis entre la probabilité de couverture du type d'utilisateur et son efficacité spectrale selon le type d'allocation de fréquence. Nous montrons que le schéma proposé offre un meilleur compromis que celui atteint par ceux de la littérature.

- Afin d'améliorer la probabilité de couverture de l'utilisateur en bord de cellule, nous proposons d'utiliser une technique de diversité de station de base pour améliorer la couverture de ce type d'utilisateurs. Notre contribution provient de l'analyse de performance de cette technique, dans le contexte d'interférence partielle que nous avons développé. D'autre part, nous proposons une analyse de l'équité entre les différentes classes d'utilisateurs en fonction de l'efficacité spectrale atteignable. L'équité est mesurée avec l'indice de Jain et permet une mesure de la variance d'un critère par rapport à sa valeur moyenne.

## Chapitre 2. Préliminaires mathématiques

Dans ce chapitre, nous décrivons l'histoire de la GS et ses applications dans l'analyse des réseaux sans fil. Ensuite, nous présentons quelques-uns des théorèmes de GS et, enfin, nous définissons les métriques de performance utilisées dans cette thèse.

Nous avons commencé ce chapitre en fournissant un bref historique de la GS en tant qu'outil analytique important pour évaluer les performances des réseaux sans fil et les enquêtes liées à la GS dans les réseaux sans fil. Nous présentons les outils mathématiques et les théorèmes de géométrie stochastique utilisés dans cette thèse pour résoudre le problème. De plus, nous donnons les caractéristiques mathématiques du processus de Poisson ponctuel utilisées comme modèle de base dans les réseaux sans fil. En raison de sa calculabilité et de sa flexibilité analytique, le PPP est largement utilisé et nous le considérons également comme un modèle spatial de BS dans cette thèse. Nous présentons les caractéristiques importantes qui sous-tendent une telle calculabilité. Le PPP est un processus de point d'attraction zéro dans lequel les points sont dispersés indépendamment sans interaction entre eux. Ce chapitre présente deux théorèmes très importantes dans le cadre des PPP, à savoir les théorèmes de Slivnyak et de Campbell. Le théorème de Slivnyak indique que la distribution du processus original est égale à sa distribution de Palm réduite. Le théorème de Campbell est soit une équation particulière ou un ensemble de résultats relatifs à l'espérance d'une fonction sommée sur un processus ponctuel en une intégrale impliquant la mesure moyenne du processus ponctuel, ce qui permet le calcul de la valeur attendue et de la variance de la somme aléatoire.

Afin d'obtenir des résultats plus complets et calculable, diverses modifications sur le PPP sont parfois essentielles pour modéliser les positions des nœuds. Dans ce chapitre, nous revisitons les propriétés des PPP utilisées dans la littérature, à savoir la superposition, l'amincissement indépendant, le déplacement. Pour donner une idée des métriques de performance étudiées dans cette thèse, nous avons mené une brève enquête sur les différents indicateurs de performance clé (IPC) les plus couramment utilisés dans les réseaux sans fil, tels que la probabilité de couverture et l'efficacité spectrale, et leurs définitions mathématiques ont été présentées.

## Chapitre 3. État de l'art

Dans ce chapitre, nous effectuons un aperçu exhaustif des approches existantes basées sur la GS qui caractérisent le caractère aléatoire des emplacements de réseau. Ces techniques pratiques, à savoir l'approche standard, l'approche processus de distance relative (PDR), l'approche des moments factoriels, l'approche d'inversion de Gil-Pelaez, l'approche d'inversion de transformation de Laplace, l'approche d'approximation par interférence, sont évaluées avec le PPP comme PP de référence, avec

diverses possibilités de calculabilité, de précision et de flexibilité mathématique.

Les déploiements pratiques de BS présentent généralement une propension croissante à l'agrégation spatiale et au regroupement dans les points chauds des utilisateurs (par exemple événements, zones urbaines) et une tendance croissante à la répulsion et à la régularité où les utilisateurs sont également répartis. Étant donné que la distribution spatiale de la BS a un impact de premier ordre sur le rapport signal sur interférence plus bruit d'un réseau cellulaire, la capture de la topologie de ces nœuds via un PP approprié aura un impact direct sur l'exactitude de l'examen des performances du réseau. Ce chapitre a examiné les nombreuses options de modélisation proposées dans la littérature de la GS pour déployer des éléments de réseau tels que la BS et les emplacements des utilisateurs. Dans les processus ponctuels agrégatifs tels que le processus de Cox, les processus de cluster Matérn (MCP) et les processus de cluster Thomas (TCP), les BS ont tendance à être placés dans les clusters des zones très peuplées. La figure 1 montre une réalisation de MCP et TCP.

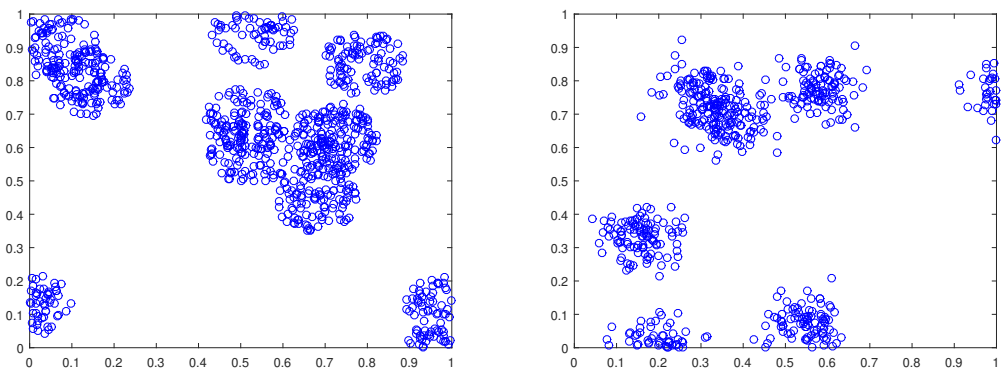

(a) (b)

FIGURE 1 – Réalisation de (a) MCP, (b) TCP.

D'autre part, le répulsion entre les points est réalisable en fixant une restriction déterministe via des distances de noyau dur. Le processus de point de Matérn dur (MHPP) est une variante significative du *hard-core* PP. La figure 2 représente une réalisation de MHPP de type-I et type-II.

Comme principal défi de la thèse, nous avons passé en revue le concept des réseaux d'interférence partielle dans la littérature et en avons donné une nouvelle définition basée sur la région de couverture dans le réseau. Dans ce modèle, la localisation à proximité des bords des cellules ne conduit pas nécessairement à une dégradation significative des performances car toutes les BS ne sont pas actives avec la même ressource. Pour avoir un paramètre d'interférence partielle, nous avons appliqué l'approche de classification des utilisateurs et de coordination des interférences. Nous avons classé ces techniques en plusieurs catégories selon leurs principes de

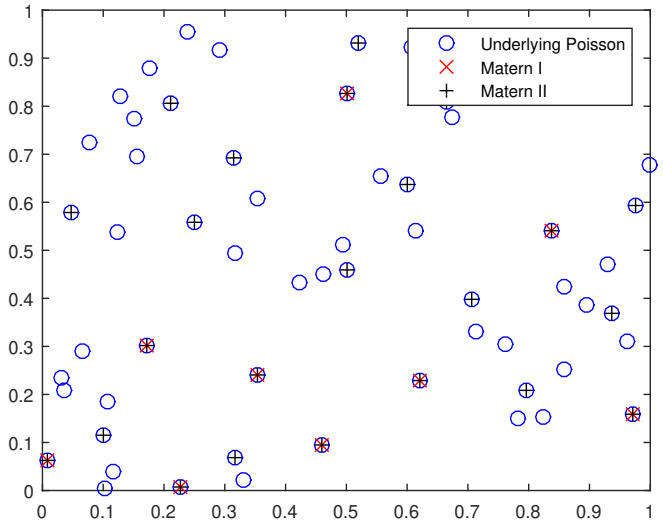


FIGURE 2 – Réalisation de MHPP type-I et type-II.

fonctionnement. La figure 3 représente une taxonomie de la gestion des interférences.

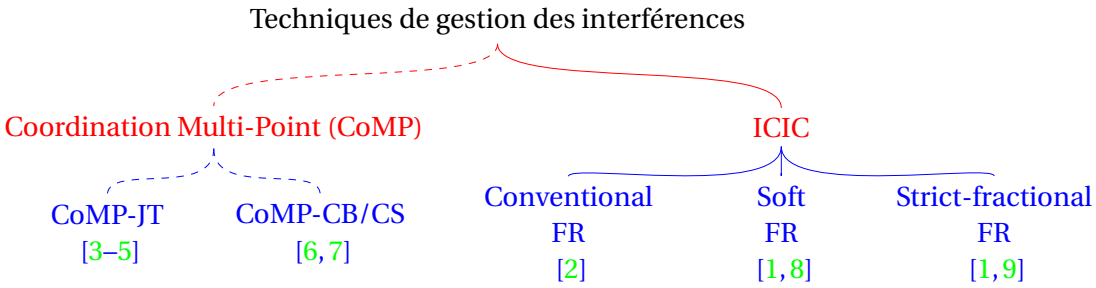


FIGURE 3 – Taxonomie de la gestion des interférences.

Des méthodes de coordination des interférences basées sur la réutilisation des fréquences ont été largement proposées pour réduire les interférences entre les cellules voisines et améliorer l'efficacité de la bande passante. Le facteur de réutilisation dans l'approche de réutilisation de fréquence traditionnelle contrôle le nombre de bandes de fréquence distinctes utilisées par le réseau, où une seule bande est utilisée par cellule. La technique CoMP est développée dans le réseau LTE-A dans le cadre d'un effort visant à minimiser les interférences, à améliorer la couverture, à augmenter le débit de l'utilisateur à la périphérie de la cellule et le débit global du système dans les déploiements co-canaux et non co-canaux. L'idée principale derrière CoMP est de s'éloigner de la structure traditionnelle du système multi-utilisateur à un seul niveau

et vers une conception multi-utilisateur à plusieurs niveaux.

Nous terminons ce chapitre en présentant le concept de gestion des ressources radio (RRM) dans les réseaux sans fil. Les fonctions RRM dans les réseaux cellulaires comprennent la division du spectre disponible entre les stations de base (macrocellules et microcellules), l'allocation des ressources entre les nombreux utilisateurs au sein de chaque cellule, l'adaptation des liaisons, la gestion de transfert et le contrôle d'admission. La modulation, le codage adaptatifs et la gestion de la puissance de transmission sont utilisés pour réaliser la fonction d'adaptabilité de la liaison. Ces capacités, notamment le partitionnement des ressources entre les cellules, la planification des utilisateurs et la régulation de la puissance de transmission, sont utilisées pour atténuer l'impact des interférences sur les performances du système. Le concept RRM comprend plusieurs défis et problèmes technologiques en matière d'évitement des interférences, d'utilisation des ressources radio, d'équité, de QoS et de complexité. Dans cette thèse, nous avons considéré les concepts d'évitement des interférences et d'équité dans les chapitres 4 et 5 lors de la mise en œuvre de notre technique proposée.

## Chapitre 4. Réseaux cellulaires à interférence partielle : analyse des performances et classification des utilisateurs

Dans les réseaux cellulaires modernes, la qualité du service est liée à la puissance du signal reçu de la BS de desserte et de toutes les autres BS interférentes via le RSIB, qui est affecté par la géométrie du réseau et les conditions du canal. Ce chapitre présente une analyse des interférences partielles pour déduire la probabilité de couverture lorsque la technique d'attribution de spectre partagé est appliquée au réseau PPP homogène. Chaque cellule est divisée en deux régions sur la base de la valeur du RSIB : la région du centre de la cellule, si le RSIB est plus important qu'un seuil, et la région de bord de la cellule sinon. Dans notre modèle, un bloc de ressources (RB) donné est alloué à un utilisateur dans une cellule et ne peut pas être partagé par un autre utilisateur. Le RB est donc divisé en deux sous-bandes qui sont utilisées exclusivement selon que l'utilisateur est un utilisateur de centre de cellule (CCU) ou de bord de cellule (CEU), laissant une partie du RB inutilisée afin de réduire les interférences avec les autres cellulse. Ce scénario implique que l'ensemble de BS interférentes dépend de la probabilité de couverture de l'utilisateur type. Nous prouvons que l'ensemble des BS interférentes est une version amincie du PPP original et qu'il est lié à la probabilité de couverture de la région du centre de la cellule.

La figure 4 (a) compare la probabilité de couverture centrale en considérant la classification CCU/CEU sous les modèles d'interférence complète et d'interférence partielle. La courbe liée à l'hypothèse d'interférence totale produit le résultat de la probabilité de couverture d'un utilisateur typique présenté dans [2]. Cependant,

le modèle d'interférence partielle réduit le PPP d'origine en deux PPP. Le processus d'amincissement réduit les interférences pour l'utilisateur central typique d'un facteur dépendant de la probabilité de couverture et du seuil de couverture central $\theta_c$. En se référant à la figure, nous pouvons voir que pour $\theta_c < -8$ dB, la proportion de CCU est élevée par rapport à celle de CEU, générant beaucoup d'interférences sur la sous-bande $B_c$, ce qui rend le résultat à convergent vers l'hypothèse d'interférence totale. La figure 4 (b) compare la probabilité de couverture périphérique en considérant la classification CCU/CEU sous les modèles d'interférence totale et d'interférence partielle. Comme le montre la figure, la probabilité de couverture de bord de cellule $p_e$ est tracée en fonction de $\theta_e$ pour un seuil cible CCU spécifique $\theta_c = 5$ dB. La valeur du seuil central modifie la densité des BS interférentes de l'utilisateur typique du bord de cellule. De plus, comme mentionné dans la description de la figure 4 (a) et étant donné que l'ensemble BS interférentes est une version amincie du PPP d'origine, la probabilité de couverture de CEU est améliorée. Cela signifie que la sous-bande $B_e$ n'est utilisée que par les CEU des autres cellules par rapport au scénario de brouillage complet.

La figure 5 représente l'efficacité spectrale (SE) pour CCU, CEU dans le réseau d'interférence partielle en fonction du seuil de classification d'utilisateur $\theta$. Le SE de CEU augmente avec $\theta$ puisque le nombre de CEU augmente. D'autre part, SE de CCU augmente d'abord puis diminue après 8 dB, car le nombre de CCU diminue et il n'est pas compensé par le gain d'être plus proche de la BS. Le SE global est compris entre les valeurs obtenues pour $\Delta = 1$ et $\Delta = 2$ de l'approche de réutilisation de fréquence (FR). D'autre part, étant donné que le CCU typique bénéficie d'une fraction de ressource dépendante de la couverture et souffre de la même fraction d'interférence, il a un SE supérieur à la FR avec $\Delta = 1$.

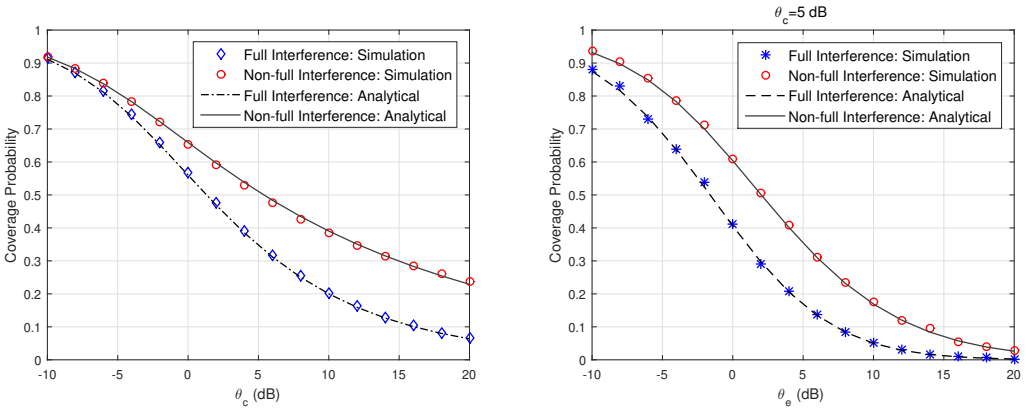


(a) Probabilité de couverture du centre de cellule

(b) Probabilité de couverture de bord de cellule

FIGURE 4 – Probabilité de couverture versus seuils RSIB.

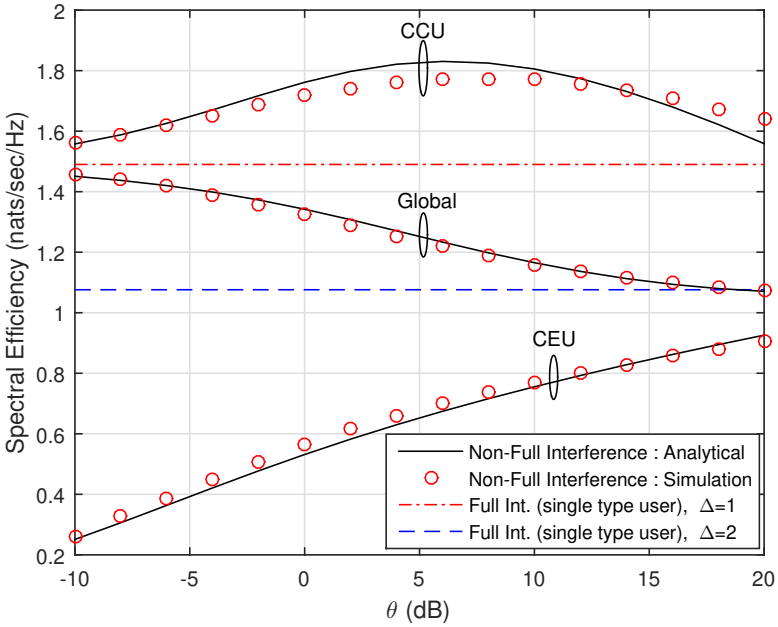


FIGURE 5 – SE versus seuils RSIB $\theta$.

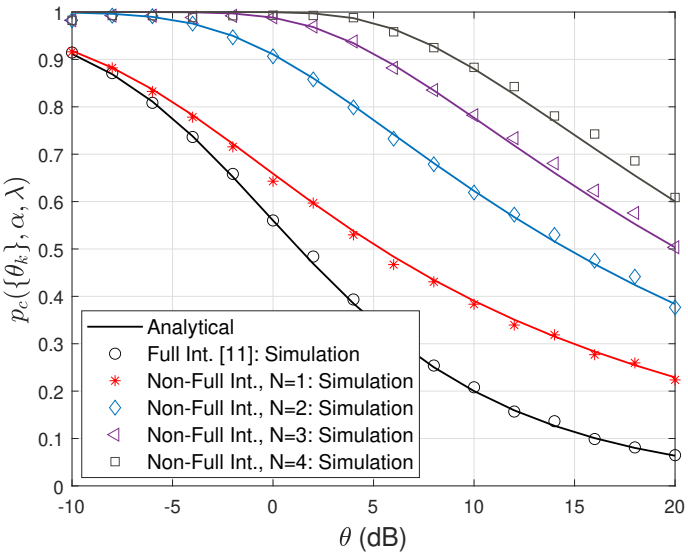


FIGURE 6 – Probabilité de couverture pour différentes valeurs de $N$.

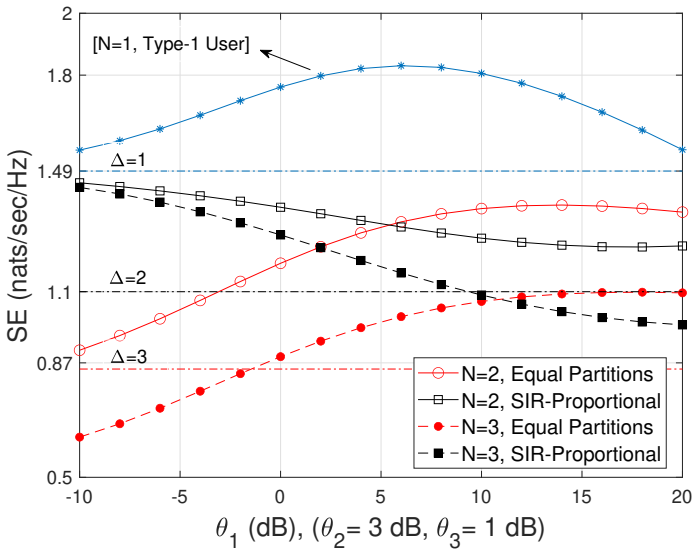


FIGURE 7 – SE avec deux stratégies de partitionnement de bande passante différentes.

Pour évaluer le modèle proposé de réutilisation de fréquence centrée sur l'utilisateur dans un scénario de classification d'utilisateurs avec plus de deux classes, nous étendons d'abord l'approche de classification d'utilisateurs basée sur le rapport signal sur interférence (SIR) à $N$ classes. De plus, nous analysons la probabilité de couverture d'un utilisateur typique localisé au hasard dans le réseau d'interférence partielle. La figure 6 montre les résultats de simulation et analytiques de la probabilité de couverture pour un utilisateur type lorsque $N \in \{1,2,3,4\}$, sous interférence partielle et totale, avec un $\theta$ unique considéré, c'est-à-dire que le seuil cible est le même pour toutes les classes d'utilisateurs. La stratégie d'interférence partielle induite par l'allocation de RB centrée sur l'utilisateur en fonction du type d'utilisateurs, conduit à une probabilité de couverture plus importante lorsque $N$ augmente. Les dérivations analytiques sont relativement proches des simulations surtout pour les petites valeurs de seuil. Cependant, le décalage augmente à mesure que le seuil et $N$ augmentent. L'écart provient du manque d'une densité appropriée de BS active dans le scénario de simulation dans les sous-canaux relatifs lorsque $N$ est grand. De plus, l'estimation de l'ensemble interférent de type $k$ de BS par simulation est un processus itératif qui est sensible à la valeur seuil et nécessite beaucoup d'itérations lorsque $\theta$ est grand. Néanmoins, cette approche convient lorsque le seuil $\theta$ n'est pas trop grand pour assurer suffisamment de BS active pour une approximation de réseau à grande échelle en simulation.

La figure 7 représente l'efficacité spectrale globale pour $N \in \{1,2,3\}$ dans le réseau d'interférence partielle par rapport au seuil cible utilisateur de type 1 $\theta_1$ lorsque $\theta_2 =$

3 dB et $\theta_2 = 1$ dB. Les SE de différents types d'utilisateurs sont comparés dans le cadre d'un partitionnement égal fixe et de stratégies adaptatives de SIR-proportionnelles.

## Chapitre 5 : Réseaux cellulaires à interférence partielle : coopération BS et partitionnement de la bande passante

Dans ce chapitre, en s'appuyant sur le modèle d'interférence partielle multi-classes présenté au chapitre 4, une technique de coopération de BS est étudiée pour améliorer la SE des utilisateurs de bord de cellule sans mettre en péril les autres utilisateurs exploitant le même RB. De plus, une allocation de bande passante (BWP) entre les utilisateurs considérant un compromis entre le SE moyen du réseau et l'équité pour tous les types d'utilisateurs est proposée et comparée à différents scénarios d'allocation de bande passante. Un schéma BWP anti-risque prenant en compte le compromis entre l'efficacité spectrale moyenne du réseau et l'équité pour tous les types d'utilisateurs est proposé. La figure 8 illustre une réalisation d'un réseau PPP pour trois types d'utilisateurs, avec un seul utilisateur par BS exploitant un RB donné. Les BS colorées en vert, rouge et noir représentent les BS actives pour les utilisateurs de type 1, 2 et 3, respectivement.

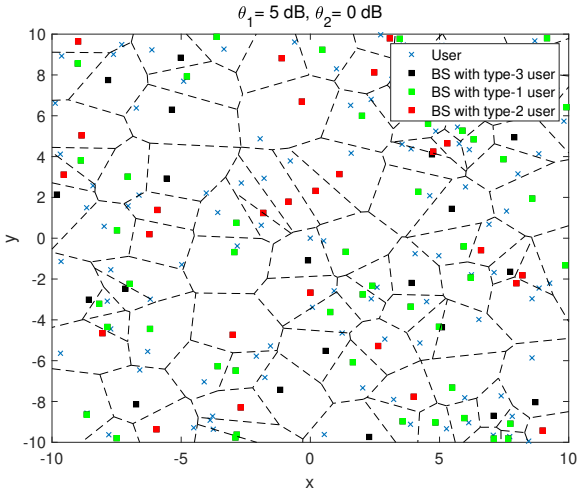


FIGURE 8 – Déploiement PPP pour BS avec un utilisateur sélectionné au hasard dans chaque cellule.

La figure 9 (a) montre les résultats de simulation et analytiques de la probabilité de couverture de bord de cellule dans le cas de deux types d'utilisateurs avec et sans sélection de point optimale (OPS) dans le réseau d'interférence partielle, avec un seuil de classification unique. D'après la figure, la probabilité de couverture de l'utilisateur de bord de cellule est améliorée avec OPS par rapport au scénario non coopératif.

Lorsque le seuil unique augmente, les deux techniques convergent car le nombre de BS desservant un utilisateur de type 1 dans le réseau diminue. De plus, la simulation et les résultats analytiques correspondent, ce qui valide les conclusions théoriques du chapitre 5.

La figure 9 (a) compare le SE moyen pour la classification d'utilisateur centre et bord de cellule dans le scénario d'interférence partielle par rapport au seuil cible d'utilisateur de type 1 $\theta_1$ sous différentes stratégies BWP. De plus, le SE moyen obtenu est comparé à la technique de réutilisation de fréquence conventionnelle avec le facteur de réutilisation $\Delta$ présentée dans [2]. La figure montre que le BWP max-moyen surpasse les autres stratégies car donner toute la bande passante au meilleur utilisateur est optimal en ce qui concerne les performances SE du réseau. De plus, la courbe correspondant au SE max-moyen augmente d'abord puis diminue après environ 8 dB car, pour les petites valeurs de $\theta_1$, presque tous les utilisateurs sont au centre de la cellule. D'un autre côté, les grandes valeurs de $\theta_1$ font que tous les utilisateurs sont des utilisateurs de bord de cellule, et cela tend vers le cas d'interférence totale, c'est-à-dire la réutilisation de fréquence avec $\Delta = 1$. De plus, on peut clairement observer que lorsque $\theta_1$ augmente, le SE moyen sous la politique de SIR proportionnelle diminue tandis que le SE augmente avec un partitionnement égal. On peut voir qu'un BWP égal finit par surpasser le BWP proportionnel au SIR en augmentant $\theta_1$ au-dessus de 5 dB. En effet, contrairement au BWP égal, le BWP proportionnel au SIR donne plus de bande passante aux utilisateurs de la périphérie de la cellule lorsque $\theta_1$ augmente, ce qui est moins efficace pour le SE global. En effet, dans la politique proportionnelle SIR, l'utilisateur type bénéficie d'une fraction des ressources qui dépend du SIR et souffre de la même fraction des interférences. Cependant, la politique proportionnelle SIR a toujours un SE plus élevé que la réutilisation de fréquence statique avec $\Delta = 2$. En outre, la figure compare la BWP moyenne-variance selon le niveau de sensibilité au risque $\beta$ avec d'autres politiques BWP. Pour $\beta = -1.5$, la BWP moyenne-variance est une politique d'aversion au risque faible et tente de maximiser le réseau SE en donnant plus de bande passante aux utilisateurs du centre cellulaire. Par conséquent, le SE obtenu par la BWP moyenne-variance est identique à la stratégie max-moyenne pour les petits $\theta_1$ et diminue ensuite lorsque $\theta_1$ augmente. Ceci est dû au fait que le nombre d'utilisateurs du centre cellulaire diminue en augmentant la valeur de seuil, et la politique tend à limiter l'augmentation de la variance dans l'attribution de débit. D'un autre côté, si $\beta = -10$, la politique est encore plus averse au risque et tend à assurer l'équité entre les utilisateurs au sens de l'index de Jain. Cela signifie également qu'en augmentant négativement le niveau de risque, la SE obtenue par la stratégie moyenne-variance tend vers celle obtenue avec le BWP max-min. La BWP max-min consiste à donner la même quantité de taux parmi les types d'utilisateurs et donc à minimiser la variance de l'allocation et SE augmente en augmentant $\theta$.

La figure 10 (a) montre le compromis entre la probabilité de couverture et le

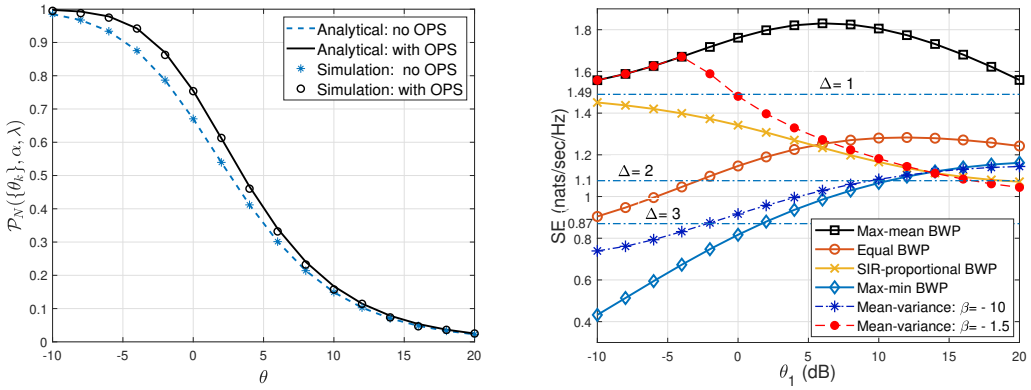


(a) OPS avec $N = 2$ (b) SE sous différentes stratégies BWP

FIGURE 9 – Résultats OPS et BWP.

SE moyenne du réseau pour un BWP proportionnel au SIR, un BWP égal et une réutilisation de fréquence (avec $\Delta = N$), avec et sans technique de coopération BS, c'est-à-dire un schéma OPS, et pour une valeur de seuil unique $\theta$ de $\{-5, 2, 10\}$ dB. Quel que soit le schéma BWP considéré, la probabilité de couverture augmente alors que la SE moyenne diminue lorsque $N$ augmente, mais avec des tendances différentes selon le seuil $\theta$. Cependant, les courbes correspondant aux politiques SIR-proportionnel et BWP égale sont au-dessus de la réutilisation conventionnelle des fréquences. De plus, pour $\theta \in \{-5, 2\}$ dB, le SE moyen obtenu avec le BWP proportionnel au SIR est plus élevé car il alloue plus de bande passante à l'utilisateur de type 1, qui a une efficacité spectrale plus élevée que les autres types d'utilisateurs du réseau. En revanche, un BWP égal alloue également la bande passante quelle que soit la densité des différents types d'utilisateurs dans le réseau. D'autre part, pour $\theta = 10$ dB, sous deux types d'utilisateurs (centre et bord de cellule), c'est-à-dire $N = 2$, un BWP égal a un SE plus élevé que le BWP proportionnel au SIR. Cela est dû au fait qu'une valeur seuil élevée rétrécit la région du centre de la cellule et l'approche proportionnelle SIR alloue plus de bande passante à l'utilisateur de bord de cellule, qui a un SE inférieur à celui de l'utilisateur du centre de cellule. Mais, lorsque $N$ augmente, le SIR-proportionnel atteint à nouveau un SE supérieur à un BWP égal. En effet, l'effet négatif de la division égale de la bande passante disponible est supérieur à l'allocation dépendante de la densité basée sur le type d'utilisateur. Enfin, la stratégie OPS améliore le front de compromis en augmentant le SE de l'utilisateur de type $N$ en utilisant un schéma de diversité de sélection BS, en particulier pour des valeurs de seuil modérées à élevées.

La figure 10 (b) illustre le compromis SE moyen de l'indice de Jain pour différentes stratégies étudiées dans ce travail. Le BWP moyenne-variance caractérise le compromis entre le SE du réseau et l'équité entre les types d'utilisateurs, lorsque la valeur de $\beta$ diminue de $-0.01$ à $-40$. Le BWP max-moyen a le SE maximal mais avec la plus

faible équité dans le partage de la bande passante. En sacrifiant le SE, les BWP proportionnels et égaux atteignent une plus grande équité en ce qui concerne la stratégie max-moyenne. Le BWP max-min offre le partage de bande passante le plus équitable, au sens de l'indice de Jain, tout en ayant le SE le plus bas. On peut remarquer que la technique de réutilisation de fréquence permet d'obtenir un SE du réseau plus grand que celui obtenu avec la politique max-min avec un indice de Jain égal à 1. En effet, la bande passante allouée ne dépend pas de la position de l'utilisateur type dans la cellule de sorte que l'équité de type utilisateur est un. L'équité mesurée est entre les types d'utilisateurs et cela ne signifie pas que l'équité entre les utilisateurs ne ferait qu'un avec la technique de réutilisation des fréquences puisque les utilisateurs ne connaissent pas le même taux. Le critère d'équité moyenne-variance avec un niveau de risque donné $\beta$ permet d'explorer le point opérationnel réalisable en fonction du SE souhaité et du niveau d'équité entre les différents types d'utilisateurs du réseau cellulaire.

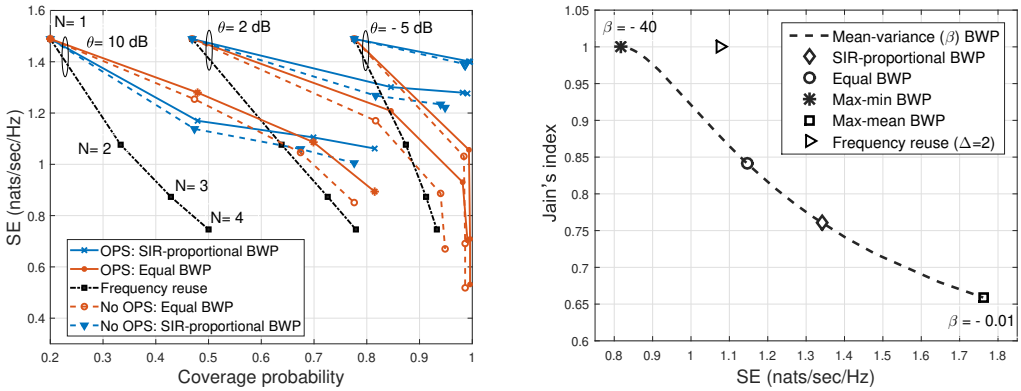


(a) SE-Couverture (b) équité-SE

FIGURE 10 – Résultats des compromis SE-Couverture et Équité-SE.

# Conclusion et travaux futurs

Ce chapitre présente l'extension possible du travail à l'avenir, par exemple, les réseaux multi-niveaux avec un modèle d'interférence partielle, un scénario de liaison montante d'un modèle d'interférence partielle, en étudiant le modèle présenté avec la technique d'accès multiple non orthogonale (NOMA), en étudiant le compromis entre l'efficacité spectrale et efficacité énergétique.

# Chapter 1

# Introduction

This introduction provides an overview of the thesis, describing the background of the study and discussing the reason for this effort as well as the contributions made to the topic.

## 1.1 Background

The successive generations of wireless networks are designed to meet an increasing demand for reliable and high data rate services [10]. The quality of service in cellular networks is determined by the relative signal strength received from the serving base station (BS) w.r.t. the signal received from all other interfering BS via the signal-to-interference-plus-noise ratio (SINR), which is determined by the network geometry and channel conditions [11].

In order to increase the global spectral efficiency (SE), network densification has been pushed as a viable technique [12]. Nevertheless, co-channel interference among base stations due to aggressive frequency reuse limits the performance of cell-edge users (CEU). In a conventional full interference cellular network, a CEU is a user who is positioned near a cell boundary. This has proven a useful criteria for determining user performance degradation. However, in network infrastructures, this is no longer a valid criteria since there are numerous inactive cells and the activity of a BS varies dynamically according to network densification and load model [13, 14]. The term "cell-edge user" is defined deliberately and differently in this thesis by tacking into account the activity of BS in the network.

In downlink, the non-full interference scenario is when all BS do not contribute to the interference received by a user in a given time-frequency resource block (RB). In a conventional full interference scenario, all BS transmit in the same frequency resource, and hence users near the cell boundary are known to experience a low SINR [13]. However, in a non-full interference scenario, locating close to the cell

edge does not necessarily lead to significant performance degradation because all BS are not active in the same resource [11]. To help users who are more vulnerable to interference, in the non-full interference scenario, the available bandwidth can be divided into smaller frequency bands and the frequency reuse technique is able to reduce the interference by not allocating the same frequencies to neighboring cells. On the other hand, if the SINR requirement remains the same, splitting the bandwidth into $N$ sub-channels results in an $N$-fold reduction in data rate [15]. A variation on this concept is to classify users into cell-center users (CCU) and CEU and then allocate different sub-bands to each class using a location-based approach [16]. However, since this is a purely geometrical approach, it ignores the user's SINR, which may be a useful metric for classifying users. Indeed, the SINR can temporally be larger in the non-full interference networks at a point located farther from the BS than the nearest one.

Traditionally, the grid model and network-level simulation were frequently used to analyze the performance of a cellular network, as well as Inter-cell Interference Coordination (ICIC) performance [17]. However, because it is idealized, the grid model becomes intractable and does not represent the features of actual networks. Since the proposal of a cellular network model based on stochastic geometry (SG) [2], an increasing number of cellular network studies have been based on SG, which represents the positions of randomly dispersed BS and users [18]. The Homogeneous Poisson Point Process (HPPP) has been frequently utilized in such investigations because it reflects the irregularity of actual networks and provides mathematically tractable solutions. In addition, coordination of radio resource management is a viable approach for improving the performance of a CEU who encounters high inter-cell interference [19, 20], and hence does not meet Quality of Service (QoS) requirements such as coverage and SE. Because of the cell deployment and the spatial distribution of CEU, the performance of ICIC depends on the network geometry. Some publications evaluating ICIC have not taken spatial distribution of CEU into account [21, 22]. Since 3GPP release 8, inter-cell interference has been identified as the primary bottleneck, and many techniques to manage inter-cell interference have been developed. The performance decrease induced by inter-cell interference is most evident for CEU. To offer adequate QoS to CEU, ICIC controls the radio resources of neighboring BS and therefore enhances edge user performance [19, 20]. ICIC is classified into two kinds. The first is cell-centric ICIC, while the second is user-centric ICIC.

The resource management in cell-centric ICIC is handled by a fixed frequency reuse scheme. This method is simple and requires few signaling overhead. Nevertheless, it is not suited for dense environments since dealing with the user mobility and dynamic channels are challenging in cell-centric ICIC. In contrast, in user-centric ICIC, resource management is coordinated based on known user locations via multi-cell interaction. This is more sophisticated and requires more signaling overhead than

cell-centric ICIC, but it is appropriate for the future generation of networks since it can handle the user mobility, and there are many initiatives ongoing to eliminate signaling overhead in 5G networks [22], [23]. The authors of [22] suggested a user-centric ICIC that employs signal strength order from the perspective of an scheduled user where a user is always served by the BS that provides the strongest signal averaged over small-scale fading. The authors of [1] investigated fractional frequency reuse methods utilizing independent thinning, which is a kind of cell-centric ICIC. The authors in [21] investigated a user-centric ICIC in small cell networks in which cross-tier interference between small cells and macro cells can be avoided through a split-spectrum assignment. BS that transmit interference with signal strength greater than a certain threshold to a scheduled user are not allowed to use the allocated resource. In addition to ICIC, several interference management techniques have been investigated. [24] investigates an inter-tier interference cooperation method in two-tier cellular networks in which small cell transmitters surrounding macro cell receivers can not use the frequency band used by macrocell receivers. [25] investigates an inter-tier interference avoidance system in two-tiers cellular networks in which small BS access macro cell frequencies using the cognitive radio strategy. [26] investigates interference cancellation, a type of interference reduction method based on signal processing at the receiver, in spectrum shared networks. The primary goal of ICIC is to improve the performance of a CEU who suffers from inter-cell interference. As a result, the performance of an ICIC scheme should be measured by the performance improvement of an edge user provided by ICIC. Nevertheless, the majority of previous studies on user-centric ICIC examines a randomly selected user known as a typical user rather than a CEU and assess the performance improvement of the typical user using ICIC. It is worth mentioning that attempts have been made to address the problem of CEU enhancement but in cell-centric ICIC framework [1], [27].

The attributes listed above are the three most important considerations in evaluating the performance of Beyond 5G (B5G) networks. Since network inter-cell interference is essential in future network design, it is critical to examine cellular network modeling methodologies, and performance measures [13]. Several approaches are used in modeling challenges in cellular networks, with SG being among the most widely utilized tools. This thesis focuses on the modeling and performance evaluation of non-full interference cellular networks using SG.

In this work, we aim to assess the performance of large scale network in a non-full interference network scenario. The challenge induced by this setting is the correlation among the activity of the BS and the coverage probability itself leading to a difficult problem. So the thesis employ SG tool to model the network and show that the spatial dependence between the desired transmitter and the interferers is critical in analysing the network's performance.

## 1.2 Contributions

As stated in the previous section, this thesis specially studies the non-full interference cellular networks from the perspective of SG. In the literature, to the best knowledge of the author of this thesis, the works that consider full interference do not capture the correlation in signal-to-interference (SIR) induced by the fact that the user's interference set is a function of its coverage probability. The non-full interference model presented in this thesis overcomes the above limitations while enabling the tractable system-level study of the typical user performance in downlink using SG. The key contributions of our study are briefly summarized below.

1. A novel non-full interference model for cellular networks to classify users with distinct link qualities is proposed. First, we mathematically define the cell center region and cell edge region for a stationary Poisson point process (PPP) in $\mathbb{R}^2$, modelling the BS deployment, based on the received users' SIR. Then, we extend the classification approach to $N$ user types. A cell is divided into $N$ classes, and a typical user belongs to a certain class depending on its SIR. Moreover, each class has its proper sub-band that may be used by the nearest interfering cell but only by the same user type in that interfering cell. In our model, a user is classified to be a type-1 when its SIR on sub-channel 1 is larger than a threshold; a user is type-2 if its SIR on sub-channel 1 is less than the first-class threshold and its SIR on sub-channel 2 is larger than the second class one, and so on. A type-$N$ user has all its SIR lower than the thresholds in all sub-channels 1 to $N-1$ and maybe in an outage in the last remaining sub-channel $N$. Contrary to the type-$N$ user, all type-$k$ users are covered with a probability equal to one. The type-1 user is the CCU while the type-$N$ is the CEU one. This user-centric model allows quantifying key performance measures, i.e., the coverage probability and the SE in the non-full interference context, based on the user type. We show that the user position within each cell drives the BS activity. In this case, user classification leads to BS classification for the considered RB, which means that the interfering BS set density is correlated with the user position in the interfering cells and depends on the user's location where the SIR is measured.

2. An accurate approximation of the user classification probability is derived. The expression is obtained in the form of a fixed-point equation that models the existing correlation between the desired signal and the interference set of each user type. In this model, the average number of interfering BS that lies within a given distance from each user type is a function of its coverage probability. On the other hand, it is shown that the correlated interfering scenario can be estimated as a thinning process: the original PPP is split into $N$ thinned complementary processes, and the thinning factor for each class is quantified.

The interference are mathematically modeled, and semi-tractable expressions for the coverage probability and SE are obtained.

3. Based on multi-point coordination technique, we apply the optimal point selection (OPS) technique to improve the performance of CEU without degrading the performance of the other user types, in our framework. Precisely, our proposed scheme exploits the fact that a BS that serves a type-$k$ user in another cell is only active on the $k$-th sub-channel and remains idle for all the other sub-channels and in particular for the $N$-th sub-channel. We mathematically characterize the mean interference seen by the typical cell edge user. We drive integral-form solutions for the coverage probability and SE.

4. The network's SE depends on the bandwidth partitioning (BWP). Hence, the bandwidth allocation strategy plays an important role in the performance achieved. We study the fairness-SE tradeoff achieved by different BWP techniques in our framework, i.e., the user-centric frequency reuse model. The fairness is measured with the Jain's index that provides a measure of the variance of a given criterion, e.g. the spectral efficiency, w.r.t. its mean value. We present a risk-averse approach to find a mean-variance tradeoff for the network performance.

5. Our numerical results demonstrate that: *i*) in comparison to the conventional frequency reuse scheme, user-centric frequency reuse boosts network efficiency, *ii*) the non-full interference-based BS cooperation can help vulnerable users without penalizing other users in other cells, *iii*) the proposed tradeoff BWP strategy assigns fair shares to the different types of users based on their performance metrics.

## 1.3 Publications

List of publications.

- Journal paper: [28], submitted on March 2022 to EURASIP Journal on Wireless Communications and Networking.

- Conference papers: [29, 30], published (SPAWC'20, Globecom'20)

# Chapter 2

# Mathematical Background

## 2.1 Introduction

In this chapter, we outline the history of SG and its application in wireless networks analysis. Then, we present some of the most famous theorems of SG, and finally, we define performance metrics used in this thesis.

### 2.1.1 Stochastic geometry

SG is an applied probability area that attempts to provide tractable mathematical formulas and adequate statistical tools for studying and analyzing random occurrences on the plane $\mathbb{R}^2$ or in higher dimensions [31]. Its advancement was motivated by applications in forestry, image analysis, geophysics, neurophysiology, cardiology, finance, and economics. In wireless communications, the various network topologies encountered in real environment make the performance analysis of a particular deployment too specific to the network geometry. In order to overcome this limitation, the positions of users and BS can be seen as particular realizations of a two-dimensional random process [32, 33]. Hence, with SG, the position of users and BS, are statistically evaluated to explore their interactions, that allows to assess the network performance in average over all possible realizations [34].

### 2.1.2 Brief history

The study in [35] is the first work in communication networks that investigates SG techniques for evaluating connectivity in a network represented by a PPP. In the 1990s, [32, 33] proposed significant ideas from SG to model and analyze communication networks, where methods based on Poisson Voronoi tessellation and Delaunay triangulation were presented to infer geometric properties of connections between stations. Notable results were reported a decade later, in the example of a single-tier

wireless network [36]. Since then, the complexity of the models used to address more and more realistic networks has increased significantly.

### 2.1.3 Related studies on SG for wireless networks

Several interesting survey and magazine papers on applications of SG in wireless networks have been developed during the last decades, e.g. [18, 37, 38] and references therein. [37] focuses on earlier references up to 2008, where SG were used to derive the main statistical properties of cables connecting subscribers and concentration points in: i) fixed-line networks to obtain the main statistical characteristics to assess infrastructure costs as a function of node density; ii) cellular networks to assess the impact of network geometry on key performance indicators (KPI) based on SINR thresholds, such as service coverage, the ergodic rate; and iii) ad hoc networks to explore the connectivity characteristics of random graphs using the SINR. Authors in [38] present a tractable approach to derive the coverage probability in wireless networks in a PPP with Rayleigh fading. Authors in [39] addressed the distance distribution when nodes are distributed: i) according to a PPP; and ii) uniformly inside a bounded region of $\mathbb{R}^2$. In addition, authors in [40, 41] review the literature results on how SG models have been used to capture the interference impact in ad hoc networks, whereas work in [42] is a tutorial study on how SG has been utilized wisely to describe interference in cellular networks.

## 2.2 Spatial point process

In this section, we will go over some of the fundamental principles of the point process (PP) theory, which plays a significant role in SG. A point process is a countable random collection of points that reside in some measurable space. Consider $N(B)$ as the cumulative counting process of a spatial PP $\Phi$, defined for any finite set $B \subset \mathbb{R}^2$. The number of points $X_i$ falling into $B$ can be stated as [43]

$$N(B) = \sum_{X_i \in \Phi} \mathbf{1}\left(X_i \in B\right). \tag{2.1}$$

The intensity measure of a point process is equal to the average number of points in a set $B \subset \mathbb{R}^2$, i.e.,

$$\Lambda(B) = \mathbb{E}[N(B)]. \tag{2.2}$$

### 2.2.1 Nearest neighbor distance

The probability mass function (PMF) of having $n$ points in a given set $B \subset \mathbb{R}^2$ is an essential measure linked to the cumulative counting process, i.e., $\mathbb{P}(N(B) = n)$. In

particular, the void probability, is $\mathbb{P}(N(B) = 0)$. Considering an area $B$ as a ball with radius $R$ centered at the typical point $X$, i.e., $B = b(X, R)$, the void probability of $B$ may be read as the probability that the distance between $X$ and the nearest point of $\Phi$, i.e., $\mathrm{d}(X, \Phi)$, is greater than $R$.

As a result, we consider the distribution of the closest neighbor distance $G_X(.)$ as the distribution of the distance among $X$ and the nearest point $Y \in \Phi \backslash \{X\}$. In terms of likelihood,

$$G_X(R) = \mathbb{P}(\mathrm{d}(X, Y) \leq R \mid X, Y \in \Phi, Y \neq X) \tag{2.3}$$
$$= \mathbb{P}(N(b(X, R) \backslash \{X\}) > 0 \mid X \in \Phi) \tag{2.4}$$
$$= 1 - \mathbb{P}(N(b(X, R)) = 1 \mid X \in \Phi), \tag{2.5}$$

where $\mathrm{d}(X, Y)$ is the distance between the typical location $X$ and the closest point $Y$. The term $N(b(X, R) \backslash \{X\})$ counts the number of points of $\Phi$ within the ball $b(X, R)$ excluding $X$.

When $X \notin \Phi$, we analyze the contact distribution function $F_X(.)$, which indicates the shortest radius required for the ball centered at $X$ to make contact with a point in $\Phi$. Theoretically,

$$F_X(R) = \mathbb{P}(\mathrm{d}(X, \Phi) \leq R) = 1 - \mathbb{P}(N(b(X, R)) = 0). \tag{2.6}$$

Expressions $G_X(.)$ and $F_X(.)$ are essential first order summary features of a specific PP [44], that allows to capture clustering of repulsive effects in PP. They are often equal in the scenario of a completely random PP, such as the PPP, whereas $G > F$ for clustered PPs (Cox, Nymann-Scott, etc.), and $G < F$ for normal PPs (shifted regular lattices, hard-core, and soft-core repulsive PPs, etc.). See figure 2.1.

| Repulsion | ⟵ Zero Attraction ⟶ | Attraction |
|---|---|---|
| Regular processes | PPP | Clustered processes |
| $F > G$ | $F = G$ | $F < G$ |

Figure 2.1 – Taxonomy of PP

### 2.2.2 Reduced Palm probability

Consider the point $X$ from a stationary point process $\Phi$, so that $X$ is in the typical location $o$ (at the origin). The function $G_X(.)$ is defined as the ratio of the mean number of points except $X$ in the ball of radius $R$ and centering at $o$ to the mean number of points inside a given set $B \subset \mathbb{R}^2$. Theoretically, it is the ratio of the reduced Campbell

measure represented as

$$\mathbb{E}_0^!(\Phi(B)) = \mathbb{E}\left[\sum_{X\in\Phi\cap B} \mathbf{1}(\mathscr{A})\right], \tag{2.7}$$

as well as the average number of points within $B$ represented as $\Lambda(B)$, where $\mathscr{A}$ is the event $N(b(X,R)\backslash\{X\}) > 0$.

The preceding interpretation of the closest neighbor distance $G_X(.)$ is referred to as the reduced Palm probability measure, which is represented by $\mathbb{P}_0^!$ as [45]

$$\mathbb{P}_0^!(\Phi \in \mathscr{A}) = \frac{1}{\Lambda(B)}\mathbb{E}\left[\sum_{X\in\Phi\cap B} \mathbf{1}(\mathscr{A})\right], \tag{2.8}$$

where the superscript ! refers to the fact that the typical point in the origin $o$ is not included, i.e., $\mathbb{P}_o(\Phi\backslash\{X\} \in \mathscr{A}) = \mathbb{P}_o^!(\Phi \in \mathscr{A})$, and $\Phi \in \mathscr{A}$ stating that $\Phi$ has the property $\mathscr{A}$. Hence, a point becomes typical when the reduced Palm distribution is the distribution of the process.

## 2.3 Poisson point process

Because of its tractability and analytical flexibility, the PPP is widely used [18], and we also consider it as the spatial model for BS in this thesis. This section reviews the important characteristics that underpin such tractability. PPP is a zero-attraction point process in which points are dispersed independently with no interaction between them. It is distinguished by two characteristics [43], that is:

1. For every compact set $B \in \mathbb{R}^2$, $N(B)$ has a Poisson distribution with mean $\Lambda(B) = \int_B \lambda(x)\mathrm{d}x$ where $\lambda(.)$ is the density of points. The PMF of PPP is

$$\mathbb{P}(N(B) = n) = \frac{\Lambda(B)^n}{n!}\mathrm{e}^{-\Lambda(B)}. \tag{2.9}$$

2. If $B_1, B_2, \ldots, B_m$ are disjoint compact sets, then $N(B_1), N(B_2), \ldots, N(B_k)$ are independent random variables.

For an HPPP ($\lambda(x) = \lambda$), the first property can be written as:

$$\mathbb{P}(N(B) = n) = \frac{(\lambda|B|)^n}{n!}\mathrm{e}^{-\lambda|B|}. \tag{2.10}$$

### 2.3.1 Slivnyak-Mecke theorem

The number of points lying in disjoint Borel sets is independent for HPPP $\Phi \subset \mathbb{R}^2$ with density $\lambda$. As a result, the points described by an HPPP are completely independent, which is why the HPPP is also known as a zero-interaction PP [43]. In HPPP, the closest neighbor distance distribution $G_X$ and the contact distance distribution $F_X$ are identical. This resemblance may be regarded as the equality between the reduced Palm probability of $\Phi$ in the usual point $X$ placed at the origin $o$, i.e., $\mathbb{P}^!_X(\Phi \in .)$, and its initial distribution counting $X$, i.e., $\mathbb{P}(\Phi \in .)$. In other terms, the spatial averages seen at $o \notin \Phi$ have the same distribution as those observed at $o$ of $\Phi \cup \{o\}$, indicating that conditioning on the typical point has no effect on the PPP distribution. That's the well-known Slivnyak-Mecke theorem [33, 45], which is formalized as

$$\mathbb{P}^!_X(\Phi \in \mathscr{A}) = \mathbb{P}(\Phi \in \mathscr{A}). \tag{2.11}$$

This theorem is frequently referred to in the literature. In a wireless network, for example, when the typical user is situated at the origin $o$, the Slivnyak-Mecke theorem may be used to calculate the mean interference at $o$, assuming that the serving BS $Y_0$ belongs to the PP of BS but does not participate to the interference.

### 2.3.2 Binomial point process

For a fixed number $n$ of nodes within a particular coverage area $W$, if $k \leq n$ nodes are placed in a specific subset $B \subset W$, the residual area $W \setminus B$ must involve $n-k$ nodes, introducing dependence between points of $W$. Thus the PPP is not a valid model for such finite networks. Instead, for such events, the binomial point process (BPP) is regarded as the most important PP [46]. It is important to note that, according to (2.8), the probability that a point $X \in W$ belongs to $B$ is dependent on the number of points lying inside $B$. Equivalently,

$$\mathbb{P}(X \in B) = \frac{\Lambda(B)}{\Lambda(W)}. \tag{2.12}$$

For a uniform BPP, the number of randomly located points being found in a region $B$ is a binomial random variable, say, $N(B)$, with probability parameter $p = \Lambda(B)/\Lambda(W)$. The PMF of $N(B)$ is

$$\mathbb{P}\left(N(B) = k\right) = \binom{n}{k} p^k (1-p)^{n-k}. \tag{2.13}$$

We can write the expression more explicitly

$$\mathbb{P}\left(N(B) = k\right) = \binom{n}{k} \left[\frac{\Lambda(B)}{\Lambda(W)}\right]^k \left[1 - \frac{\Lambda(B)}{\Lambda(W)}\right]^{n-k}. \tag{2.14}$$

In a more formal way, the conditional multivariate PDF $f(X_1,\ldots,X_n \mid N(W)=n)$ defined w.r.t. the Lebesgue measure on $\left(\mathbb{R}^2\right)^n$ is expressed as

$$f(X_1,\ldots,X_n \mid N(W)=n)=\frac{\prod_{i=1}^{n}\lambda(X_i)}{\Lambda(W)^k}. \tag{2.15}$$

Remarkably, the notion of (2.15) is investigated in order to describe the structure of point configurations with inter-point interactions. In other words, it is utilized in a more sophisticated structure known as the Papangelou conditional intensity to create the family of Gibbs PPs [44].

### 2.3.3 Simulation of Poisson point process

1. Realization of PPP:

   In numerical simulations, a binomial distribution in a limited window $W$ is often utilized to produce a PPP with density $\lambda$ [44]. In practice, we first construct a Poisson variate $N$ with the parameter $\lambda$, and then we generate $N$ independent and uniformly distributed points inside $W$. The resulting PP inside $W$ corresponds to a PPP with density $\lambda$. Figure 2.2 depicts a realization of the homogeneous PPP produced in the $W=[0,1]\times[0,1]$ window.

2. Voronoi tessellation

   Let $\Phi$ be a stationary [1] point process on $\mathbb{R}^2$. The set

   $$V(X):=\left\{Y\in\mathbb{R}^2, X\in\Phi : \|Y-X\|\leq \inf_{X\in\Phi}\|Y-X\|\right\} \tag{2.16}$$

   is called the Voronoi cell of $X$ with respect to $\Phi$. An example of the Voronoi cell is presented in 2.2.

### 2.3.4 Laplace functional and Campbell theorem

In the preceding section, the PPP were built using the PMF in (2.9). A PPP $\Phi$ may be created using probability densities on Borel subsets and then generalized to the entire plane. Analysis of wireless networks can be greatly aided by calculating the sum and product of functions evaluated at the point of a PP.

[1] A point process $\Phi$ defined on a $A$ of $\mathbb{R}^2$ is said to be stationary if the number of points lying in $A$ depends on the size of $A$ but not its location [47].

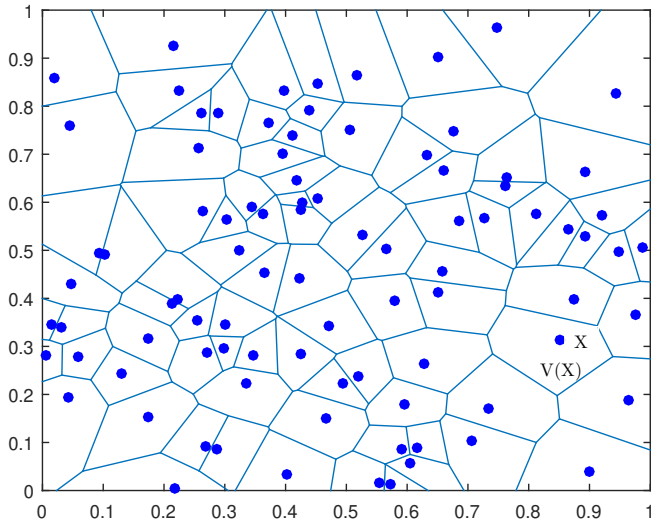


Figure 2.2 – Realization of an HPPP on the window $W = [0,1] \times [0,1]$ with density $\lambda = 100$. Voronoi tessellation shows cells boundaries based on the nearest points.

**Theorem 1** (Sum over PPP (Campbell theorem) [40])**.** *Let* $\Phi$ *be a PPP of density* $\lambda$ *and* $f(x) : \mathbb{R}^2 \to \mathbb{R}^+$

$$\mathbb{E}\left[\sum_{X_i \in \Phi} f(X_i)\right] = \lambda \int_{\mathbb{R}^2} f(x)\mathrm{d}x. \tag{2.17}$$

*Proof.* Referring to [40], we have

$$\mathbb{E}\left[\sum_{X_i \in \Phi} f(X_i)\right] = \lim_{R\to\infty} \mathbb{E}\left[\sum_{X_i \in \Phi \cap B(o,R)} f(X_i)\right]. \tag{2.18}$$

Let $N = \Phi(B(o,R))$. Conditioning on the number of points $N$,

$$\mathbb{E}\left[\sum_{X_i \in \Phi \cap B(o,R)} f(X_i)\right] = \mathbb{E}_N\left[\mathbb{E}\left[\sum_{X_i \in \Phi \cap B(o,R)} f(X_i) \mid N = n\right]\right]. \tag{2.19}$$

Since conditioned on the number of points, the points are i.i.d. uniform

$$\mathbb{E}\left[\sum_{X_i \in \Phi \cap B(o,R)} f(X_i) \mid N = n\right] = n \int_{B(o,R)} \frac{f(x)}{|B(o,R)|}\mathrm{d}x. \tag{2.20}$$

Averaging over $n$

$$\mathbb{E}\left[\sum_{X_i \in \Phi \cap B(o,R)} f(X_i)\right] = \mathbb{E}[N] \int_{B(o,R)} \frac{f(x)}{|B(o,R)|}\mathrm{d}x. \tag{2.21}$$

As $\mathbb{E}[N] = \lambda|B(o,R)|$, and tending $R \to \infty$ we obtain the result. □

**Theorem 2** (Product over PPP (probability generating functional (PGFL)) [40])**.** *Let $\Phi$ be a PPP of density $\lambda$ and $f(x) : \mathbb{R}^2 \to [0,1]$ be a real valued function. Then*

$$\mathbb{E}\left[\prod_{X_i \in \Phi} f(X_i)\right] = \exp\left(-\lambda \int_{\mathbb{R}^2} (1 - f(x)) \mathrm{d}x\right). \tag{2.22}$$

*Proof.* We prove the result for $\Psi_r = \Phi \cap B(o,r)$. Observe that $\Psi_r$ is a PPP with number of points $n$ distributed as a Poisson random variable with mean $\lambda\pi r^2$.

$$\mathbb{E}\left[\prod_{X_i \in \Psi_r} f(X_i)\right] = \mathbb{E}_N \mathbb{E}\left[\prod_{X_i \in \psi_r} f(X_i) \mid N = n\right] \tag{2.23}$$

$$= \mathbb{E}_N \mathbb{E}[f(X_i)]^n. \tag{2.24}$$

But $\mathbb{E}[f(X_i)] = \frac{1}{\pi r^2} \int_{B(o,r)} f(x) \mathrm{d}x$. Hence

$$\mathbb{E}\left[\prod_{X_i \in \Psi_r} f(X_i)\right] = \mathbb{E}_N \left[\left(\frac{1}{\pi r^2} \int_{B(o,r)} f(x) \mathrm{d}x\right)^n\right]. \tag{2.25}$$

Let $z > 0$. Let $n$ be a Poisson random variable with mean $a$. Then

$$\mathbb{E}\left[z^n\right] = \exp(-a(1-z)). \tag{2.26}$$

$$\mathbb{E}\left[\prod_{X_i \in \Psi_r} f(X_i)\right] = \exp\left(-\lambda\pi r^2 \left(1 - \frac{1}{\pi r^2} \int_{B(o,r)} f(x) \mathrm{d}x\right)\right) \tag{2.27}$$

$$= \exp\left(-\lambda \int_{B(o,r)} (1 - f(x)) \mathrm{d}x\right), \tag{2.28}$$

where by tending $R \to \infty$ we obtain the result. □

Formally, the probability generating functional (PGFL) of a PPP $\Phi$, also known as the Laplace functional, and we have [33]

$$\mathscr{L}_f(s) = \mathbb{E}\left[\exp\left(-s \sum_{X_i \in \Phi} f(X_i)\right)\right] \tag{2.29}$$

$$= \exp\left(-\lambda \int_{\mathbb{R}^2} \left(1 - \mathrm{e}^{-sf(x)}\right) \mathrm{d}x\right), \tag{2.30}$$

where $f$ is any measurable non-negative function on the space $\mathbb{R}^2$.

### 2.3.5 Properties of a Poisson point process

In order to achieve more comprehensive and tractable findings, various modifications on the PPP are sometimes essential to model node's positions. In this section, we revisit popular properties of PPP used in literature [33], i.e.,

1. **Superposition**:

   The combination of independent PPP $\{\Phi_k\}$ with intensities $\{\lambda_k\}$ is a PPP $\Phi = \bigcup_k \Phi_k$ with intensity measure $\lambda = \sum_k \lambda_k$. For instance, consider the superposition of K-tiers independent networks investigated in [48]. The superposition of two separate layers of line-of-sight (LOS) and non-line-of-sight (NLOS) BS investigated in [49]. It is also discussed in the context of infrastructure sharing [50] and spectrum sharing [14, 51], to show how separate PPP can abstract the network of many competing operators.

2. **Independent thinning**:

   Independent thinning is a selection process $\Phi^p$ of particular points from the original PPP $\Phi$ such that each point $X$ is randomly and independently chosen with certain probability distribution $P_X$. As a result, $\Phi^p$ is a PPP with density equals to $\int_{\mathbb{R}^2} P_X(x)\Lambda(\mathrm{d}x)$ [33]. Generally, independent thinning is employed to produce the family of Cox PP (e.g., Neyman-Scott, log-Gaussian), which is an extension of the PPP and is used to identify clustered point patterns [52]. For instance, independent thinning has been used to separate LOS and NLOS transmissions in [50]. In [53], it is used to separate the transmissions in half-duplex while it is used for to model active device-to-device (D2D) links in [54]. Independent thinning has been used to model medium access control (MAC) protocols, e.g. ALOHA, by considering the set of concurrent packet transmissions as a thinning process in [33, 54].

3. **Displacement**:

   In displacement, points of $\Phi$ from $\mathbb{R}^2$ are transformed to some new location in $\Phi^p$ from $\mathbb{R}^{d'}$ according to a distribution $P_X(x)$. The Poisson law is passed down to the next PP and its density will be $\Lambda'(A) = \int_{\mathbb{R}^2} P_X(x \in A)\Lambda(\mathrm{d}x)$, $A \subset \mathbb{R}^{d'}$, according to the displacement theorem [33]. In some cases, a given point $X \in \Phi$ may be moved deterministically with probability 1 into a function $f(x) \in \Phi^f$ [3], and hence the new PP remains a PPP with intensity measure $\Lambda'(A) = \Lambda\left(f^{-1}(.)\right)$. This feature is sometimes referred to as the mapping theorem [43]. An example application is explored in [55], where the authors evaluated an arbitrary path loss model and a generalized fading model, and then constructed a series of equivalence between the shotgun cellular system and a stochastically equivalent system, namely the canonical model.

## 2.4 Key performance indicators

A study of the comprehensive literature on SG-based research for wireless network modeling and analysis indicates that nearly all accepted performance measures are generally based on SINR. It is defined as the desired received power divided by the total received interference power plus noise and may be written as:

$$\text{SINR} = \frac{\text{Direct signal power}}{\text{Noise power} + \text{Interference power}}. \tag{2.31}$$

The definition of important representative performance measures utilized in the thesis will be discussed further below.

### 2.4.1 Coverage probability

The coverage probability $\mathrm{P}_{\mathrm{cov}}$ is the complementary probability of the outage probability $\mathrm{P}_{\mathrm{out}}$, and is defined as the probability that the typical user can exceed a target threshold $\theta$ [36]. It is written as

$$\mathrm{P}_{\mathrm{cov}}(\theta) = 1 - \mathrm{P}_{\mathrm{out}}(\theta) = \mathbb{P}(\text{SINR} \geq \theta). \tag{2.32}$$

This may alternatively be understood as the average success chance of a typical transmission/link over all geographical connections [40, 56]. Formally, we first condition on the BS process and the typical user situated at the origin $X_0$ of the PP $\Phi$, and then average over all spatial connections

$$\mathrm{P}_{\mathrm{cov}}(\theta) = \mathbb{E}\left(\mathbb{P}^{!}_{X_0}(\text{SINR} \geq \theta \mid \Phi)\right). \tag{2.33}$$

### 2.4.2 Spectral efficiency

The spectral efficiency $\eta$, accounts for the possible information rate attainable over a cell in a given bandwidth and is another metric of interest. It is calculated in units of [nats/s/Hz] as [2, 48, 57]

$$\eta \triangleq \mathbb{E}\left[\log(1+\text{SINR})\right]. \tag{2.34}$$

The spectral efficiency in (2.34) can be computed as

$$\eta = \int_{t>0} \mathbb{P}(\log(1+\text{SINR}) > t)\,\mathrm{d}t \tag{2.35}$$

$$= \int_{t>0} \mathbb{P}\left(\text{SINR} > \mathrm{e}^{t} - 1\right)\mathrm{d}t \tag{2.36}$$

$$= \int_{x>0} \frac{\mathrm{P}_{\mathrm{cov}}(x)}{x+1}\,\mathrm{d}x. \tag{2.37}$$

The achievable rate $R$ is defined as the maximum number of bits that can be sent across a given bandwidth $B$ in units of nats/s as

$$R \triangleq \mathrm{B}\log(1+\mathrm{SINR}). \tag{2.38}$$

It is necessary to have knowledge about the channels between the BS and the users in order to compute the rate value.

### 2.4.3 Fairness measure

Fairness in resource allocation is an essential performance evaluation criterion. Resource allocation is a stage in network system management in which users must get a piece of a resource to deliver a service. When the available resources are limited and insufficient to meet consumers' demand fully, resource allocation becomes a difficult task. In such cases, resource allocation algorithms must provide some fairness. Fairness measures can be classified as quantitative or qualitative [58]. We explicate them in the sequel.

- Quantitative fairness measures: in these methods, a given fairness index is computed by averaging the throughput for each user within some formulas. Two most applied quantitative measures are Jain's Index [59] and Entropy [60]. Jain's index is one of well-known and widely studied fairness measures [58]. Jain's fairness index is calculated as follows:

$$\mathrm{J}\left(\eta_1,\eta_2,\ldots,\eta_K\right) = \frac{\left(\sum_{k=1}^{K}\eta_k\right)^2}{K\cdot\sum_{k=1}^{K}\eta_k^2}, \tag{2.39}$$

  where $J$ rates the fairness of a set of throughput values; $K$ is the number of users. Jain's fairness index ranges from $1/K$ (worst case) to 1 (best case). When all users receive the same throughput, it achieves its maximum value. The Jain's index has the following good properties:

  1. Population size independence: applicable to any user set, finite or infinite.
  2. Scale and metric independence: not affected by the scale.
  3. Boundedness: can be expressed as a percentage.
  4. Continuity: able to capture any change in the allocation.

- Qualitative fairness measures: in these measures, each user's throughput is subject to a constraint based on the throughput distributions of all other users. Two most relevant measures are max-min [61] and proportional fairness. Max-min fairness is achieved when a system cannot increase any user's resources

without decreasing another user's resources who was already allocated less resources. On the other hand, proportional fairness considers multi-resource allocation from the perspective of each user. Proportional fairness may become max-min fairness in special cases discussed in [62].

In chapter 5, we employ Jain's index to compare different resource allocation in term of the amount of fairness they can achieve among various types of user in the network. We use Jain's index because it is simple to adapt and the aim is only comparing different bandwidth partitioning approaches with different fairness features.

### 2.4.4 Meta distribution

Expressions such as the reduced Palm expectation over the PP does not reveal how concentrated the well-covered regions or what the connection success probabilities are. Author in [63] introduces the notion of meta-distribution (MD) to acquire fine-grained information regarding performance

$$\bar{F}(\theta, u) = \mathbb{P}\left(\mathbb{P}^{!}_{X_0}(\mathrm{SINR} \geq \theta \mid \Phi) > u\right), u \in [0,1]. \tag{2.40}$$

The coverage probability in (2.33) then becomes

$$\mathrm{P}_{\mathrm{cov}}(\theta) = \int_0^1 \bar{F}(\theta, u)\mathrm{d}u = \lim_{u\to 1}\int_0^u \bar{F}(\theta, x)\mathrm{d}x. \tag{2.41}$$

MD seeks to assess fine-grained information about the SINR distribution.

## 2.5 Conclusion

In this chapter, after describing a brief history of stochastic geometry and its application to analyze network performance, we presented general definitions and notions of the spatial point processes that will be used in this thesis. We outlined the Poisson point process and its properties. Then, we gave useful theorems of the point processes that found important applications in wireless communication. We also introduced some KPIs to investigate the performance of wireless networks and that will be used in the subsequent chapters of this manuscript. In the next chapter, we present a state of art of approaches that deal with the performance analysis in PPP networks. In particular, we review the recent techniques that have been proposed to reduce the interference for cell-edge users.

# Chapter 3

# State of the Art

## 3.1 Introduction

Next-generation wireless networks are projected to be highly diverse and multi-layered [64–66]. In such a case, random modeling of networks is critical for developing valuable insights into the tradeoffs that control such a complicated system. Over the last decade, SG has been an essential analytical tool for evaluating average performance of randomly deployed models for wireless networks. Furthermore, SG is likely to be an active field of study for the purposes:

- First, the spatial distribution of transmitters and receivers will remain important in predicting performance measures in 5G/B5G wireless networks, such as performance scaling laws in ultra-dense networks (UDN) [67];

- Second, the ability to evaluate the effect of coupling user and BS locations on average performance study [38].

## 3.2 Derivations based on SG

This section aims at investigating practical SG-based techniques in the literature to evaluate the coverage probability under PPP as the reference PP. These techniques are different in various aspects such as mathematical tractability and accuracy of evaluation. We take the standard definition of the received SINR at the typical user located in $X_0 \in \mathbb{R}^2$ from a serving BS $Y_0$. We have

$$\mathrm{SINR}\left(Y_0; X_0\right) = \frac{H_0\, \ell\left(R_0\right)}{\sigma^2 + I}, \tag{3.1}$$

where $\ell(.)$ is the path loss function. The term $I$ is the signal power of the inter-cell interference, and can be expressed as

$$I = \sum_{Y_k \in \Phi \setminus \{Y_0\}} H_k \, \ell(R_k), \tag{3.2}$$

where $\{Y_k\}$ are BS locations modeled by an homogeneous PPP $\Phi$ of density $\lambda$, $Y_0$ is the serving BS under a given association strategy, $R_k = \|Y_k - X_0\|$ is the Euclidean distance between the BS $Y_k$ and the typical user $X_0$, and $\{H_k\}$ are the fading channel coefficients between the typical user and the BS $k$, and $\sigma^2$ is the noise power.

In the following, we investigate six approaches to characterize the interference to derive the coverage probability in PPP wireless networks.

### 3.2.1 Standard approach

The standard approach introduced in [2], consists in calculating the Laplace transform of the inter-cell interference at the typical user, conditioned on $R_0$ and then averaging over it. It is worth nothing that closed-form expression can only be computed for Rayleigh fading channels. Accordingly, for $H \sim \exp(1)$, the coverage probability in (2.33) is simplified as

$$\begin{aligned} \mathrm{P}_{\mathrm{cov}}(\theta) &= \mathbb{P}\left(H_0 \geq \theta \, \ell^{-1}(R_0)\,(\sigma^2 + I)\right) && (3.3)\\ &= \mathbb{E}_{R_0}\left[\mathbb{P}\left(H_0 \geq \theta \, \ell^{-1}(R_0)\,(\sigma^2 + I) \mid R_0\right)\right] && (3.4)\\ &\overset{(a)}{=} \mathbb{E}_{R_0}\left[\exp\left(-\theta \, \ell^{-1}(R_0)\,\sigma^2\right) \mathscr{L}_I\left(\theta \, \ell^{-1}(R_0)\right)\right], && (3.5) \end{aligned}$$

where (a) follows from the Laplace transform definition.

The expectation in (3.5) is expressed under the form $\mathbb{E}_{R_0}\left[\varphi(R_0)\right] = \int_0^\infty \varphi(x) f_{R_0}(x) \mathrm{d}x$, where the function $f_{R_0}(.)$ depends on the BS association scheme [68]. Typically, when considering the nearest-neighbor cell association [2, 57, 68], $f_{R_0}$ is the probability density function (PDF) of the random variable $R_0$, i.e., $f_{R_0}(r_0) = 2\pi r_0 \mathrm{e}^{-\pi\lambda r_0^2}$. However, if the maximum recieved SINR (max-SINR) association is considered, $f_{R_0}(r_0) = 2\pi\lambda r_0$ [38, 48]. Besides, the Laplace transform of the interference can be expressed via the PGFL theorem (2.29) as [2, 68]

$$\mathscr{L}_I\left(\theta \, \ell^{-1}(R_0)\right) = \exp\left(-\pi\lambda \, \mathbb{E}_H\left[\int_{\vartheta(R_0)}^{\infty} \left(1 - \exp\left(-H \frac{\theta \, \ell^{-1}(R_0)}{\ell^{-1}(u)}\right)\right) u \, \mathrm{d}u\right]\right), \tag{3.6}$$

where $\vartheta(.)$ determines the interfering exclusion boundary. Generally, $\vartheta(x) = x$ in the nearest-neighbor cell association, when interferers are not allowed to be closer to the typical user than the serving BS. There is no exclusion area for interferers in the max-SINR relationship and $\vartheta(x) = 0$.

Remarkably, (3.6) may be reduced further by changing variables, as in [69, (34)]. Considering Rayleigh fading channels, (3.6) is reduced as

$$\begin{aligned}\mathscr{L}_I\left(\theta\,\ell^{-1}(R_0)\right) &= \exp\left(-\pi\lambda\int_{\vartheta(R_0)}^{\infty}\left(1-\mathbb{E}_H\left[\exp\left(-H\frac{\theta\,\ell^{-1}(R_0)}{\ell^{-1}(u)}\right)\right]u\,\mathrm{d}u\right)\right)\\ &= \exp\left(-\pi\lambda\int_{\vartheta(R_0^2)}^{\infty}1-\frac{1}{1+\frac{\theta\,\ell^{-1}(R_0)}{\ell^{-1}(\sqrt{x})}}\mathrm{d}x\right)\\ &= \exp\left(-\pi\lambda\int_{\vartheta(R_0^2)}^{\infty}\frac{\mathrm{d}x}{1+\frac{\ell^{-1}(\sqrt{x})}{\theta\,\ell^{-1}(R_0)}}\right).\end{aligned} \tag{3.7}$$

Despite the Rayleigh assumption on the desired signal and interferers, coverage probability in (3.5) is commonly stated as an inappropriate integral that requires a two-fold numerical integration [2, Theorem 1]. In literature, certain attempts are made to obtain closed-form formulas or approximations of the coverage probability. In [2], for example, tractable formulations have been derived by assuming an interference-limited environment or a path loss exponent equal to 4. A somewhat more generalized closed-form equation has been provided in [70, 71], considering an integer value for the path loss exponent.

### 3.2.2 Relative distance process (RDP) approach

Given the assumption of

- the standard path loss model with path loss exponent $\alpha$,
- Rayleigh fading model for the channel,
- the nearest BS cell association strategy, and
- the interference-limited regime for the environment,

another method can be used to derive the coverage probability in (3.3) via the RDP of the PPP $\Phi$. A new PP $\Phi^{\mathscr{R}}$ is defined as [63]

$$\Phi^{\mathscr{R}} = \left\{\frac{R_0}{R_k}\middle| Y_k \in \Phi\setminus\{Y_0\}\right\} \subset [0,1], \tag{3.8}$$

where its density function is given based on (2.15), as [72]

$$\Lambda(\mathrm{d}r) = 2r^{-3}\,\mathrm{d}r. \tag{3.9}$$

where d$r$ is a 2-dimensional area element. The PGFL of the RDP can be represented as [72, Lemma 1]

$$G_{\Phi^{\mathscr{R}}}\{f\} = \frac{1}{1+2\int_0^1 \frac{1-f(r)}{r^3}\,\mathrm{d}r}. \tag{3.10}$$

Then (3.3) is obtained by $G_{\Phi^{\mathscr{R}}}$, as

$$\begin{aligned} \mathrm{P}_{\mathrm{cov}}(\theta) &= \mathbb{E}\left[\mathbb{P}(\mathrm{SIR} > \theta \mid \Phi)\right] && (3.11)\\ &= \mathbb{E}\left[\mathbb{P}\left(H_0 \geq \theta\, R_0^{\alpha} \sum_{Y_k \in \Phi\setminus\{Y_0\}} H_k\, R_k^{-\alpha} \mid \Phi\right)\right] && (3.12)\\ &= \mathbb{E}\left[\prod_{Y_k \in \Phi\setminus\{Y_0\}} \frac{1}{1+\theta\left(\frac{R_0}{R_k}\right)^{\alpha}}\right], && (3.13) \end{aligned}$$

we can directly apply the PGFL of the RDP and obtain

$$\mathrm{P}_{\mathrm{cov}}(\theta) = \frac{1}{1+2\int_0^1 \left(1-\frac{1}{1+\theta r^{\alpha}}\right) r^3\,\mathrm{d}r}. \tag{3.14}$$

The expression obtained in (3.14) is a particular case of the $k$-th moment, as

$$\begin{aligned} M_k(\theta) &= \mathbb{E}\left[\left(\mathbb{P}(\mathrm{SIR} > \theta \mid \Phi)\right)^k\right] && (3.15)\\ &\overset{(a)}{=} \int_0^1 k u^{k-1} \bar{F}(\theta, u)\mathrm{d}u, && (3.16) \end{aligned}$$

where (a) is the MD introduced in (2.40). It is important to note that $M_1(\theta)$ is the coverage probability defined in (2.33). Moreover, by repeating the steps from (3.11) to (3.14), the $k$-th moment $M_k(\theta)$ in (3.16) can be written in closed-form [73].

### 3.2.3 Factorial moment approach

In the case of the max-SINR association policy, the authors of [74, 75] defined the coverage probability of the typical user $X_0$, as the probability that the $k$-th weakest BS meets the SINR threshold $\theta$. If at least $k$ BS meet the necessary SINR target, the typical user is covered. Technically,

$$\mathrm{P}_{\mathrm{cov}}^{(k)}(\theta) = \mathbb{P}\left(\left[\sum_{Y\in\Phi} \mathbf{1}(\mathrm{SINR}(Y; X_0) > \theta)\right] \geq k\right). \tag{3.17}$$

Let us define by $n \geq 1$, the number of BS having an SINR higher than the threshold level. The authors then added a quantity of importance, the factorial moment measure

$S_n(\theta)$ of the SINR process, which is defined as the average number of ways that the typical user may be linked with $n$ different BS. Strictly speaking, it can be stated as

$$S_n(\theta) = \mathbb{E}\left[\sum_{Y_1,\ldots,Y_n\in\Phi}^{\neq} \mathbf{1}\left(\bigcap_{i=1}^{n}\left\{\mathrm{SINR}\left(Y_i;X_0\right)>\theta \mid Y_i\in\Phi\right\}\right)\right], \tag{3.18}$$

where $\sum^{\neq}$ indicates that the sum is taken over n-tuples of distinct points.

Remarkably, (3.17) may be reduced using the well-known inclusion-exclusion concept [74, 75], as shown below.

$$\mathrm{P}_{\mathrm{cov}}^{(k)}(\theta) = \sum_{n=k}^{\infty}(-1)^{n-k}\binom{n-1}{k-1}S_n(\theta). \tag{3.19}$$

The sum in (3.19) is actually finite since $n\theta/(1+\theta)$ needs to be lowered by 1 as demonstrated in [33, Proposition 6.2]. That is, (3.19) is simplified as

$$\mathrm{P}_{\mathrm{cov}}^{(k)}(\theta) = \sum_{n=k}^{\lceil 1/\theta\rceil}(-1)^{n-k}\binom{n-1}{k-1}S_n(\theta). \tag{3.20}$$

The calculation of the $k$-coverage probability in (3.20) necessitates a previous assessment of $S_n(\theta)$ for $n \geq k$, which may be obtained using higher-order Campbell's theorem as in [74, Theorem 6] [76, Theorem 7]. Although the factorial moment-based technique reflects numerous connectivity scenarios of the typical user, it offers less-tractable expressions of coverage probability.

### 3.2.4 Gil-Pelaez inversion approach

Another method to obtain the coverage probability under Rayleigh fading channel assumption is to use the Gil-Pelaez inversion theorem [77], which states that the cumulative distribution function (CDF) $F_X(.)$ of a random variable $X$ may be written based on the characteristic function $\Phi_X(\omega)$, as

$$F_X(x) = \frac{1}{2} - \frac{1}{\pi}\int_0^{\infty}\frac{\mathrm{Im}\left(e^{-j\omega x}\Phi_X(\omega)\right)}{\omega}\mathrm{d}\omega. \tag{3.21}$$

Relevant applications may be seen in [63, 69, 78, 79], where the coverage probability in (3.3) is recast as

$$\mathrm{P}_{\mathrm{cov}}(\theta) = \mathbb{E}_{R_0,H}\left[\mathbb{P}\left(I \leq \frac{H}{\theta\,\ell^{-1}(R_0)}\middle|R_0,H\right)\right] \tag{3.22}$$

$$= \frac{1}{2} - \frac{1}{\pi}\mathbb{E}_{R_0}\left[\int_0^{\infty}\mathrm{Im}\left(\Phi_H\left(\frac{-\omega}{\theta\,\ell^{-1}(R_0)}\right)\Phi_I(\omega)\right)\frac{\mathrm{d}\omega}{\omega}\right], \tag{3.23}$$

where the characteristic function of the interference $I$ may be calculated as

$$\Phi_I(\omega) = \exp\left(-2\pi\lambda \int_{\vartheta(R_0)}^{\infty} \left[1 - \mathbb{E}_H\left[\exp\left(\frac{j\omega H}{\ell(u)}\right)\right]\right] u \, \mathrm{d}u\right), \tag{3.24}$$

such that $\vartheta(.)$ is the exclusion bound relative to the association technique. Interestingly, the Gil-Pelaez approach may also be used to invert the $jw$-moment of the conditional success probability in order to extract traffic metrics such as mean delay and peak edge of information [80, 81].

### 3.2.5 Laplace transform inversion approach

The PDF of a random variable $X$ can be calculated using the Fourier inversion theorem. The Fourier inversion theorem is also known as the Laplace transform inversion [46, 82], the characteristic function inversion [83], or even the moment generating function (MGF) inversion [84]. Formally, the PDF $f_X(.)$ of $X$ is derived by the Bromwich contour inversion integral [46], as

$$f_X(y) = \mathscr{L}^{-1}\{\mathscr{L}_X(s)\}(y) = \frac{1}{2\pi j} \int_{\gamma - j\infty}^{\gamma + j\infty} \mathscr{L}_X(s) \mathrm{e}^{ys} \, \mathrm{d}s, \tag{3.25}$$

where $\gamma$ is a real constant. As for the CDF of $X$, it can be derived equivalently as

$$F_X(x) = \int_0^x f_X(y) \mathrm{d}y = \mathscr{L}^{-1}\left\{\frac{\mathscr{L}_X(s)}{s}\right\}(x). \tag{3.26}$$

The coverage probability in (3.22), simplifies then as

$$\mathrm{P}_{\mathrm{cov}}(\theta) = \mathbb{E}_{R_0,H}\left[\mathscr{L}^{-1}\left\{\frac{\mathscr{L}_I(s)}{s}\right\}\left(\frac{H}{\theta\,\ell^{-1}(R_0)}\right)\right]. \tag{3.27}$$

This approach, like above inversion approaches, yields accurate expressions of coverage probability under generalized fading distributions, but it has limited design insights [76]. A more flexible alternative is to use characteristic function inversion to eliminate contour integration, as presented in [83].

### 3.2.6 Interference approximation approach

Approximating the interference distribution is another approach to obtain the coverage probability without using less tractable inversion techniques [18]. One may find two methods in literature.

- The first is to assess the interference impact from only a subset of transmitters depending on the association policy. When adopting the max-SINR association

criterion [41], for example, when the $k$ strongest interferers are considered. In contrast, in [85], the $k$-nearest interferers are deemed and in [86], the $n$-th nearest neighbor association strategy is considered. This method allows one to calculate an upper bound of coverage probability, where bound accuracy rises when path loss exponent increases. This allows to neglects the contribution of distant interferers [18].

- Second, the distribution of interference can be approximated by a known distribution whose parameters are estimated to match the empirical distribution. The authors of [87] demonstrated that the interference behavior could be represented by the $\alpha$-stable distribution family, and the authors in [88], approximate the true interference distribution with the gamma distribution.

We summarized six commonly used techniques to find the coverage probability reported in literature. These techniques have various degrees of mathematical tractability and approximation accuracy. For example, the factorial moment technique gives a mathematical expression to tackle various user-BS association strategies, but it offers less tractability. It is because the computation of $S_n(\theta)$ needs to apply higher-order Campbell's theorem. Furthermore, regardless of the fading model, the Gil-Pelaez inversion approach allows finding an exact expression for coverage probability. In this thesis, we follow the standard approach, the most popular one applied in the literature, to derive the coverage probability. Using standard approach, we can derive tractable expressions in particular scenarios of our non-full interference framework.

## 3.3 Network deployment

Several network attributes can be included in the model of deployment in order to account realistic characteristics of real networks:

1. Network elements based on a deterministic or random model, node type (transmitter, receiver, or both).

2. Their attributes, such as transmit power and antenna types.

3. The environmental properties such as propagation effects.

4. Node interaction properties, such as association strategy, coordination.

This section will look at the many modeling options made in literature of SG-based modeling and analysis.

### 3.3.1 Base station deployment

Practical BS deployments typically exhibit a growing propensity towards spatial aggregation and clustering in user hotspots (e.g., events, urban areas) and a growing trend into repulsion and regularity where users are homogeneously distributed [88–90]. A cellular network's SINR has a direct correlation with the spatial distribution of its base stations. Capturing the topology of this type of node through an appropriate PP will directly impact the validity of the performance prediction [38, 89, 91–94]. The Poisson point method is widely employed to analyze the SINR of mobile networks [91, 95–97]. As all points in a Poisson process are independent, there is no interaction between them.

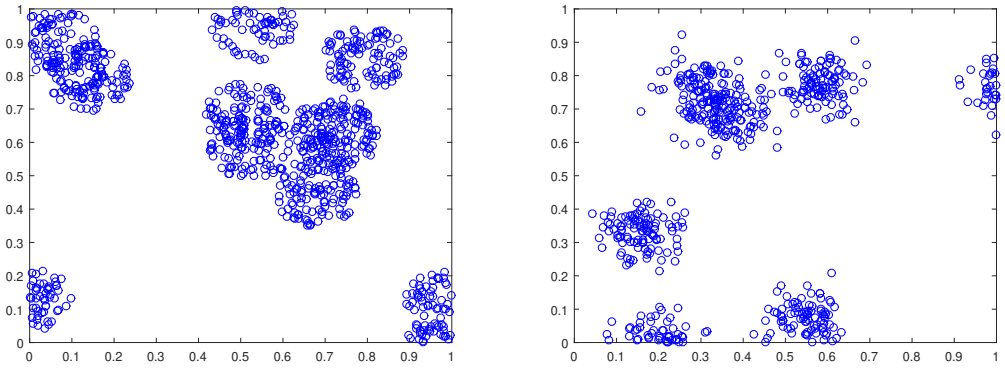

(a) (b)

Figure 3.1 – Realization of (a) MCP, (b) TCP.

In the following, we will review the other PP processes used in literature to model the location of nodes with interactions and outline the key methods used to deal with them.

1. Aggregative point processes

   In realistic wireless networks, BS tend to be placed in clusters in highly populated areas. Aggregative PP are necessary in such cases for a correct evaluation of system performance. The notable aggregative PP utilized in literature are reviewed briefly.

   - Cox process
     The Cox process stands as an Inhomogeneous PPP (IPPP) with a random intensity measure, which is deemed doubly stochastic. Its structure has two levels. First, create a general PP $\Phi^p$ as parent points. Second, conditioned on a configuration $\Phi^p$, a PPP $\Phi^d$ with density $\lambda$ is generated as

daughter points. On the other words, it first consider a non-negative random measure, called a driving measure. A Poisson point process, which is independent of the random driving measure, is then generated with a random intensity measure. For instance, the Cox PP is studied in vehicular networks [86], where a doubly stochastic process helps achieve the unpredictability of roadways and the randomness of node positions.

- Poisson cluster process (PCP)
  Contrarily to the Cox PP, where $\phi^p$ follows a general PP and $\Phi^d$ is a PPP, in the PCP, the number of parent points follows a PPP, and the number of daughter points follows a general PP. In particular cases, the PCP yields the family of the Neyman-Scott PP namely Matérn cluster processes (MCP). In the latter, the points in $\Phi^d$ are i.i.d. in a ball centered at each parent point. PCP also leads to Thomas cluster processes (TCP), in which the points in $\Phi^d$ are distributed according to a symmetric normal distribution with a variance. In related literature, empirical data of modern shared networks was examined using PP from the MCP and TCP [98], and Fig. 3.1 illustrates a realization of both.

2. Repulsive point process
   In this kind of processes, some locations are forbidden in order to impose regularity in the distribution of the points over the space. Matérn hard-core point process (MHPP) is a significant variant of hard-core PP, where there are no points at a distance less than a particular threshold. Remarkably, MHPP is used in literature to assess the minimum safe distance between cars in vehicular ad hoc networks [99]. The study in [100] focuses more on theoretical aspects of the MHPP. Fig. 3.2 represents a realization of MHPP (Type-I and Type-II).

   - Determinantal point processes (DPP)
     DPP is an example of a soft-core repulsive point process. A DPP acting with kernel $K : B^2 \to \mathbb{C}$, is a PP $\Phi$ described over a given Borel $B$ and its $n$-th joint intensity is expressed as

     $$\varrho^{(n)}(X_1, \ldots, X_n) = \det\left(K\left(X_i, X_j\right)\right)_{1 \le i,j \le n}, \forall (X_1, \ldots, X_n) \in B^n, \qquad (3.28)$$

     where $\det(\cdot)$ is the determinant function.

     The kernel function $K(X, Y)$ is a continuous, Hermitian, locally square-integrable, and non-negative definite function. The DPP's repulsiveness derives from the observation that the determinant of a kernel matrix cannot be higher than the product of its eigenvalues [101] and then $\varrho^{(n)}(X_1, \ldots, X_n) \le \prod_{i=1}^{n} \varrho^{(1)}(X_i)$, where equality prevails in a PPP. Concentrating on DPP de-

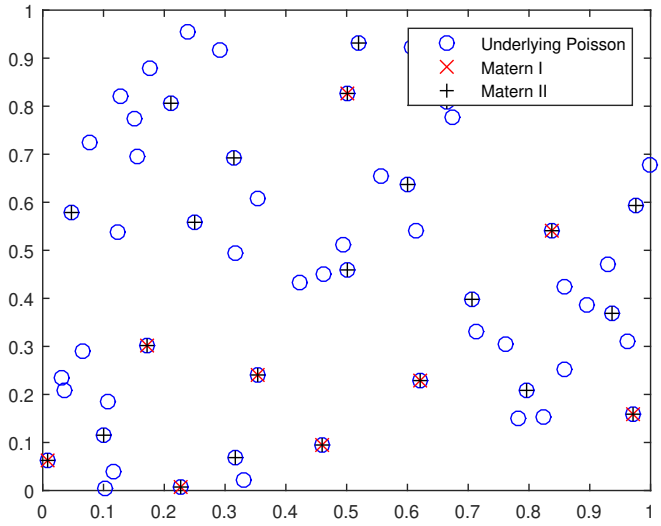


Figure 3.2 – Realization of MHPP (Type-I and Type-II).

fined on the Euclidean plane $\mathbb{R}^2$, the generalized contact distance distribution for DPP is as follows:

$$F_y(R) = \sum_{n=1}^{+\infty} \frac{(-1)^{n-1}}{n!} \int_{(b(0,R))^n} \det\left(K\left(x_i, x_j\right)\right)_{1\leq i,j\leq n} dx_1 \ldots dx_n, \qquad (3.29)$$

where $\mathrm{F}_y(.)$ is a kernel-dependent function. DPP is divided into several types with various degrees of repulsiveness and tractability. For instance, it is a Gauss DPP if for every $X, Y \in \mathbb{R}^2, K(X,Y) = \lambda \exp\left(-\|X-Y\|^2/\gamma^2\right)$, where $\lambda$ is the density of the Gauss DPP and $\gamma$ is a parameter for modifying the DPP's repulsiveness, such as $\pi\lambda\gamma^2 \leq 1$ for the condition of existence. The Cauchy DPP is obtained for $K(X,Y) = \lambda/\left(1+\|X-Y\|^2/\gamma^2\right)^{m+1}$ with a condition of existence such that $\pi\lambda\gamma^2 \leq m$, where $\lambda$ is the spatial intensity of the process and $\alpha$ and $m$, are shape parameters that can be used to fine-tuned repulsiveness. Another type of motion-invariant DPP is introduced for more tractability and mathematical simplicity, namely the scaled Ginibre PP ($\beta$-GPP), by considering a kernel as $K(X,Y) = c\pi^{-1}\mathrm{e}^{-\frac{c}{2\beta}\left(|X|^2+|Y|^2\right)}\mathrm{e}^{\frac{c}{\beta}X\ Y}$, where the resulting density $\lambda$ is scaling with $c$ as $\lambda = c/\pi$ and $\beta$ can change the repulsion intensity [102]. Authors in [56] showed that a $\beta$-GPP, whose parameters have been correctly chosen, has better fit to a real BS deployment compared Gauss DPP and Cauchy DPP. However, $\beta$-GPP is less tractable than Gauss DPP and Cauchy DPP.

- Lattice point process

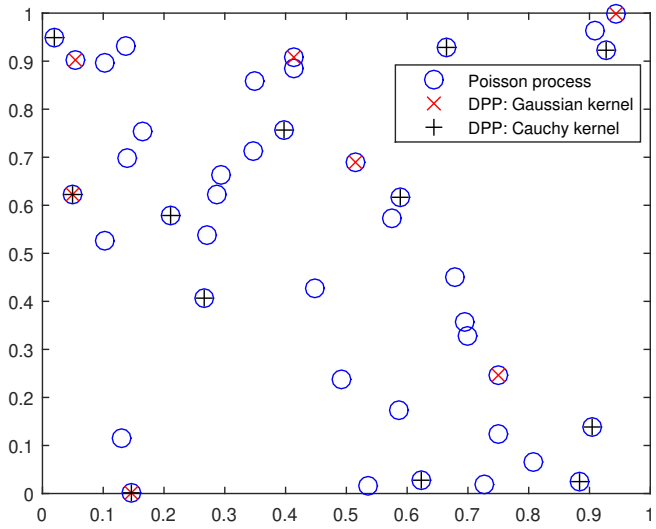


Figure 3.3 – A simulation of DPP (Gaussian and Cauchy kernel) underlying a realization of PPP.

The actual regular square lattice point process may be readily created by deploying points uniformly with a set spacing between nearby points [46]. A regular stationary lattice in $\mathbb{R}^2$ can be represented as follows:

$$\Phi^{Lattice} = \{cG + U; c \in \mathbb{Z}\}, \tag{3.30}$$

where $G$ is the grid's generator matrix, and to guarantee lattice stationarity, $U$ is an uniformly distributed random vector across the Voronoi cell of the origin. The contact distance distribution is calculated as follows [103]

$$F_{\mathrm{y}}(R) = \begin{cases} \frac{\pi R^2}{D^2} & R < D/2 \\ \frac{R}{D^2}\left(\pi R + 2D\sqrt{1-\frac{D^2}{4R^2}} - 4R\,\mathrm{ArcCos}\left(\frac{D}{2R}\right)\right) & D/2 \le R < \frac{\sqrt{2}}{2}D, \\ 1 & \frac{\sqrt{2}}{2}D \le R \end{cases} \tag{3.31}$$

where D is the distance between two points in the Lattice PP.

It's true that non-PPP models can represent the geometry of real networks with nodes that are negatively correlated, such as spatial inhibition or repulsion or positively correlated, such as spatial aggregation and clustering. In this way, since the received SINR is directly influenced by the degree of interaction between nodes,

capturing the geometrical relationships between nodes through a PP will directly influence the mathematical complexity of network performance evaluation. This thesis aims to employ PPP model which is a widely used model in the relevant literature and also provide tractable mathematical solutions for the network performance metrics.

### 3.3.2 Load modeling

For the study of downlink cellular networks, it is important to consider the user point process. This section briefly reviews two popular models encountered in literature.

1. Type-I model

   The Type-I user distribution model considers one user uniformly distributed in each cell. It is the most famous and frequently used model in literature to represent the distribution of user per RB [104]. This model is appropriate for a fully loaded network where each cell has an active user in each RB. Its model relies only on a single point process.

   Nevertheless, fully-loaded BS are not always accurate in practice, as user movement may introduce random features that impact BS performance [104].

2. Type-II model

   Consider that the spatial distribution of BS follows a PPP with the density $\lambda_1$, over which users are scattered according to another PPP with the density $\lambda_2$. The nearest BS serves each user. In this model, only one user is scheduled per RB. In other words, if there are multiple users in the Voronoi cell of a BS, then the BS can serve only one of them in the RB. Some BS may not have any user in their Voronoi cells at any given time. The authors suggest a novel model in [105, (12)], to estimate the PDF of the size of a typical Voronoi cell $Z$,

   $$f_Z(z) = \frac{3.5^{3.5}}{\Gamma(3.5)} z^{2.5} \exp(-3.5z). \tag{3.32}$$

   This distribution function is an approximation based on curve fitting, it is undoubtedly less accurate than a more complex three-parameter fit proposed in [105]. However, this model gains in tractability what it looses in accuracy and hence keeps a practical interest in performance analysis.

   In this case, the random positioning of active BS follows a thinned version of the original PPP of BS with the thinning parameter given as [106]:

   $$p_{\text{active}} = 1 - \left(1 + 3.5^{-1} \frac{\lambda_2}{\lambda_1}\right)^{-3.5}. \tag{3.33}$$

This concept is used in a variety of circumstances. In [107], the optimal proportion of traffic offloaded to maximize the coverage in SINR is not always the same as the optimal proportion of traffic offloaded to maximize the coverage in rate. In [108], using this model, a tractable model for rate in self-backhauled millimeter wave cellular networks is provided.

In this thesis, we employ Type-I load model and assume that all BS have users to serve in their cells. However, unlike the relevant literature that assume full interference condition in case of Type-I model, we correlate the activity of BS to their coverage regions.

### 3.3.3 Propagation model

Communication in a wireless network consisting of many spatially dispersed nodes is typically hampered by various wireless propagation effects such as:

1. The degradation of transmitted signals with blockages (shadowing).
2. Receiving duplicates of the same transmitted signal (multipath fading).
3. Signal losses with distance (path loss).

In terms of path loss functions, the vast majority of works consider the simple single slope unbounded path loss model because of its ability to derive reliable and tractable results [38]. The standard (power-law) path loss function is defined as [2]

$$\ell(r) = r^{-\alpha}, \tag{3.34}$$

where $\alpha$ is the path loss exponent.

Even though the standard path loss model does not correctly reflect the dependency of the path loss exponent on link distance in many critical cases, it provides the framework for modern cellular network theory, analysis, simulation, and design.

In addition to the distance-dependent path-loss degradation, each connection experiences independent and rapidly changing channel fading, indicated by $H$. It is assumed to have an exponential distribution (i.e., Rayleigh fading channel) with a mean square value of $\mu$. The PDF of $H$ is

$$f_H(h) = \frac{1}{\mu}\exp(-\frac{h}{\mu}). \tag{3.35}$$

The propagation channels associated with network are considered independent and identically distributed (i.i.d.) throughout this thesis. If we examine a typical link, the received signal by the typical user from its serving BS is

$$S_0 = H_0 R_0^{-\alpha}, \tag{3.36}$$

where $H_0$ and $R_0$ are the fading channel and the distance between the typical user and its serving BS, respectively. We use this channel model throughout of this thesis.

### 3.3.4 Cell association

In downlink cellular network where BS send data with the same transmit power, users are associated with their spatially nearest BS without taking channel effects into account, which is known as the nearest-neighbour cell association [2, 3, 48, 68]. An extended version of it is the $n$-th nearest BS association policy [3, 27, 39, 40, 46, 109, 110]. When channel effects are taken into account, interferers may be closer to the typical user than the serving BS. That is, we must consider the channel effect $H$, which causes the typical user to connect to the strongest BS instantly, i.e., the maximum instantaneous power-based cell selection, or equivalently the max-SINR association strategy [38, 48, 83, 111]. The max-SINR association strategy can be expressed as

$$Y_0 = \arg\max_{Y \in \Phi} H_0 \ell(\|Y - X_0\|), \tag{3.37}$$

where the typical user $X_0$ selects the serving BS $Y$ as that providing the maximum instantaneous power.

## 3.4 Non-full interference model

In cellular networks, quantifying co-channel interference among base stations is crucial for providing an analytical framework using stochastic geometry. In downlink, the non-full interference terminology refers to the case where all BS do not contribute to the interference received by a user in a given bandwidth. In literature, if there is no user in a cell, the BS of the cell is inactive [11]. Under this scenario, the work in [106] approximated the interference as a thinned version of the original PPP of BS.

In a conventional full interference network, all BS transmit in the same frequency resource, i.e., full frequency reuse, and hence users near to the cell boundary are known to experience a low SINR [13]. However, in a non-full interference network, locating close to the cell edge does not necessarily lead to significant performance degradation because all BS are not active in the same resource [11]. In [11], the authors proposed a new definition for the cell edge users in small cell deployments based on the nearest active base stations (non-empty cells) to evaluate the user performance degradation in practice. The work in [11] employed a type-II user distribution to model a non-full interference network. However, considering the full load model (type-I user distribution model), it is still possible to have a non-full interference setting by applying user classification and interference coordination approach, that will be the topic of chapter 4 and 5.

## 3.5 User classification

In cellular networks, the quality of service (QoS) depends on the relative signal strength received from the serving BS and all other interfering BS through the so-called SIR, which in turn depends on the network geometry and channel conditions. In a conventional full interference network, users near to the cell boundary are known to experience a low SIR. Users placed near to the serving BS experience modest path-loss attenuation, and the received signal strength from its serving BS is substantially greater than the received interference. In contrast, users who are farther from their serving BS get reduced signal power from their associated BS compared to the detected interference, resulting in much worse performance. As a result of these considerations, each cell in such a large-scale configuration may be split into two sub-regions: cell center and edge regions. CCU are positioned in the cell center region, whereas CEU are users placed in the cell edge region. Then, by utilizing fair spectrum allocation among CCU and CEU, the interference seen by the users may be reduced, resulting in enhanced network performance.

The classification of users has been explored in numerous studies [1, 112–114] in grid or PPP-based cellular networks. Authors in [112] explored the categorization of users by utilizing fractional frequency reuse (FFR) [1]. However, the approach described in [112] is only applicable to a grid-based cellular network. Authors in [113] expanded the approach to stochastic-based two-tier heterogeneous networks (HetNets) by employing an SINR threshold for user classification. Given that the SINR-based approach leads a user to often move between CCU and CEU, the distances ratio-based method was presented in [114] for heterogeneous cellular networks based on separate PPP. In the open literature, user classification schemes mainly focus on distance-based [11, 16, 114–117], and SIR based classification [1, 118]. However, since all BS are active in the classical full interference scenario, both aspects lead to similar conclusions on average, and a user located at the cell border undergoes severe performance degradation. However, this ignores the correlation in the BS activity, which is a function of the randomly selected user location in the cell in the scheduled resource.

For instance, in [114–116], the ratio of the distance between the typical user and the serving BS to the distance between the typical user to the nearest interfering BS is computed. If the ratio is larger than a threshold, the user is a CEU; otherwise, it is a CCU. Authors in [116] studied a MD of the CCU/CEU under orthogonal and non-orthogonal multiple access. A similar approach for classifying users is also used at 3GPP to analyze the performance of schemes such as SFR [119]. Inspired by this, base station cooperation techniques have been investigated to enhance the CEU's coverage [11, 16, 117]. However, this approach for incorporating a user as a CCU/CEU is not proper for the next-generation cellular networks because of neglecting the effects of fading channel and inter-cell interference seen by the users, which can make them

experience low coverage performance even in the cell center area [120]. The SIR ratio is a more suitable way of classifying the users [1, 118]. In [1], the entire frequency band has been split into CCU/CEU frequency sub-bands using spectrum access strategies such as fractional and soft frequency reuse to increase the CEU's coverage. In [118], the authors used the instantaneous SINR to classify users and got an approximation of the coverage probability of the typical CEU for a PPP-modeled 3-tier heterogeneous network. However, these approaches apply full interference assumption and do not consider the correlation in the computation of received SIR by users. However, these approaches did not take into account the correlation of the signal and interference in the calculation of received SINR by a user which is considered in this thesis.

## 3.6 Interference management

Coordination of radio resource management is a viable approach for improving the performance of a CEU who encounters high inter-cell interference [19, 20], and hence does not meet QoS requirements such as coverage probability and SE. Because of the randomness of BS and user locations the performance of ICIC is dependent on the network deployment. Despite the relevance of spatial distribution of CEU with ICIC for performance improvement, some publications evaluating ICIC have not taken spatial distribution of CEU into account [21, 22]. Since 3GPP release 8, inter-cell interference has been identified as the primary bottleneck, and many techniques to manage inter-cell interference have been developed. The decrease in performance induced by inter-cell interference is most evident when a user is a CEU. To offer adequate QoS to CEU, ICIC controls the radio resources of neighboring BS and therefore enhances edge user performance [19, 20].

ICIC is classified into two kinds.

- The first is cell-centric ICIC. The resource management in cell-centric ICIC is handled by a pre-designed fixed frequency reuse scheme. These methods have the benefit of being simpler and requiring less signaling overhead. Nevertheless, it is not suited for dense environments since dealing with the changes of user locations and channel variations are challenging in cell-centric ICIC.

- The second one is user-centric ICIC. Contrarily to cell-centric, in user-centric ICIC, resource management is coordinated based on known user locations via multi-cell interaction. This is more sophisticated and requires more signaling overhead than cell-centric ICIC, but it is appropriate for the future generation of networks since it can handle the dynamism of user locations effectively, and there are many ongoing initiatives to eliminate signaling overhead in 5G networks [22], [23].

This section will review some of the several inter-cell interference coordination strategies used to manage radio resources. Fig. 3.4 represents a taxonomy of interference management.

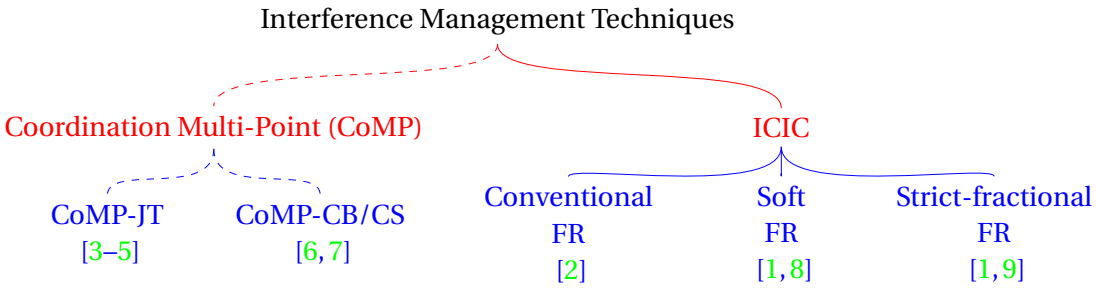


Figure 3.4 – Taxonomy of interference management

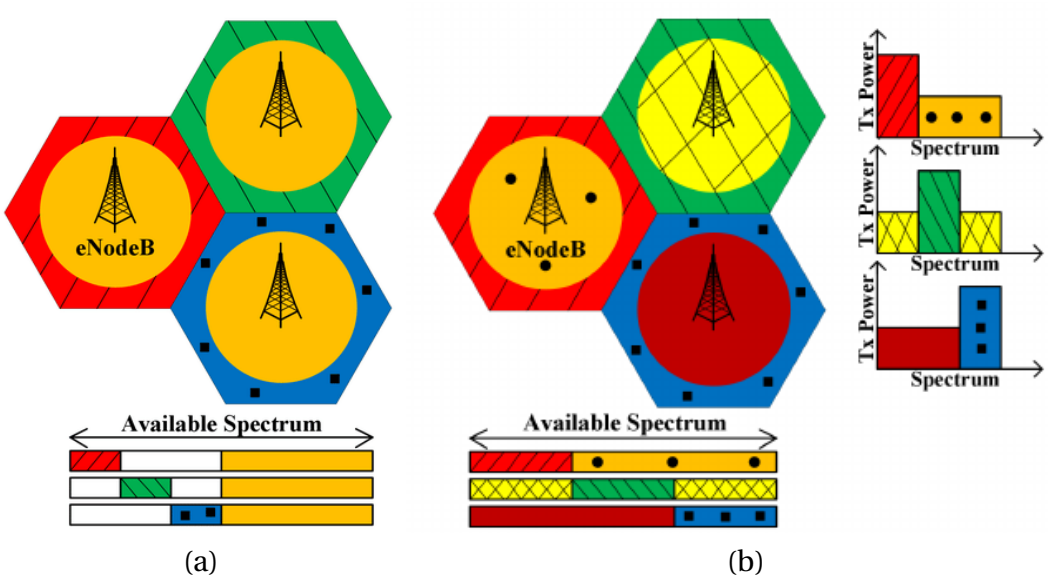


Figure 3.5 – (a) Strict-FFR technique, (b) SFR technique [1].

### 3.6.1 Frequency reuse

Interference coordination methods based on frequency reuse have been widely proposed to reduce interference between neighboring cells and enhance bandwidth efficiency. The reuse factor in the traditional frequency reuse approach controls the number of distinct frequency bands used by the network, where only one band is used per cell, and reused from one cell to another according to the level of interference

we accept to support. In [1], authors provide an analytical framework to evaluate the effect of strict-FFR and soft frequency reuse (SFR) on downlink by determining the coverage probability and the average rate in the cellular system. The whole available spectrum is split into two divisions in strict-FFR to serve CCU and CEU. The BS operates with a frequency reuse of 1 in the bandwidth allocated for CCU, justified by the concept that the strong signal from the chosen BS can deal with inter-cell interference received from all the other BS. The BS employs the standard frequency reuse with a reuse factor (>1) in the second partition. In this case, CEU receive less interference because each BS transmits in only one subband, and adjacent BS do not send signals in the same subbands. This results in higher SINR and more coverage for CEU, but at the price of less efficient spectrum utilization [1]. In SFR scenario, the BS interacts with the CEU in the same way as in the strict-FFR method; however, the BS transmits with lower power in the unused subbands, extending coverage to CCU. Because of the lower transmit power, the BS of neighbouring cells cause less interference to CEU in this technique. This method is more economical in terms of bandwidth than strict-FFR, but it falls short in delivering coverage to CEU [22]. Fig. 3.5 depicts a cluster of three LTE cells where a spectrum is allocated between cell center and cell edge regions using the FFR techniques. By combining frequency reuse with SG, the authors found the performance of FFR where co-channel interference is thinned by a factor of frequency reuse from original PPP in [1]. This approach allows them to calculate the average performance of frequency reuse in randomly deployed networks.

| Mode | Metric | BS set |
|---|---|---|
| NC-JT | Coverage | Different tiers closest BS [3, 121] |
| | Rate | Number-based/Distance-based cooperation [122] |
| | Coverage, rate | Channel-dependent cooperation activation [5] |
| C-JT | Coverage | N BS with the strongest average received power [123] |
| | SE | Constant-distance / Fixed-power-difference [124] |
| | Coverage, SE | Optimal/Random point selection [125] |
| BS silencing | Coverage, rate | Fixed cluster structures [126–128] |
| CB/CS | Coverage | Second nearest BS [129] |
| | Coverage, rate | Intracell diversity (Sending massage in M RB) [130] |
| | Coverage, rate | Cluster of BS [131] |
| SIC | Coverage | Strongest interferer [132] |
| Cell-free | SE | All access points [133] |

Table 3.1 – Taxonomy of SG-based CoMP schemes.

### 3.6.2 Coordinated Multipoint (CoMP)

CoMP is being developed in the LTE-A network as part of an effort to minimize interference, enhance data rate coverage, boost CEU throughput, and overall system throughput [134]. The main idea behind CoMP is to move away from the traditional single-tier multi-user system structure and toward a multi-tier multi-user design. Data and channel state information are exchanged across neighboring cellular BS in CoMP to synchronize their downlink transmissions and collaboratively process the received signals in the uplink. CoMP approaches successfully change destructive inter-cell interference into positive signals, allowing for large power gain, channel rank advantage, and/or diversity advantages to be utilized. CoMP needs a high-speed backhaul system for data exchange between the BS. This is often accomplished through the use of an optical fiber fronthaul [3].

Coordination scheduling/beamforming (CS/CB) and cooperative processing are two essential CoMP techniques discussed. Data for a user is only available in the CoMP cooperation set in a time-frequency RB in the CS/CB strategy. On the other hand, under the joint processing approach, data for a user is available at more than one point in the CoMP cooperating set. The combined processing method outperforms the CS/CB, albeit at the expense of increased backhaul load. There are two primary implementation strategies for the joint processing strategy: joint transmission (JT) and dynamic point selection/silencing [125].

BS JT can be classified as non-coherent joint transmission (NC-JT) [3, 121] or coherent joint transmission (C-JT) [123] depending on whether the channel state information (CSI) between the cooperative BS and the given user is accessible. The cooperative BS communicate data to the user concurrently in NC-JT without previous phase mismatch correction or strict synchronization. On the other hand, the concept of successive interference cancellation (SIC) is to decode the signals in a specific order and sequentially remove the decoded signals from the aggregate received signal. Full-duplex technology and non-orthogonal frequency division multiplexing (NOMA) are two promising solutions to improve the capacity of the 5G system [132]. Using Full-duplex technology, wireless networks will be able to simultaneously transmit and receive wireless signals over a single spectrum channel. NOMA transmissions employ superposition coding at the transmitter, which allows the SIC receiver to distinguish users both in uplink and downlink channels. Fig. 3.1 reviews a taxonomy of SG-based CoMP schemes. Furthermore, Fig. 3.6 presents a related literature on CoMP. The analysis of the performance enhancement of a typical user based on BS cooperation in cellular networks using stochastic geometry has been investigated in several works [3, 129]. In [11], a semi-closed form expression for the typical edge user's coverage probability has been obtained. It assumed that each BS serving a cell center user and placed within the so-called cooperation radius from an edge user cooperates and does not transmit any signal at the tagged time slot. A user-centric BS cooperation scheme

with the joint transmission has been analyzed in [16], where users are grouped by their relative received signal strengths to the three strongest BS. The typical edge user's performance in mmWave cellular networks under two cooperative schemes, namely fixed-number BS cooperation scheme and fixed-region BS cooperation scheme, has been investigated in [117]. A Poisson-Delaunay triangulation-based BS cooperation approach has been proposed to improve cell edge users' performance in cellular networks in [125]. In [120], the authors proposed a hybrid cooperation scheme for sub-6 GHz/millimeter wave cellular networks where an edge user independently chooses its mode of operation with or without cooperation. The follow-up works applied the BS cooperation at the typical link, representing all links' average performance in a snapshot of the network under a full interference scenario. The main disadvantage of these works is that all BS participating in cooperation should sacrify their scheduled user in their cells by postponing them to the next round of transmissions that may increase traffic load in the network.

In contrast, in the non-full interference network presented in this work, each BS is allowed to transmit a signal to its served user in the assigned fraction of the scheduled RB, and it is off in the remaining subchannels of the RB. In this scenario, an edge user can send it's cooperation request to BS who serve different user types. In this chapter, a cooperation technique, named optimal point selection, is applied to improve the cell edge user's performance under the non-full interference model. In OPS technique, data is concurrently available at multiple BS; only one BS out of the BS cooperation set sends data to a user [135, 136]. This means that the model aims at improving the performance of the cell edge user without jeopardizing other scheduled users in the same RB and without raising the interference level in the network. It is the opposite of the conventional approach in BS cooperation that focuses on a typical user and drops connected users in other cells to help the tagged typical user [11]. This thesis focuses on improving QoS of cell edge users in the non-full interference framework by employing optimal point selection approach where in a set of cooperative BS, only the BS that has the highest channel quality (the product of the high path loss and small fading) is chosen to serve the target user.

### 3.6.3 Radio resource management (RRM)

RRM functions in cellular networks deal with the sharing of spectrum between base stations (macrocells and small cells), resource allocation, link adaptation, handover management, and admission control. Adaptive Modulation and Coding and transmission power management are used to achieve the link adaptability function. These capabilities, including resource partitioning across cells, user scheduling, and transmission power regulation, are utilized to mitigate the impact of interference on system performance [19].

Cellular network still has many challenges that must be addressed to increase

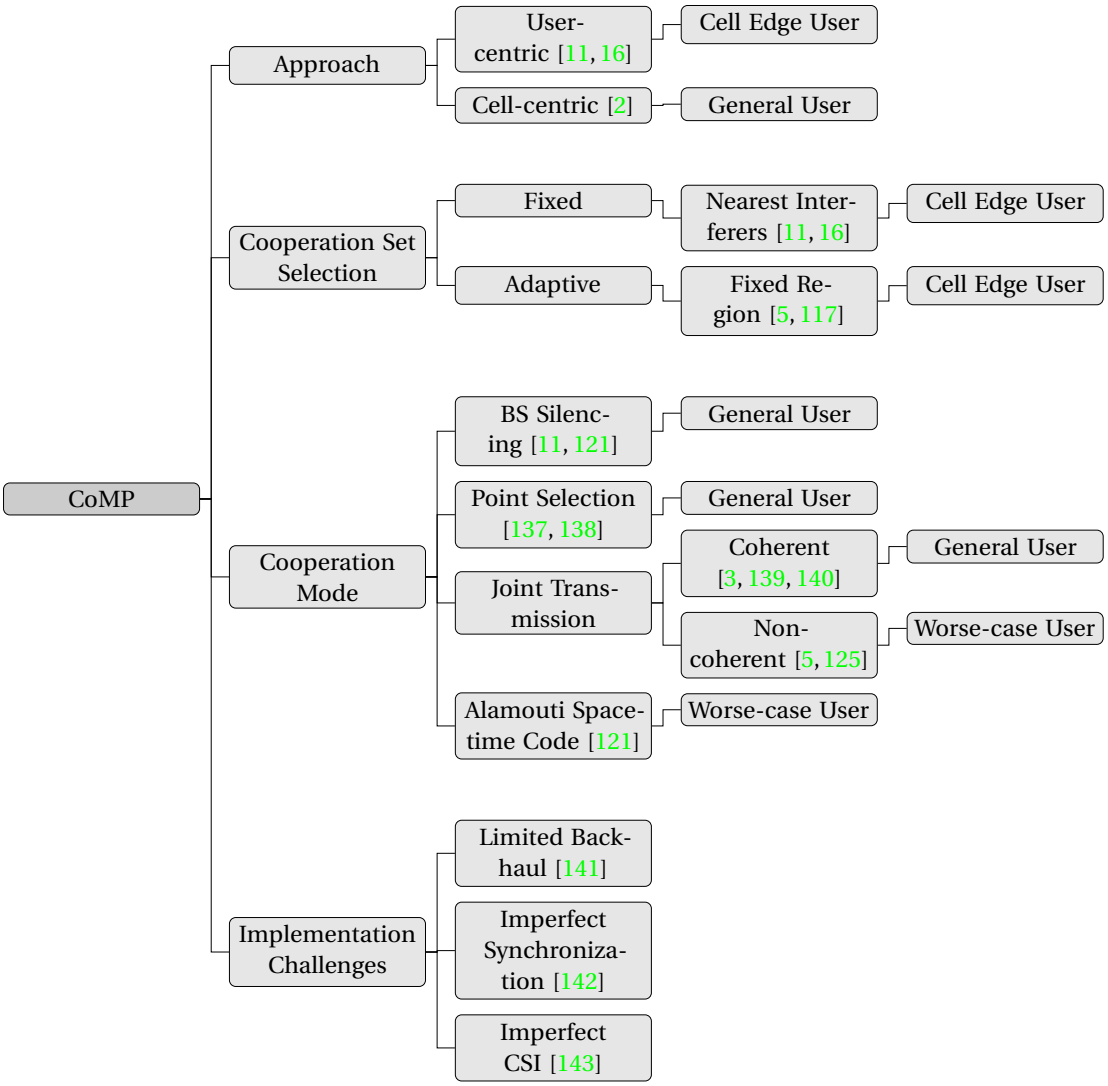


Figure 3.6 – Related literature on CoMP.

capacity in order to meet the rising demand for data rate by users. A scheduler assigns resource units, known as RB, to users. An RB is defined as in OFDMA, and is made of a set of orthogonal subcarriers and a number of OFDM symbols. Inter-cell interference occurs when users in separate cells utilize the same RB. If these BS are close together, the situation gets more intense. A static RB assignment, in which different resources are assigned to cells, may lower the interference level.

Alternatively, assignments for a fixed number of neighbour cells can be centralized to improve spatial utilization of resources and tailor RB assignments to the load in each cell. The scheduler that handles RB assignments increases the frequency reuse factor by allocating the same RB to different users to enhance capacity. Authors in [19, 144] presented assignment techniques conducted at the scheduler to minimize global interference. These techniques are validated using simulations for various conditions. However, understanding the effect of different assignment systems on a larger scale and in more usual scenarios is a significant challenge. Various SG-based designs have been suggested in related literature [22, 82, 106]. Studies in [22, 82, 106] offered spatial and tractable models for interference computing that consider traffic demand. Furthermore, these models imply that a homogeneous point process represents users. Therefore the load associated with a cell is proportional to its size (the greatest cell having the highest load).

RRM includes several technological challenges and issues in interference avoidance, radio resource utilization, fairness, QoS, and RRM complexity [145].

- Radio resource utilization
  Given existing challenges like restricted spectrum availability and poor spectrum usage, efficient radio resource usage is critical for reaching such high peak data rates. A full frequency reuse factor of one appears to be the most effective solution for meeting SE performance goals. However, this introduces a tradeoff between radio resource utilization efficiency and interference management. As a result, an RRM scheme must be constructed to minimize interference and maximize spectral efficiency [146].

- QoS management
  One of the primary goals of RRM is to improve QoS. QoS management becomes more complicated in heterogeneous networks with many cells since each cell may have limited frequency resources available to serve users. As a result, meeting each user's QoS requirements necessitates a more complex RRM solution that considers interference and limited radio resources [145].

- Fairness
  In many wireless networks, fairness is a key aspect of RRM. The conventional fairness problem in RRM is linked to packet scheduling among users, where each user should get an equitable share of radio resources for wireless access.

Fairness is extended and defined in heterogeneous networks as the fairness of resource distribution among cells. In other words, radio resources are assigned so that each cell's resource need is entirely met. The allocation of radio resources, on the other hand, is considered to be max-min fair if it maximizes the lowest attainable rate among users. In other words, users with low channel quality will receive more radio resources, while those with high channel quality will get fewer radio resources. A performance indicator known as Jain's fairness index has been used to assess fairness [147].

- Implementation and computational complexity
  There are two kinds of complexity, computational complexity and implementation complexity. Implementation complexity refers to the amount of signalling overhead and information sharing between BS. The computational complexity of an RRM scheme, on the other hand, relates to the processing time required by the RRM scheme to run specific algorithms at the BS. The requirement for a combined consideration of both implementation and computational complexities complicates RRM configuration [145].

A new feature in 5G, called BWP, inspired authors in [148] to propose a bandwidth allocation model that is able to adapt bandwidth allocation to individual users based on data rate requirements. A wide bandwidth is divided into chunks of smaller bandwidths in adaptive bandwidth allocation, the number of bandwidth chunks assigned to each user based on the type of user. However, although the proposed bandwidth allocation model mandates the allocation of contiguous bandwidth chunks in 5G, it leaves room for other assumptions on chunk allocation such as the selection of any set of bandwidth chunks, as in, for example, the LTE resource allocation where chunks are randomly selected. The proposed bandwidth allocation model is probabilistic, in that the locations of users are assumed to be the realization of a Poisson process, and each user determines independently his type of usage with some probability. Based on this model, we can quantify spectrum sharing and service differentiation in this particular context, namely what performance will be delivered to a user based on their type as well as overall performance. These analyses rely on precise representations of key performance metrics for each type of user, such as the success probability, signal-to-interference ratio, and Shannon throughput. In [15], author investigates the effect of BWP on the reliability and delay performance. Performance of reliability is measured in terms of simultaneous transmission density that meets certain reliability constraints, whereas the performance of delay is measured in terms of average number of time slots for successful transmission of a packet. The emphasis is on the ultra-reliable domain, in which the target outage probability is near zero. The BWP has two opposing effects: while interference is significantly reduced because concurrent transmissions are split over multiple bands, SIR requirements are increased because

the bandwidth allocated is smaller if the data rate is to be kept consistent. However, if the SIR requirement remains the same, the BWP will reduce the data rate and thus increase the local delay. In both approaches, the author has derived closed-form expressions for the maximum density of reliable transmissions and the local delay, which are applicable to the ultra-reliable regime. According to the analysis, in the ultra-reliable regime, BWP results in reliability-delay trade-offs. On these lines, the prior works have investigated BWP for the downlink full interference system using various performance metrics, such as user fairness [149] and weighted sum-rate maximization [150]. Assuming that an RB is partitioned into $N$ parts, i.e., for $N$ user types, we study different BWP strategies in this thesis. A risk-averse BWP scheme considering tradeoff on the average spectral efficiency of the network and the fairness for all user types is proposed. we use modern portfolio theory (MPT), which is a well-known optimization tool in economics [151, 152].

## 3.7 Conclusion

In this chapter, we have first presented practical techniques in the literature evaluated under the PPP as the reference PP, with various tractability, accuracy, and mathematical flexibility to analyze the network's performance. Then, BS and user deployments with different modelling options addressed in the literature of SG-based analysis is provided. The standard propagation model and the cell association strategy for the whole thesis is also described. We outlined the non-full interference concept as all BS do not contribute to the interference received by a user in a given bandwidth. Moreover, we have revisited the user classification solution to help cell edge users who suffer from poor SINR. A survey of the research approaches aiming to improve the network's performance using interference management is given. Inter-cell interference coordination via coordinated radio resource management is a promising solution for improving network performance. This approach can help cell edge users who are more vulnerable to interference to improve their coverage probability and spectral efficiency. The performance of inter-cell interference coordination is function of different aspects such as spatial distribution of BS, load model, etc.. Several works analyzing inter-cell interference coordination have considered a full interference network which introduce cell edge users as a user located in the cell boundary. In this thesis, in order to have a better metric to detect performance degradation, we give a new definition for non-full interference concept. The non-full interference model captures the correlation between the received signal and the inter-cell interference by performing user classification based on the link qualities. We follow tractable scenario by considering a PPP as network deployment. This enables us to give a tractable system-level study of the typical user performance in downlink non-full interference networks using stochastic geometry.

# Chapter 4

# Non-full Interference Cellular Networks: Performance Analysis and User Classification

## 4.1 Introduction

This chapter deals with modeling wireless communication networks under non-full interference assumption. Most of the work in the literature assumes that all base stations are transmitting all the time. This is called the full interference model on which the work of Andrews *et al.* in [2] is based in particular. However, a cell which does not have a covered user would not transmit and would not cause interference on the user of interest, said to be a typical user. This chapter focuses on the performance analysis of large-scale networks precisely in this case. In particular, we take up the notion of classifying users according to the quality of their SINR for which we associate a fixed RB. On the other hand, combining sophisticated user classification methods based on the link qualities and inter-cell interference is challenging [116]. It is because of the correlation between the received signal and the inter-cell interference seen by the users in the network. Therefore, most of the existing studies in the literature ignore this correlation by considering full interference assumption and instead sort the users according to their mean desired signal strength (i.e., link distances) such that the $k$-th nearest users are the $k$-th strongest user [153]. The difficulty of the analysis is due to the fact that the probability of activity of the base stations in a RB depends on the probability of coverage which one seeks to calculate, thus creating a dependence in the point process. This chapter focuses on the derivation of a theoretical framework to deal with this scenario. The key contributions of our study in this chapter are briefly summarized below.

- We provide a novel definition of a non-full interference network that correlates

the activity of a BS to the user classification within the cell;

- An accurate approximation of the user classification probability is derived. The expression is obtained in the form of a fixed-point equation that models the existing correlation between the desired signal and the interference set of each user type. Besides, we also provide per user type performance metrics, namely coverage probability and SE.

## 4.2 CCU/CEU classification

### 4.2.1 System model and assumptions

Let us consider an OFDMA-based single-tier downlink cellular network where the location of BS is modeled as an homogeneous PPP $\Phi \equiv \{X_1, X_2, ...\}$ with density $\lambda$ and $X_i \in \mathbb{R}^2$. The set of nucleus at $X_i \in \Phi$ divides the space into Poisson-Voronoi regions as

$$V_i = \left\{ Y \in \mathbb{R}^2 : \|Y - X_i\| \leq \|Y - X_j\|, \forall\, j \neq i,\ X_j \in \Phi \right\}. \tag{4.1}$$

Similarly to the works in [104], the location of the users on a given RB is a point process such that each BS selects a user at random from the set of users inside its cell. Hence, only one randomly chosen user per RB is considered to communicate with its BS. In order to analyze cellular networks, one can consider the typical user, who could be located anywhere on the plane. The performance for the typical user is defined as the performance average over all users, if point processes are ergodic (which is satisfied using homogeneous Poisson processes). Consequently, the coverage probability of the typical user is interpreted as the proportion of network users who will be able to connect to the cellular network. Since by Slivnyak's theorem, conditioning on a point is the same as adding a point to the PPP, we consider that the nucleus of the typical cell of the point process $\Phi \cup \{X_0\}$ is located at $X_0$ with its typical cell $V_0$. In this context, the point process of the interfering BS that the typical user sees is a subset of $\Phi$.

The standard power-law path loss model with exponent $\alpha > 2$ is considered for signal propagation. We assume that all BS and users are equipped with a single antenna, and users are experiencing an independent block Rayleigh fading channel on each RB. In each cell, a user can be classified as a CCU or CEU, depending on the value of its received SINR relatively to a threshold that, in turn, depends on the location of other BS and channel conditions. Fig. 4.1 illustrates a realization of the PPP network and its boundary of Voronoi tessellation (dot-dash black lines), where green and red squares present active BS for CCU and CEU, respectively, for the classification threshold value $\theta_c = 5dB$.

We consider that the time/frequency resource is a RB allocated to one user in each cell. In a conventional full interference network, as presented in (3.1), all BS

contribute to the interference received by the typical user in the given RB. In this work, RB is divided into two sub-bands, i.e., $B_c$ and $B_e$, the former will be used if the user is a CCU and the later if the user is a CEU. However, since the entire RB is dedicated to the given user, the BS cannot allocate the remaining part of RB, e.g., $B_c$ if the user is CEU or $B_e$ if the user is CCU, to another user in the cell. This setting leads to a non-full interference context in each sub-band because only a part of the RB, i.e. $B_e$ or $B_c$, is used in a given cell.

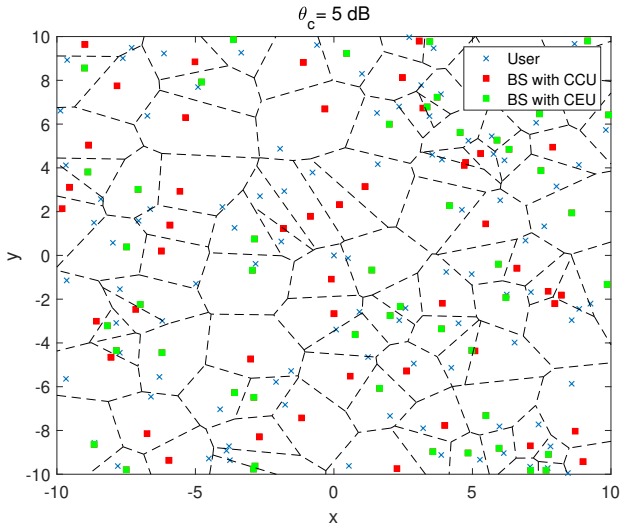


Figure 4.1 – PPP deployment for BS with a randomly selected user in each cell.

In that context, the typical user, located at the origin $(0,0)$, is classified as a CCU if its SINR is larger than a threshold $\theta_c$, i.e. $\Gamma_c \geq \theta_c$:

$$\Gamma_c = \frac{H^c_{0,0} R_0^{-\alpha}}{\sigma^2 + \sum\limits_{i>0} H^c_{0,i} R_i^{-\alpha} \mathbf{1}(\Gamma_{c,i} \geq \theta_c)}, \tag{4.2}$$

and

$$\Gamma_{c,i} = \frac{H^c_{i,i} \| X_i - Y_i \|^{-\alpha}}{\sigma^2 + \sum\limits_{j \neq i} H^c_{i,j} \| X_j - Y_i \|^{-\alpha} \mathbf{1}(\Gamma_{c,j} \geq \theta_c)}, \tag{4.3}$$

where $R_i$ is the distance between BS $i$ and the typical user, $X_i$ is the position of BS $i$, $\Gamma_{c,i}$ is the SINR of a randomly selected user located at $Y_i$ within the cell $i$ whose BS is located at $X_i$, $H^c_{i,j}$ is the channel gain between the CCU $i$ and BS $j$.

The indicator function in (4.2) and (4.3) ensures that the typical user experiences interference only from BS that serves another CCU. This model enlightens the fact

that this is a dependent thinning process, and we prove that it is equivalent to an independent thinning process on BS PPP by a factor depending on the coverage probability.

Also, if the typical user is not covered as a CCU, it becomes a CEU and will be covered if its SINR is larger than a threshold $\theta_e$, i.e. $\Gamma_e \geq \theta_e$, where

$$\Gamma_e = \frac{H^e_{0,0} R_0^{-\alpha}}{\sigma^2 + \sum\limits_{i>0} H^e_{0,i} R_i^{-\alpha} \mathbf{1}(\Gamma_{c,i} < \theta_c)}. \tag{4.4}$$

Since separated frequency sub-bands are allocated to CCU and CEU, we assumed that they do not experience the same channel gains. Hence the typical CEU experiences a new direct and interference channel gains, i.e., $H^e_{0,0}$ and $H^e_{0,i}$, respectively, exponentially distributed and independent from $H^c_{0,0}$ and $H^c_{0,i}$.

### 4.2.2 Coverage probability

Consider two real numbers, $\theta_c > 0$ and $\theta_e > 0$, as the cell center and cell edge thresholds, respectively. The coverage probability is the probability that the SINR of the typical user exceeds a threshold [2] in the classical approach, and two thresholds in our case. Since the classification in CCU or CEU is related to SINR, the probability to be covered for a CCU is equal 1 and the probability to be a CCU can be defined as follow.

**Definition 1.** *The probability to be a CCU of a typical user is defined as*

$$p_c(\theta_c, \lambda, \alpha) \triangleq \mathbb{P}(\Gamma_c \geq \theta_c). \tag{4.5}$$

Since the probability be covered for a CCU; let's call $p_c$ the central coverage probability.

**Definition 2.** *The edge coverage probability of a typical user is defined as*

$$p_e(\theta_e, \theta_c, \lambda, \alpha) \triangleq \mathbb{P}(\Gamma_e \geq \theta_e | \Gamma_c < \theta_c). \tag{4.6}$$

Further, the global coverage probability of a typical user randomly located in the considered model can be defined by the next definition.

**Definition 3.** *The global coverage probability of a typical user*

$$p(\theta_e, \theta_c, \lambda, \alpha) \triangleq \mathbb{P}(\Gamma_c \geq \theta_c) + p_e(\theta_e, \theta_c, \lambda, \alpha)\mathbb{P}(\Gamma_c < \theta_c). \tag{4.7}$$

The next theorem states a result on the approximation of the probability to be a CCU.

**Theorem 3.** *The central coverage probability in the non-full interference context is well approximated by*

$$p_c(\theta_c,\lambda,\alpha) \approx \pi\lambda \int_0^{\infty} e^{-\pi\lambda v(1+p_c(\theta_c,\lambda,\alpha)\rho(\theta_c,\alpha))} e^{-\theta_c\sigma^2 v^{\alpha/2}} \mathrm{d}v, \tag{4.8}$$

*where*

$$\rho(\theta,\alpha) = \frac{2\theta}{\alpha-2}\, {}_2F_1\left(1, 1-\frac{2}{\alpha}; 2-\frac{2}{\alpha}; -\theta\right). \tag{4.9}$$

*Proof.* See Appendix A.1. □

The expression (4.8) is a fixed point equation which approximates the correlation when computing the received SIR by users.

**Theorem 4.** *The edge coverage probability in the non-full interference context is*

$$p_e(\theta_e,\theta_c,\lambda,\alpha) \approx \frac{\pi\lambda}{1-p_c(\theta_c,\lambda,\alpha)} \int_0^{\infty} \left( e^{-\pi\lambda v(1+\mathcal{K}_2(\theta_e,\lambda,\alpha))} e^{-\theta_e\sigma^2 v^{\alpha/2}} - e^{-\pi\lambda v(1+\mathcal{K}_3(\theta_e,\theta_c,\lambda,\alpha))} e^{-(\theta_c+\theta_e)\sigma^2 v^{\alpha/2}} \right) \mathrm{d}v, \tag{4.10}$$

*where*

$$\mathcal{K}_1(\theta_c,\lambda,\alpha) = p_c(\theta_c,\lambda,\alpha)\,\rho(\theta_c,\alpha), \tag{4.11}$$

$$\mathcal{K}_2(\theta_e,\lambda,\alpha) = (1-p_c(\theta_c,\lambda,\alpha))\,\rho(\theta_e,\alpha), \tag{4.12}$$

$$\mathcal{K}_3(\theta_e,\theta_c,\lambda,\alpha) = \mathcal{K}_1(\theta_c,\lambda,\alpha) + \mathcal{K}_2(\theta_e,\lambda,\alpha). \tag{4.13}$$

*Proof.* See Appendix A.2. □

In the following, some closed-form expressions can be further obtained when considering particular values of system parameters.

1. Noise, $\alpha = 4$

   Theorem 3 simply becomes

$$p_c(\theta_c,\lambda,4) = \frac{\pi^{3/2}\lambda}{\sqrt{\theta_c\sigma^2}} e^{\frac{(\pi\lambda(1+\mathcal{K}_1(\theta_c,\lambda,4)))^2}{4\theta_c\sigma^2}} Q\left(\frac{\pi\lambda(1+\mathcal{K}_1(\theta_c,\lambda,4))}{\sqrt{2\theta_c\sigma^2}}\right), \tag{4.14}$$

   where

$$Q(x) = \frac{1}{\sqrt{2\pi}} \int_x^{\infty} \exp\left(-y^2/2\right) \mathrm{d}y \tag{4.15}$$

is the standard Gaussian tail probability.

Also, Theorem 4 can be given by (4.16) at the following

$$p_e(\theta_e,\theta_c,\lambda) = \frac{\pi^{3/2}\lambda}{1-p_c(\theta_c,\lambda,4)}\left(\frac{\exp\left(\frac{(\pi\lambda(1+\mathcal{K}_2(\theta_e,\lambda,4)))^2}{4\theta_e\sigma^2}\right)}{\sqrt{\theta_e\sigma^2}}Q\left(\frac{\pi\lambda\,(1+\mathcal{K}_2(\theta_e,\lambda,4))}{\sqrt{2\theta_e\sigma^2}}\right)\times\right.$$
$$\left.-\frac{\exp\left(\frac{(\pi\lambda(1+\mathcal{K}_3(\theta_e,\theta_c,\lambda,4))^2}{4(\theta_e+\theta_c)\sigma^2}\right)}{\sqrt{(\theta_e+\theta_c)\sigma^2}}Q\left(\frac{\pi\lambda\,(1+\mathcal{K}_3(\theta_e,\theta_c,\lambda,4)))}{\sqrt{2(\theta_e+\theta_c)\sigma^2}}\right)\right). \quad (4.16)$$

As an asymptotic analysis of the global coverage probability, it can be found that for $\theta_c \to \infty$, then $p_c(\infty,\lambda,\alpha) \to 0$ and

$$p_e(\theta_e,\infty,\lambda,4) = \frac{\pi^{3/2}\lambda}{\sqrt{\theta_e\sigma^2}}e^{\frac{(\pi\lambda(1+\mathcal{K}_2(\theta_e,\lambda,4)))^2}{4\theta_e\sigma^2}}Q\left(\frac{\pi\lambda\,(1+\mathcal{K}_2(\theta_e,\lambda,4))}{\sqrt{2\theta_e\sigma^2}}\right). \quad (4.17)$$

The reason is that increasing $\theta_c$ shrinks the center region, thereby makes the global coverage probability a function of the edge threshold $\theta_e$. Also, setting $\theta_c \to 0$ makes all users as CCU, then the global coverage will be equal to the central coverage probability and $p_c(\theta_c \to 0,\lambda,\alpha) \to 1$.

2. No Noise, $\alpha > 2$

   It can be shown that the central and edge coverage probabilities become

$$p_c(\theta_c,\lambda,\alpha) = \frac{\sqrt{1+4\rho(\theta_c,\alpha)}-1}{2\rho(\theta_c,\alpha)}, \quad (4.18)$$

   and

$$p_e(\theta_e,\theta_c,\lambda,\alpha) = \frac{1}{1-p_c(\theta_c,\lambda,\alpha)}\times\left(\frac{1}{1+\mathcal{K}_2\left(\theta_e,\lambda,\alpha\right)}-\frac{1}{1+\mathcal{K}_3\left(\theta_e,\theta_c,\lambda,\alpha\right)}\right). \quad (4.19)$$

3. No Noise, $\alpha = 4$, unique $\theta$

   The global coverage probability simplifies to

$$p(\theta,\theta,\lambda,4) = \frac{1}{1+\frac{\lambda_c}{\lambda}\rho(\theta,4)}+\frac{1}{1+(1-\frac{\lambda_c}{\lambda})\rho(\theta,4)}-\frac{1}{1+\rho(\theta,4)}, \quad (4.20)$$

   where $\lambda_c = p_c(\theta,\lambda,\alpha)\lambda$ is the equivalent density of BS dedicated to CCU and $\rho(\theta,4) = \sqrt{\theta}\left(\frac{\pi}{2}-\arctan(\frac{1}{\sqrt{\theta}})\right)$. Since $\frac{\lambda_c}{\lambda} \le 1$, the derived coverage probability in (4.20) is larger than the coverage probability of the full interference network model with a single type user given in [2].

   As the coverage does not take into account the resource used, we need another measure to evaluate and compare the proposed method fairly. So, we investigate spectral efficiency as follows.

### 4.2.3 Spectral efficiency

If only one kind of user is considered, the average achievable SE for the typical user is $\mathscr{R} = \mathbb{E}[\ln(1+\text{SINR})]$ [2]. In our case, the SE in nats/s/Hz for a CCU/CEU is defined as follows.

**Definition 4.** *The SE of a typical CCU is defined as*

$$\eta_c(\theta,\lambda,\alpha) \triangleq \delta\mathbb{E}[\ln(1+\Gamma_c)|\Gamma_c \geq \theta], \tag{4.21}$$

*where* $\delta = \frac{B_c}{B_c+B_e}$.

**Definition 5.** *The SE of a typical CEU is defined as*

$$\eta_e(\theta,\lambda,\alpha) = (1-\delta)\mathbb{E}[\ln(1+\Gamma_e)|\Gamma_c < \theta]. \tag{4.22}$$

Since for a positive random variable $Z$, we have

$$\mathbb{E}[Z] = \int_{t>0} P(Z>t)\mathrm{d}t, \tag{4.23}$$

we can find the SE of a typical CCU/CEU from the following theorems.

**Theorem 5.** *Given $\alpha$ and threshold value $\theta_c$, the spectral efficiency of the typical CCU in the non-full interference can be obtained as*

$$\eta_c(\theta,\lambda,\alpha) = \frac{\delta}{p_c(\theta,\lambda,\alpha)}\mathbb{E}_{R_0}\left[\int_{t>0} e^{-\max(e^t-1,\theta)R_0^\alpha\sigma^2}\mathscr{L}_{I_c}\left(\max\left(e^t-1,\theta\right)R_0^\alpha\right)\mathrm{d}t\right], \tag{4.24}$$

*and*

$$\mathscr{L}_{I_c}\left(\max\left(e^t-1,\theta\right)R_0^\alpha\right) = \exp\left(-\pi\lambda R_0^2 p_c(\theta,\lambda,\alpha)\,\rho\left(\max\left(e^t-1,\theta\right),\alpha\right)\right). \tag{4.25}$$

*Proof.* Using the expressions 4.21 and (4.23), the SE of the typical CCU is

$$\begin{aligned}\eta_c(\theta,\lambda,\alpha) &= \delta\mathbb{E}[\ln(1+\Gamma_c)|\Gamma_c>\theta] \\ &= \delta\int_0^\infty \mathbb{P}\Big(\Gamma_c > e^t-1|\Gamma_c>\theta\Big)\mathrm{d}t.\end{aligned} \tag{4.26}$$

By using the Bayes rule, we have

$$\eta_c(\theta,\lambda,\alpha) = \delta\int_0^\infty \frac{\mathbb{P}\Big(\Gamma_c > e^t-1,\Gamma_c>\theta\Big)}{\mathbb{P}\Big(\Gamma_c>\theta\Big)}\mathrm{d}t$$

$$= \frac{\delta}{\mathbb{P}\Big(\Gamma_c > \theta\Big)} \int_0^\infty \mathbb{P}\Big(\Gamma_c > \max(e^t - 1, \theta)\Big) \mathrm{d}t$$

$$= \frac{\delta}{p_c(\theta,\lambda,\alpha)} \int_0^\infty \mathbb{P}\Big(H_{0,0}^c > \max(e^t - 1, \theta) R_0^\alpha (\sigma^2 + I_c)\Big) \mathrm{d}t \tag{4.27}$$

By Conditioning on $R_0$ and following steps presented in the Appendix (A.1), the term (4.27) becomes

$$\eta_c(\theta,\lambda,\alpha) = \frac{2\pi\lambda\delta}{p_c(\theta,\lambda,\alpha)} \int_0^\infty \int_0^\infty e^{-\max(e^t-1,\theta) r_0^\alpha \sigma^2} e^{-\pi\lambda r_0^2 p_c(\theta,\lambda,\alpha)\rho(\max(e^t-1,\theta),\alpha)} r_0 \mathrm{d}t\mathrm{d}r_0. \tag{4.28}$$

□

**Theorem 6.** *Given $\alpha$ and threshold values $\theta_c, \theta_e$, the spectral efficiency of the typical CEU in the non-full interference can be obtained as*

$$\eta_e(\theta,\lambda,\alpha) = \frac{1-\delta}{1-p_c(\theta,\lambda,\alpha)} \mathbb{E}_{R_0}\Bigg[\int_{t>0}\Big(e^{-(e^t-1)R_0^\alpha\sigma^2}\mathscr{L}_{I_e}((e^t-1)R_0^\alpha) - e^{-((e^t-1)+\theta)R_0^\alpha\sigma^2}\mathscr{L}_{I_e,I_c}((e^t-1)R_0^\alpha, \theta R_0^\alpha)\Big)\mathrm{d}t\Bigg], \tag{4.29}$$

*and*

$$\mathscr{L}_{I_e}\left(\left(e^t-1\right)R_0^\alpha\right) = \exp\left(-\pi\lambda R_0^2\left(1-p_c\left(\theta,\lambda,\alpha\right)\right)\rho\left(\left(e^t-1\right),\alpha\right)\right), \tag{4.30}$$

$$\mathscr{L}_{I_e,I_c}\left(\left(e^t-1\right)R_0^\alpha, \theta R_0^\alpha\right) = \mathscr{L}_{I_e}\left(\left(e^t-1\right)R_0^\alpha\right)\mathscr{L}_{I_c}\left(\theta R_0^\alpha\right). \tag{4.31}$$

*Proof.* Using the expressions (4.22) and (4.23), the SE of the typical CEU is

$$\eta_e(\theta,\lambda,\alpha) = (1-\delta)\mathbb{E}\left[\ln\left(1+\Gamma_e\right)|\Gamma_c < \theta\right]$$

$$= (1-\delta)\int_0^\infty \mathbb{P}\Big(\Gamma_e > e^t - 1 | \Gamma_c < \theta\Big)\mathrm{d}t$$

$$= \frac{1-\delta}{1-p_c(\theta,\lambda,\alpha)}\int_0^\infty \mathbb{P}\Big(\Gamma_e > e^t - 1, \Gamma_c < \theta\Big)\mathrm{d}t. \tag{4.32}$$

By conditioning on $R_0$ and following steps presented in the Appendix (A.2), the term (4.32) becomes

$$\eta_e(\theta,\lambda,\alpha) = \frac{2\pi\lambda(1-\delta)}{1-p_c(\theta,\lambda,\alpha)}\int_0^\infty\int_0^\infty e^{-(e^t-1)r_0^\alpha\sigma^2} e^{-\pi\lambda r_0^2\left(1-p_c(\theta,\lambda,\alpha)\right)\rho(e^t-1,\alpha)} \times \left(1 - e^{-\theta r_0^\alpha\sigma^2} e^{-\pi\lambda r_0^2 p_c(\theta,\lambda,\alpha)\rho(\theta,\alpha)}\right) r_0 \mathrm{d}t\mathrm{d}r_0. \tag{4.33}$$

□

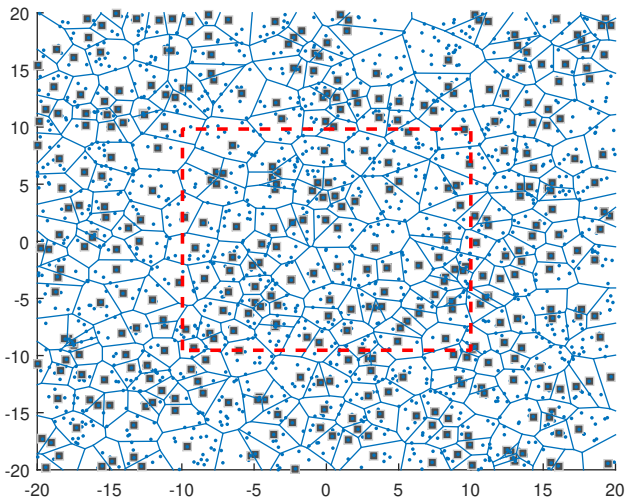


Figure 4.2 – Realization of a simulation area.

The global SE in the non-full interference network is then

$$\eta(\theta,\lambda,\alpha) = p_c(\theta,\lambda,\alpha)\eta_c(\theta,\lambda,\alpha) + (1 - p_c(\theta,\lambda,\alpha))\eta_e(\theta,\lambda,\alpha). \tag{4.34}$$

### 4.2.4 Simulation and numerical results

Now that we have established expressions for cellular network coverage and SE, one can evaluate the accuracy of these analytical findings by comparing them to Monte Carlo simulations. Performance analysis is conducted for the cell bordering the plane's origin, which is referred as the typical cell, which implies that simulations must be performed under the Palm measure. The network is assumed to be interference limited, i.e. $\sigma^2 = 0$ and $\lambda = 1$ and $\alpha = 4$ [2]. Figure 4.2 illustrates the realization of the main area of the network and selected simulation area to avoid cell edge effect to simulated numerical results.

Fig. 4.3 compares the central coverage probability considering CCU/CEU classification under conventional full interference and non-full interference models. The curve related to the full interference assumption produces the coverage probability of a typical user presented in [2] when all BS are transmitting in the tagged RB. However, the non-full interference is a thinning of the original PPP. The thinning process reduces the interference to the typical user by a factor depending on the coverage probability itself and $\theta_c$ as it can be inferred from (4.18). Referring to the figure, we can see that for $\theta_c < -8$ dB, the proportion of CCU is high compared to the proportion of CEU, generating a lot of interference in sub-band $B_c$. In that case, the non-full and full interference assumptions lead to the same result.

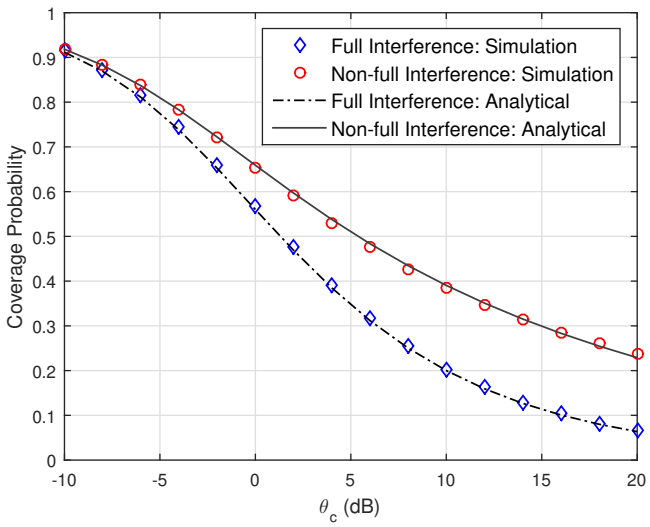


Figure 4.3 – Coverage probability versus SIR thresholds.

Fig. 4.4 compares the edge coverage probability considering CCU/CEU classification under conventional full interference and non-full interference models. As shown in the figure, the cell edge coverage probability $p_e$ is plotted versus $\theta_e$ for specific CCU target threshold $\theta_c = 5$ dB. The value of central threshold changes the density of interfering BS of the typical cell edge user. Moreover, as mentioned in the description of Fig. 4.3, since the interfering BS set is a thinned version of original PPP, the coverage probability of CEU is enhanced. It means that the sub-band $B_e$ is only used by CEU of the other cells compared to the full interference scenario.

Fig. 4.5 presents the global coverage probability of a typical user when a unique $\theta$ is considered, i.e. the CCU target threshold is equal to the CEU one. The gain of considering non-full interference strategy, i.e., when a sub-band is dedicated to a single kind of user is clear from this figure. Fig. 4.6 presents the global coverage probability of a typical user randomly located in the typical cell versus the CCU target threshold for different CEU target thresholds. As expected, reserving some fraction of resources to CEU increases the global coverage probability.

In order to improve the global SE, [1] proposed a SIR-proportional resource sharing approach. Under this approach, the fraction of bandwidth allocated to CCU is determined based on a chosen threshold value by assessing the CCDF of $\Gamma_c$ at $\theta_c$, i.e., $\delta = \mathbb{P}(\Gamma_c \geq \theta_c)$ in (4.24) and (4.33).

Fig. 4.7 represents the SE for CCU, CEU in the non-full interference network versus a single user classification threshold $\theta$, which means that we consider $\theta_e = \theta_c = \theta$. The SIR-proportional spectral resource sharing in [1] is applied. SE of CEU increases with $\theta$ since the number of CEU increases. On the other hand, SE of CCU first increases and then decreases after 8 dB, because the number of CCU decreases and it is not

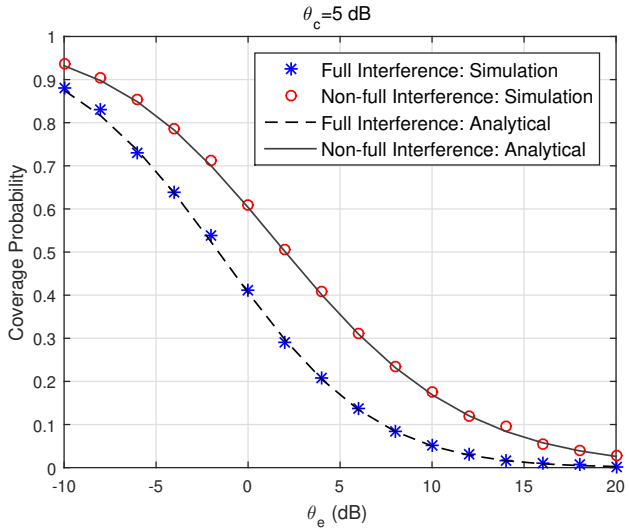


Figure 4.4 – Coverage probability versus SIR thresholds.

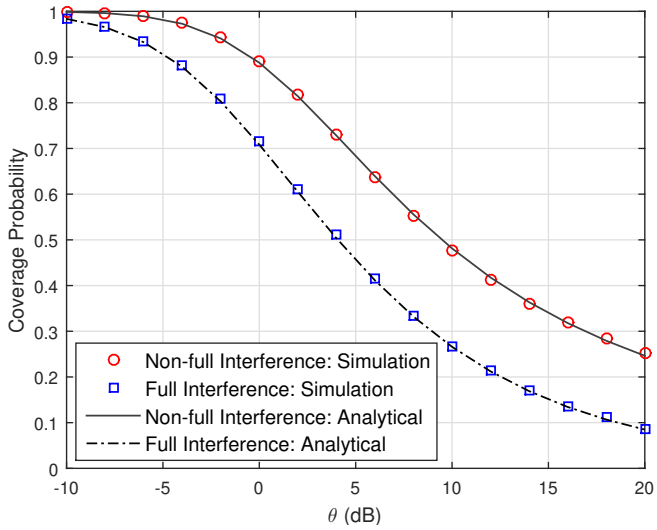


Figure 4.5 – Coverage probability versus unique SIR threshold.

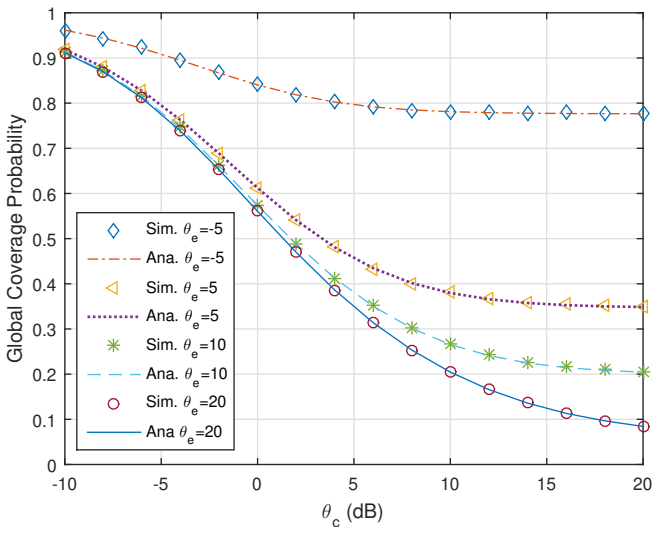


Figure 4.6 – Comparison of the coverage probability results versus $\theta_c$ for various $\theta_e$.

compensated by the gain of being closer to the BS. The result is that global SE, in (4.34), is nonetheless decreasing with $\theta$ because of the waste of the resource to create band with less interference. However, global SE is compared with the frequency reuse (FR) technique with reuse factor $\Delta$ presented in [2], under full interference network, i.e. only one type of user. The global SE is between the values obtained for $\Delta = 1$ and $\Delta = 2$ in FR approach. On the other hand, since the typical CCU benefits from coverage-dependent fraction of resource and suffers from the same fraction of the interference, it has higher SE than FR with $\Delta = 1$. The small mismatch in the figure between analytical and simulation results is because of taking independence assumption to find a approximation for the coverage probability in (4.8), in step (b) to (c) in A.1, which indicates a interference thinning factor in the calculation of SE.

## 4.3 Extension to multiple user classes

In this section, to evaluate the proposed user-centric frequency reuse model under user classification scenario with more than two classes, we first extend the SIR-based user classification approach to $N+1$ classes. Moreover, we analyze the coverage probability of a typical randomly located user in the non-full interference network. Next, the conditional coverage probability of each user type is investigated. Finally, to fairly evaluate the proposed method, the SE of the network is studied.

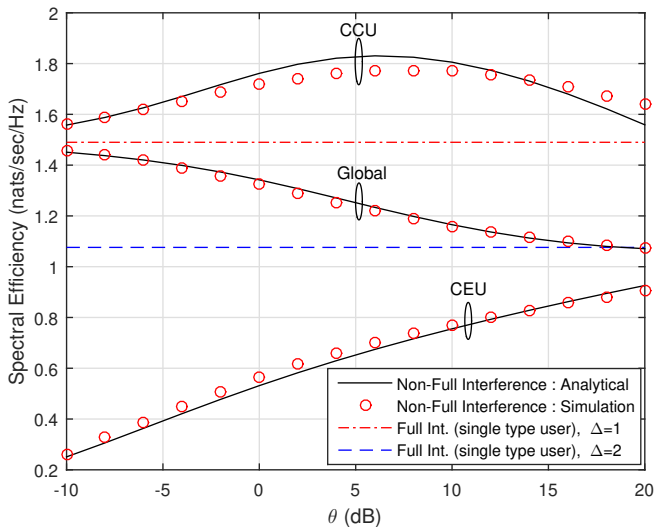


Figure 4.7 – SE versus $\theta$ for SIR-proportional [1] resource sharing.

### 4.3.1 System model and assumptions

Consider the system model same as section 4.2, except that the number of user classes is extended to $N+1$. In this context, a cell is divided into $N+1$ classes, and a typical user belongs to a certain class depending on its SIR. Moreover each class has its proper sub-band that may be used by the nearest interfering cell but only by the same type of user in that interfering cell.

In our model, a user is classified to be a type-1 when its SIR is larger than a threshold, a user is type-2 if its SIR is less than the first-class threshold and larger than the second class one, and so on. A user type-$N+1$ has the weakest SIR and is in outage from the network. By the above construction, the typical user is a type-$k$ user according to the relative value of its SIR w.r.t. some thresholds that, in turn, depends on the location of others BS and the channel conditions.

Fig. 4.8 illustrates one realization of a PPP network for two types of served users, with only one user per BS. The BS colored in green, red and black represent the active BS for users of type-1, type-2 and outage users respectively.

### 4.3.2 Proposed User-BS classification

Let us consider the typical BS at $X_0$ and divide the interfering BS set $\Phi$ into $N+1$ complementary subsets $\Phi_k$ such that $\Phi = \cup_{k=1}^{N+1}\Phi_k$ and $\Phi_k \cap \Phi_l = \emptyset$ for all $k \neq l$. $\Phi_k$ is the subset gathering the BS that are serving type-$k$ users across the network and hence $\Phi_{N+1}$ is the set of BS that have the typical user in outage. Let $X_i$ be the position of the BS $i$ and $\mathrm{SIR}_i^k$ the SIR experienced by a randomly selected user in the cell $i$ over

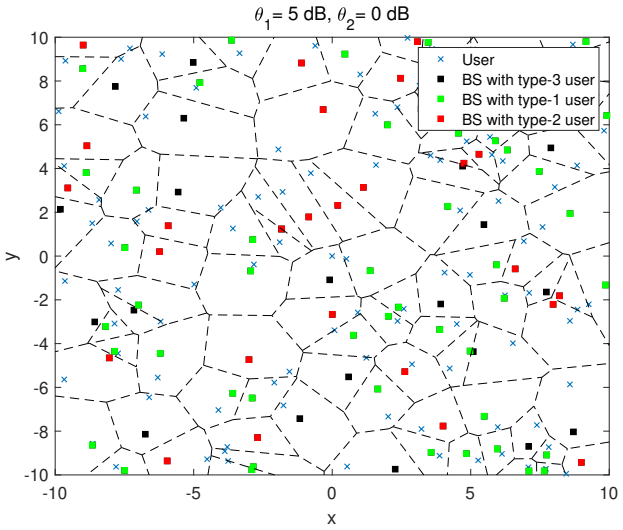


Figure 4.8 – PPP deployment for BS with a randomly selected user in each cell.

the sub-channel $k$. The subset $\Phi_k$ for all $1 \leq k \leq N$ is

$$\Phi_k \triangleq \left\{ X_i \,:\, \mathrm{SIR}_i^k \geq \theta_k \text{ and } \mathrm{SIR}_i^m < \theta_m, \forall m, 1 \leq m < k \right\}, \tag{4.35}$$

and $\Phi_{N+1} = \left\{ X_i \,:\, \mathrm{SIR}_i^m < \theta_m, \forall m, 1 \leq m \leq N \right\}$, where real numbers $\{\theta_k\}_1^N \geq 0$ are the SIR classification thresholds. Let $\mathrm{SIR}_0^k$ be the received SIR by the typical user in $V_0$, using the subchannel $k$, then

$$\mathrm{SIR}_0^k = \frac{H_{0,0}^k R_0^{-\alpha}}{\sum\limits_{X_i \in \Phi} H_{0,i}^k R_i^{-\alpha} \mathbf{1}(X_i \in \Phi_k)} = \frac{S_0}{I_{0,k}}. \tag{4.36}$$

### 4.3.3 Coverage probability

In interference-limited wireless networks, the standard coverage probability describes the probability that the SIR of the typical link exceeds a threshold [2]. In our model, we have a set of thresholds $\{\theta_k\}_{1 \leq k \leq N}$ to successfully demodulate and decode the received signal. Then, the typical user placed at the origin is covered on downlink if one of the subsequent events occurs:

$$\{X_0 \in \Phi_k\}, \; k = 1, ..., N. \tag{4.37}$$

Referring to the law of total probability, the coverage probability of the typical user is as follows.

**Theorem 7.** *The coverage probability $p_c$ of a randomly located typical user in a non-full interference network with $N$ type of covered users is given by*

$$p_c(\{\theta_k\},\alpha,\lambda) = \sum_{k=1}^{N} p_k \tag{4.38}$$

*where $p_k$ is well estimated with a fixed point equation as*

$$p_k = \int_0^{\infty} e^{-v(1+p_k\rho(\theta_k,\alpha))} \prod_{i=1}^{k-1} \left(1 - e^{-p_i\rho(\theta_i,\alpha)v}\right) \mathrm{d}v\,. \tag{4.39}$$

*Proof.* Based on the law of total probability, the coverage probability $p_c$ of the typical user is the probability that it satisfies the required condition of at least one of the $N$ type user classes in (4.35).

$$\begin{aligned} p_c(\{\theta_k\},\alpha,\lambda) &= \mathbb{P}\left(\bigcup_{k=1}^{N} \{X_0 \in \Phi_k\}\right) \\ &\overset{(a)}{=} \sum_{k=1}^{N} \mathbb{P}\left(X_0 \in \Phi_k\right), \end{aligned} \tag{4.40}$$

where (a) comes from that sets $\{\Phi_k\}_{1\le k\le N}$ are disjoint. Hence, the coverage probability can be expressed as $p_c = \sum_{k=1}^{N} p_k$ where $p_k$ is the probability of being a type-$k$ user, i.e.

$$\begin{aligned} p_k &= \mathbb{P}\left(X_0 \in \Phi_k\right) \\ &= \mathbb{P}\left(\mathrm{SIR}_0^k \ge \theta_k, \bigcap_{m=1}^{k-1} \mathrm{SIR}_0^m < \theta_m\right). \end{aligned} \tag{4.41}$$

Conditioning on $R_0$ the two events in (4.41) are independent and it can be written as

$$p_k = \int_0^{\infty} \mathbb{P}\left(\mathrm{SIR}_0^k \ge \theta_k | r_0\right) \mathbb{P}\left(\bigcap_{m=1}^{k-1} \mathrm{SIR}_0^m < \theta_m | r_0\right) f_{R_0}(r_0)\mathrm{d}r_0. \tag{4.42}$$

The first term in (4.42) is the probability that the SIR at the typical receiver exceeds $\theta_k$ and it follows

$$\begin{aligned} \mathbb{P}(\mathrm{SIR}_0^k \ge \theta_k | r_0) &= \mathbb{P}\left(H_{0,0}^k \ge \theta_k R_0^{\alpha} \sum_{X_i\in\Phi} H_{0,i}^k R_i^{-\alpha} \mathbf{1}(X_i \in \Phi_k)\right) \\ &\overset{a}{=} \mathbb{E}\left[\exp\left(-\theta_k R_0^{\alpha} \sum_{X_i\in\Phi} H_{0,i}^k R_i^{-\alpha} \mathbf{1}(X_i \in \Phi_k)\right)\right] \\ &= \mathbb{E}\left[\prod_{X_i\in\Phi} \exp\left(-\theta_k R_0^{\alpha} H_{0,i}^k R_i^{-\alpha} \mathbf{1}(X_i \in \Phi_k)\right)\right] \end{aligned} \tag{4.43}$$

$$= \mathbb{E}\Big[\prod_{X_i\in\Phi} \mathbf{1}(X_i\in\Phi_k)e^{-\theta_k R_0^\alpha H_{0,i}^k R_i^{-\alpha}} + 1 - \mathbf{1}(X_i\in\Phi_k)\Big]$$
$$\stackrel{b}{=} \mathbb{E}\Big[\prod_{X_i\in\Phi}\Big(1-\mathbb{E}[\mathbf{1}(X_i\in\Phi_k)](1-e^{-\theta_k R_0^\alpha H_{0,i}^k R_i^{-\alpha}})\Big)\Big],$$

where (a) comes from the i.i.d. exponential distribution of $H_{0,0}^k$ with mean 1 as in [2], (b) comes from averaging over interfering fading channels, the law of total expectation, $\mathbb{E}_X[f(X)] = \mathbb{E}_Y[\mathbb{E}_X[f(X)|Y]]$, the independence of $\{\mathrm{SIR}_i^k\}_{1\le i\le N}$, which is a reasonable assumption whose correctness has been verified by simulations, and finally by factoring out $\mathbb{E}[\mathbf{1}(X_i\in\Phi_k)]$. By applying PGFL [31] of the PPP and identically distributed $\{\mathrm{SIR}_i^k\}_i$, we have

$$\mathbb{P}(\mathrm{SIR}_0^k \ge \theta_k | r_0) = \exp\left(-2\pi\lambda\, p_k\, \rho(\theta_k,\alpha) r_0^2\right). \tag{4.44}$$

The second term of (4.42) means that the received SIR by the typical user is less than all $\{\theta_i\}_{i=1}^{k-1}$ and can be derived as

$$\mathbb{P}\left(\bigcap_{m=1}^{k-1}\mathrm{SIR}_0^m < \theta_m | r_0\right) \stackrel{a}{=} \prod_{m=1}^{k-1}\mathbb{P}\left(\mathrm{SIR}_0^m<\theta_m|r_0\right) \tag{4.45}$$
$$= \prod_{m=1}^{k-1}\left(1-\mathbb{P}(\mathrm{SIR}_0^m\ge\theta_m|r_0)\right)$$
$$= \prod_{m=1}^{k-1}\left(1-\exp\left(-2\pi\lambda\, p_m\,\rho(\theta_m,\alpha)r_0^2\right)\right).$$

The independence in (a) comes from the independence of channels and interference in different sub-channels which leads to independence of $\{\mathrm{SIR}_0^m\}_{m=1}^{k-1}$ conditioned on $r_0$. By putting (4.44) and (4.45) in (4.42) and taking expectation over $r_0$, we reach to (4.39). Also, deconditioning (4.45) and with $v = \pi\lambda r_0^2$, we have

$$\mathbb{P}\left(\bigcap_{m=1}^{k-1}\mathrm{SIR}_0^m<\theta_m|r_0\right) = \int_0^\infty e^{-v}\prod_{i=1}^{k-1}\left(1-e^{-p_i\rho(\theta_i,\alpha)v}\right)\mathrm{d}v. \tag{4.46}$$

□

Theorem 7 for coverage probability does not depend on BS density $\lambda$ but on path loss exponent $\alpha$ and SIR thresholds $\{\theta_k\}_{1\le k\le N}$ as expected. It goes to 1 for all $\theta_k\to 0$ and 0 for all $\theta_k\to\infty$.

**Corollary 1.** *Given $\alpha$ and classification thresholds $\{\theta_k\}_{1\le k\le N}$, we have*

$$p_c(\{\theta_k\}_{k=1}^N,\alpha,\lambda) \le p_c(\{\theta_k\}_{k=1}^M,\alpha,\lambda),\ \forall\, N\le M \tag{4.47}$$

*Proof.* Referring to (4.37), for $M = N+1$, we can write

$$\begin{aligned} p_c(\{\theta_k\}_{k=1}^N, \alpha, \lambda) &= \mathbb{P}(X_0 \in \Phi_1 \cup \cdots \cup \Phi_{N-1} \cup \Phi_N) \\ &\leq \mathbb{P}(X_0 \in \Phi_1 \cup \cdots \cup \Phi_{N-1} \cup \underbrace{\{\Phi_N, \mathrm{SIR}_0^N \geq \theta_N\}}_{\Phi_N' \subseteq \Phi_N} \cup \underbrace{\{\Phi_N, \mathrm{SIR}_0^N < \theta_N\}}_{\Phi_{N+1} \subseteq \Phi_N}) \\ &= \mathbb{P}(X_0 \in \Phi_1 \cup \cdots \cup \Phi_{N-1} \cup \Phi_N' \cup \Phi_M) \\ &= p_c(\{\theta_k\}_{k=1}^M, \alpha, \lambda). \end{aligned}$$

□

Corollary 1 ensures that increasing the number $N$ of user types can not decrease the coverage probability.

Furthermore, the conditional coverage probability $\mathscr{P}_k$ of type-$k$ user in the non-full interference network is defined as

$$\mathscr{P}_k(\{\theta_k\}, \alpha, \lambda) \triangleq \mathbb{P}\left( \mathrm{SIR}_0^k \geq \theta_k \middle| \bigcap_{m=1}^{k-1} \mathrm{SIR}_0^m < \theta_m \right). \tag{4.48}$$

**Corollary 2.** *Conditioning on* $\{\bigcap_{m=1}^{k-1} \mathrm{SIR}_0^m < \theta_m\}$*, the probability that* $\mathrm{SIR}_0^k$ *satisfies a threshold* $\theta_k$ *is given by*

$$\mathscr{P}_k(\{\theta_k\}, \alpha, \lambda) = \frac{p_k}{\int_0^\infty e^{-\nu} \prod_{i=1}^{k-1} \left(1 - e^{-p_i \rho(\theta_i, \alpha) \nu}\right) \mathrm{d}\nu} \tag{4.49}$$

*Proof.* Starting with (4.48) and using the Bayes rule, we have conditioned on $\{\bigcap_{m=1}^{k-1} \mathrm{SIR}_0^m < \theta_m\}$ , the coverage probability of type-k user $\mathscr{P}_k$ is

$$\begin{aligned} \mathscr{P}_k(\{\theta_k\}, \alpha, \lambda) &= \mathbb{P}\left( \mathrm{SIR}_0^k \geq \theta_k \middle| \bigcap_{m=1}^{k-1} \mathrm{SIR}_0^m < \theta_m \right) \\ &= \frac{\mathbb{P}(\mathrm{SIR}_0^k \geq \theta_k, \bigcap_{m=1}^{k-1} \mathrm{SIR}_0^m < \theta_m)}{\mathbb{P}(\bigcap_{m=1}^{k-1} \mathrm{SIR}_0^m < \theta_m)}. \end{aligned} \tag{4.50}$$

The rest of the proof straightforwardly follows from Theorem 7. □

The coverage and conditional coverage probability in (4.38) and (4.49) can not be expressed in closed-form except for the typical type-1 (cell center) user, i.e.,

$$\mathscr{P}_1(\theta_1, \alpha, \lambda) = p_1 = \frac{\sqrt{1 + 4\rho(\theta_1, \alpha)} - 1}{2\rho(\theta_1, \alpha)}. \tag{4.51}$$

In particular, when $\alpha = 4$, i.e., high path-loss condition, we have $\rho(\theta, 4) = \sqrt{\theta}\left(\frac{\pi}{2} - \arctan(\frac{1}{\sqrt{\theta}})\right)$.

In the single-user type case, i.e., $N=1$, if $\theta_1=1$ (0 dB), the coverage probability of a typical user in (4.38) is equal $2\pi^{-1}(\sqrt{1+\pi}-1)=0.66$ which gains 0.7 dB rather than the coverage probability of a typical user in the classical full interference network given in [2].

### 4.3.4 Spectral efficiency

Considering the system setting of [2], where only one type of user is considered, i.e., the user is covered, the average SE per unit RB for the typical user is $\mathbb{E}[\ln(1+\mathrm{SINR})]$. In our case, a given RB is divided into $N$ sub-channels each assigned to its corresponding user type and the SE in nats/s/Hz of the typical user of type-$k$ is defined as follows.

**Definition 6.** *In the non-full interference context, the achievable SE is defined as*

$$\mathscr{R}_k \triangleq \mathbb{E}[\ln(1+\mathrm{SIR}_0^k)\,|\,X_0\in\Phi_k], \tag{4.52}$$

*and then the weighted SE is expressed as*

$$\eta_k=\omega_k\mathscr{R}_k. \tag{4.53}$$

*where $\omega_k\geq 0$ is the fraction of bandwidth allocated to type-$k$ user and $\sum_{k=1}^{N}\omega_k=1$.*

**Theorem 8.** *Conditioning on the typical user being of type-$k$, the spectral efficiency $\eta_k$ is given by*

$$\eta_k=\frac{\omega_k}{p_k}\left(p_k\ln(1+\theta_k)+\int_{\theta_k}^{\infty}g_k(z)\mathrm{d}z\right), \tag{4.54}$$

*where*

$$g_k(z)=\frac{1}{1+z}\int_0^{\infty}e^{-v(1+p_k\rho(z,\alpha))}\prod_{m=1}^{k-1}\left(1-e^{-p_m\rho(\theta_m,\alpha)v}\right)\mathrm{d}v. \tag{4.55}$$

*Proof.* Conditioning on the fact that typical user being of type-$k$, the spectral efficiency $\eta_k$ is given as

$$\eta_k=\omega_k\mathbb{E}[\ln(1+\mathrm{SIR}_0^k)|\mathrm{SIR}_0^k\geq\theta_k,\bigcap_{m=1}^{k-1}\mathrm{SIR}_0^m<\theta_m], \tag{4.56}$$

Considering (4.23), we have

$$\eta_k=\int_0^{\infty}\frac{\omega_k\mathbb{P}\left(\mathrm{SIR}_0^k\geq e^u-1,\mathrm{SIR}_0^k\geq\theta_k,\cap_{m=1}^{k-1}\mathrm{SIR}_0^m<\theta_m\right)}{\mathbb{P}\left(\mathrm{SIR}_0^k\geq\theta_k,\cap_{m=1}^{k-1}\mathrm{SIR}_0^m<\theta_m\right)}\mathrm{d}u. \tag{4.57}$$

From the same approach used in the proof of Theorem 5, it can be written as

$$\eta_k = \frac{\omega_k}{p_k} \int_0^{\infty} \mathbb{P}\Big(\mathrm{SIR}_0^k \geq \max(\theta_k, e^u - 1), \bigcap_{m=1}^{k-1} \mathrm{SIR}_0^m < \theta_m\Big) \mathrm{d}u, \tag{4.58}$$

and the term inside the integral can be simplified by dividing the integral bound into $[0, \ln(1+\theta_k)]$ and $[\ln(1+\theta_k), \infty]$. Hence, we can rewrite (4.58) as follows

$$\begin{aligned} \eta_k = \frac{\omega_k}{p_k} \Big[ \int_0^{\ln(1+\theta_k)} & \mathbb{P}\Big(\mathrm{SIR}_0^k \geq \theta_k, \bigcap_{m=1}^{k-1} \mathrm{SIR}_0^m < \theta_m\Big) \mathrm{d}u \\ + \int_{\ln(1+\theta_k)}^{\infty} & \mathbb{P}\Big(\mathrm{SIR}_0^k \geq (e^u - 1), \bigcap_{m=1}^{k-1} \mathrm{SIR}_0^m < \theta_m\Big) \mathrm{d}u \Big]. \end{aligned} \tag{4.59}$$

Using (4.44) and (4.45), and applying the change of variable $z = e^u - 1$, (4.54) is obtained. □

The overall SE of the typical user in the non-full interference network is $\overline{\eta} = \sum_{k=1}^{N} p_k \eta_k$.

### 4.3.5 Bandwidth allocation

In this part, we investigate two strategies to allocate the available bandwidth [154] among $N$ class of users to have the maximum overall spectral efficiency or fair bandwidth allocation among different user types. To maximize the overall spectral efficiency, the maximization problem can be written as

$$\max_{\{\omega_k\}_{1 \leq k \leq N}} \sum_{k=1}^{N} \omega_k \left( p_k \ln(1+\theta_k) + \int_{\theta_k}^{\infty} g_k(z) \mathrm{d}z \right) \tag{4.60}$$

$$\text{subject to:} \quad \sum_{k=1}^{N} \omega_k = 1, \ \omega_k \geq 0.$$

The optimal solution of (4.60) is simply given by $\omega_k = 1$ for the index $k$ corresponding to the largest value of $p_k \ln(1+\theta_k) + \int_{\theta_k}^{\infty} g_k(z) \mathrm{d}z$, which is function of the classification thresholds set, and $\omega_k = 0$ otherwise. However, this strategy does not allow fairness among users and it can be preferable to share the RB among all the covered users, i.e., $\omega_k > 0$ for all $k$. Two policies can be followed.

1. *Equal bandwidth partitions.* This model assigns a value in $\omega_k \in (0,1)$, regardless of the quality of service required by the type-$k$ user. The simplest partition policy, which does not need any other information from the system, is an equal partitioning method where the RB is equally divided into $N$ equal sub-channels, i.e. $\omega_k = 1/N$. In this case, the overall SE of the given typical user is obviously

$$\overline{\eta} = \frac{1}{N} \sum_{k=1}^{N} \left( p_k \ln(1+\theta_k) + \int_{\theta_k}^{\infty} g_k(z) \mathrm{d}z \right). \tag{4.61}$$

2. *SIR-proportional bandwidth partitions.* The available bandwidth is shared among the users according to the SIR distribution and traffic load. In a regular grid network, the frequency reuse scheme relies on a geometry-based policy to allocate a set of contiguous bandwidth chunks among cell center and cell edge users which is proportional to the square of the ratio of the interior radius and the cell radius [1]. In PPP models, geometric foreknowledge for chunk allocation is not employed and, instead, the allocation can be made based on the SIR distribution [1]. Hence, in the SIR-proportional model, we have $\omega_k = p_k$ and the overall SE is

$$\overline{\eta} = \sum_{k=1}^{N} \left( p_k^2 \ln(1+\theta_k) + p_k \int_{\theta_k}^{\infty} g_k(z) \mathrm{d}z \right). \tag{4.62}$$

### 4.3.6 Simulation and numerical results

In this scenario, we evaluate the average performance of the bandwidth allocation detailed above in a PPP network. To this end, we compare the average SE obtained with our theoretical findings with Monte Carlo simulations. In particular, we investigate the behavior of known bandwidth allocation strategies, i.e., equal and SIR-proportional, in the non-full interference framework.

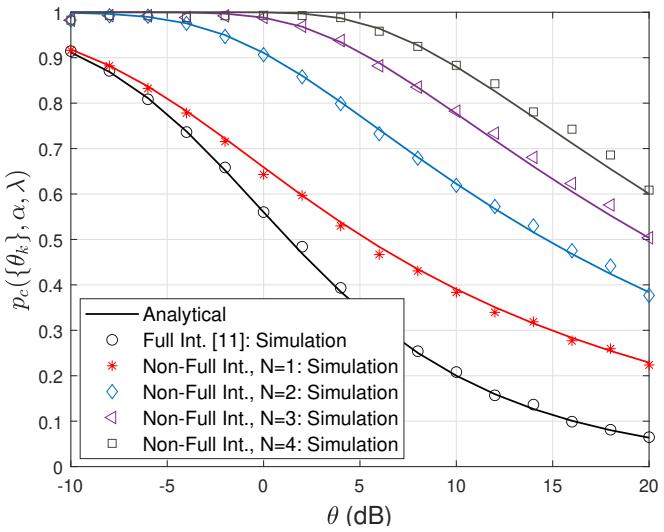


Figure 4.9 – Coverage probability.

Fig. 4.9 shows the simulation and the analytical results for the coverage probability (4.38) for a typical user when $N \in \{1,2,3,4\}$, under non-full and full interference scenarios when a unique $\theta$ is considered, i.e., the target threshold is the same for all user classes. The non-full interference strategy induced by the user-centric RB

allocation according to the type of users, leads to a larger coverage probability when $N$ increases. The analytical derivations are relatively close to the simulations especially for small values of threshold. However, the mismatch increases as the threshold and $N$ increase. The gap comes from the lack of a proper density of active BS in the simulation scenario in relative sub-channels when $N$ is large. Moreover the estimation of the type-$k$ interfering set of BS by simulation is an iterative process that is sensitive to the threshold value and requires a lot of iterations when $\theta$ is large. Nonetheless, this approach fits when the threshold $\theta$ is not too large to ensure enough active BS for large scale network approximation in simulation.

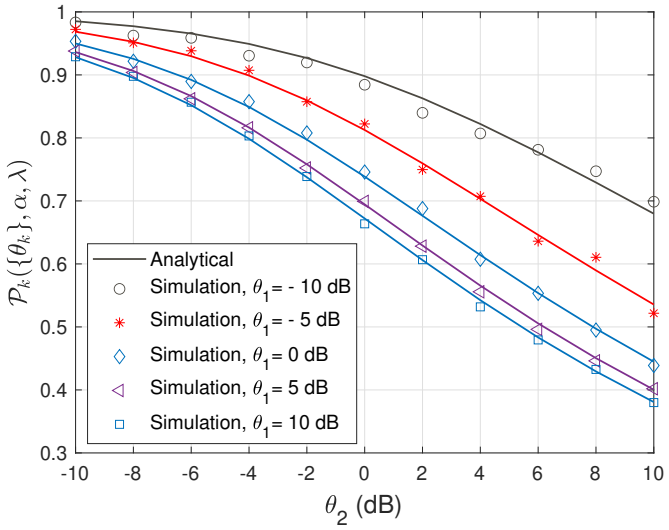


Figure 4.10 – Conditional coverage probability for $k = 2$ users case.

In Fig. 4.10, the type-2 user conditional coverage probability $\mathscr{P}_2$ in (4.49) is plotted versus $\theta_2$ for specific type-1 target thresholds $\theta_1 = \{-10, -5, 0, 5, 10\}$ dB. When $\theta_1$ decreases, the number of active BS in the type-2 class, i.e., interfering BS, decreases and consequently the conditional coverage probability of the typical type-2 user increases, because there is less interference in this type of user.

Fig. 4.11 shows the probability $p_k$ derived in expression (4.39) that the typical user be a type-$k$ user for $k \in \{1,2,3,4\}$. From the figure, it can be seen that when increasing the unique target threshold $\theta$, the probability $p_1$ decreases, but $p_2$, $p_3$ and $p_4$ increase and then decrease after a specific threshold value. It is because, by increasing the unique threshold value, the number of type-1 users decreases. Hence the chance of that the users become type-2 users is increase. However by increasing $\theta$ value, the probability of type-2 users also decreases and the chance of being type-3 and type–4 increases. Finally for large threshold values, all type user probabilities decrease and go to zero value.

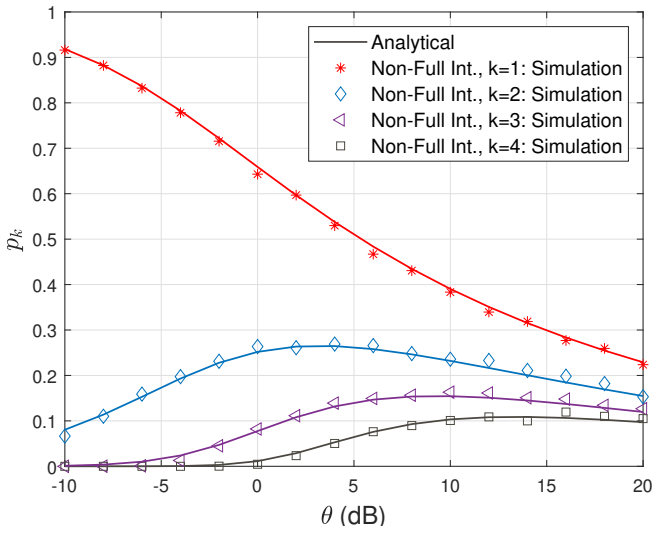


Figure 4.11 – Probability of being type-k user.

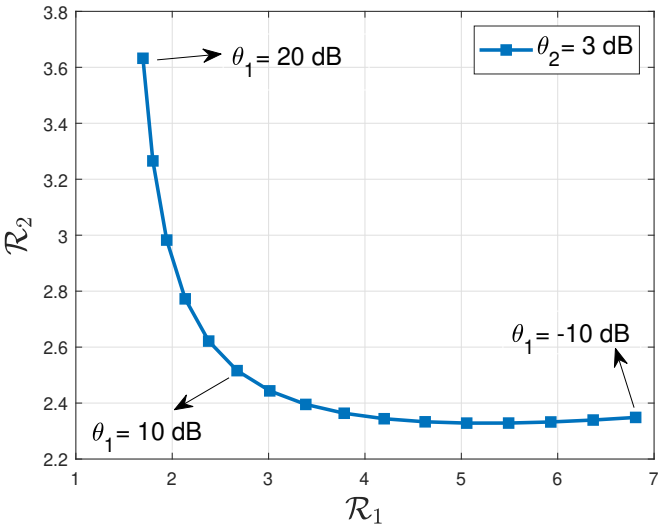


Figure 4.12 – Type-1 and type-2 SE tradeoff.

Fig. 4.12 represents the tradeoff between the spectral efficiencies of type-1 and type-2 user classes regardless of the bandwidth allocation strategy and evaluated with (4.54). The tradeoff curve varies according to the value of $\theta_1 = [-10, 20]$ dB when the threshold of type-2 is $\theta_2 = 3$ dB. The type-2 spectral efficiency increases with $\theta_1$, since the number of type-2 user increases. However, decreasing $\theta_1$ is favorable for type-1 users and increases the number of users who can satisfy the threshold in cell center area which increases the type-1 user SE.

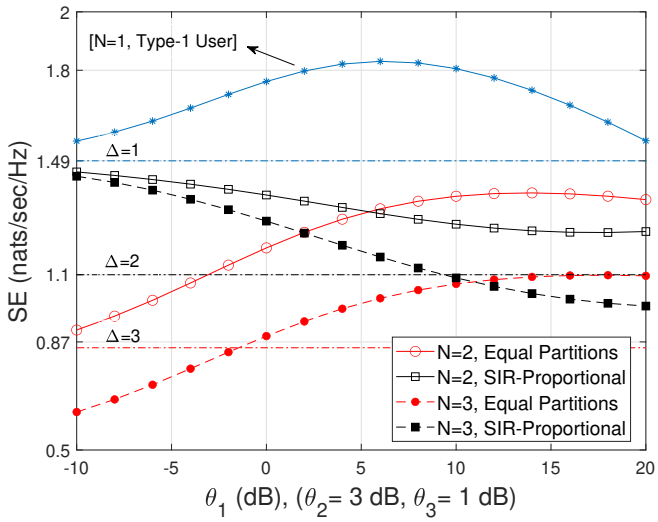


Figure 4.13 – SE under equal and SIR-proportional partitioning strategies.

Fig. 4.13 represents analytical results of the overall spectral efficiency for $N \in \{1,2,3\}$ in the non-full interference network versus the type-1 user target threshold $\theta_1$ when $\theta_2 = 3$ dB and $\theta_2 = 1$ dB. The SE of different types of users are compared under fixed equal partitioning (4.61) and adaptive SIR-proportional (4.62) strategies. When $\theta_1$ increases, the total SE under SIR-proportional policy decreases and it increases under equal partitioning. It is because under SIR-proportional scheme we have more allocated bandwidth to type-1 users who have large SE as well. By increasing the value of $\theta_1$, SIR-proportional gives less bandwidth to CCU and more bandwidth to other user-types to compensate their achievable spectral efficiencies in the network. On the other side, since equal BW partitioning scheme allocates same portion of bandwidth to all user-types, increasing $\theta_1$ leads to increase SE of other user types and finally the total SE increases when $\theta_2 = 3$ dB and $\theta_3 = 1$ dB. Moreover, the total SE is compared with the frequency reuse technique with reuse factor $\Delta$ presented in [2], under full interference network, i.e., only one type of user. Since in SIR-proportional policy, the typical user benefits from a fraction of resources that depends on the SIR, and suffers from the same fraction of the interference, it has higher SE than FR with $\Delta = 1$, $\Delta = 2$ and $\Delta = 3$, respectively.

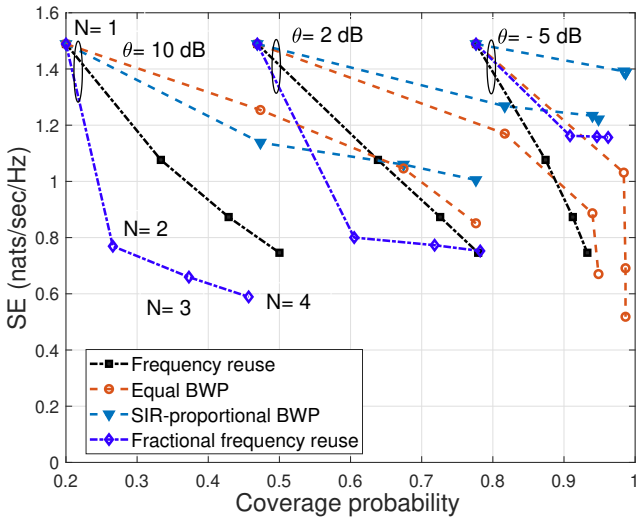


Figure 4.14 – SE-Coverage probability tradeoff under equal and SIR-proportional partitioning strategies.

Fig. 4.14 compares the network average SE-coverage probability tradeoff for SIR-proportional, equal BW partition schemes, fractional frequency reuse [1] and frequency reuse (with $\Delta = N$) [2] for an unique threshold value $\theta$ ranging in $\{-5, 2, 10\}$ dB. In the case of fractional frequency reuse, $N$ type user classification means that we still have full interference in cell center sub-channel, but the remained part of bandwidth is partitioned by frequency reuse approach with reuse factor $N-1$ which leads to classifying CEU to $N-1$ classes. Regardless of the bandwidth partitioning scheme used, the coverage probability increases, whereas the average SE declines as $N$ increases, but with different trends as $\theta$ increases. Fractional frequency scheme allocates the available bandwidth between CCU and CEU based on their SIR values w.r.t. a given threshold [1]. For $\theta = -5$ dB, it achieves better results than frequency reuse approach because most of the bandwidth is allocated to CCU who have larger SIR. However, increasing $\theta$ decreases the SE of fractional frequency reuse because it allocates more bandwidth to cell edge area. Moreover, it is above the equal BWP for $\theta = -5$ dB, which is because of using SIR based BWP approach that gives more bandwidth to CCU. However, a large value $\theta = 10$ dB shrinks cell center area and gives more bandwidth to cell edge area. Since fractional frequency uses reuse factor $N-1$, it is lower than frequency reuse approach with reuse factor $N$. Equal partitioning, on the other hand, allocates bandwidth equally regardless of the user type density. When $\theta = 10$ dB and $N = 2$, an equal partitioning has higher SE than SIR-proportional partitioning. Because a high threshold value shrinks the cell center region, and the SIR-proportional approach allocates more bandwidth to CEU, whose SE are lower than that of CCU.

## 4.4 Conclusion

In this chapter, we have provided a novel definition of a non-full interference network that correlates the activity of a BS to the user's position within the cell. An accurate approximation of the user classification probability is derived. The expression is obtained under the form of a fixed-point equation that models the existing correlation between the desired signal and the interference set of each user type. In particular, this chapter has presented an accurate expression of the global coverage probability when the users are classified to CCU and CEU. We have developed an analytic framework for evaluating the coverage probability of a typical cell edge user in a single-tier cellular network where the locations of BS are modeled as PPP. To be consistent with the existent models [2], we also assumed the typical user and the nearest BS association approach. The presented approach has been extended to multiple classes of users, and semi-closed-form performance metrics based on the received SIR level for each user type have been obtained. The results show that the user-centric resource allocation approach outperforms the conventional frequency reuse approach, which is BS-centric. The next chapter investigates a BS cooperation-based method to help CEU in the non-full interference networks. Several bandwidth partitioning schemes are presented to improve network SE and a SE-fairness tradeoff based bandwidth allocation is investigated that considers the fairness among different type of users in the network.

# Chapter 5

# Non-full Interference Cellular Networks: BS Cooperation and Bandwidth Partitioning

## 5.1 Introduction

In this chapter, relying on the presented multi-class non-full interference model in the previous chapter, a BS cooperation technique is studied to improve the SE of cell edge users without jeopardizing other scheduled users in the same RB. Moreover, a bandwidth allocation among users considering tradeoff on the average SE of the network and the fairness for all user types is proposed and compared with different bandwidth allocation scenarios in our non-full interference context.

As discussed in the previous chapter, the related works do not capture the correlation in SIR induced by the fact that the user's interference set is a function of its coverage probability. The non-full interference model presented in this thesis is a first step to overcome the above limitations while enabling the tractable system-level study of the typical user performance in downlink using stochastic geometry. The key contributions of our study in this chapter are briefly summarized below.

- Optimal point selection BS cooperation techniques are used to improve the performance of cell edge users without degrading the performance of the other user types;
- Different BWP formulations under the user-centric frequency reuse model are evaluated. From the network perspective, the objective is to maximize the average SE under constraints, minimizing SE's variance to guarantee fairness among different user types. We propose a risk-averse approach to find a mean-variance tradeoff for the network performance;

- Our numerical results demonstrate that: *i*) in comparison to the conventional frequency reuse scheme, user-centric frequency reuse boosts network efficiency and allows high SE, *ii*) the non-full interference-based BS cooperation can help vulnerable users without penalizing other users in other cells, *iii*) the proposed tradeoff BWP strategy assigns fair shares to the different types of users based on their performance metrics.

## 5.2 System model and assumptions

The system model follows the model presented in the previous chapter. However, in the non-full interference setting in chapter 4, $\Phi_{N+1}$ is the set of idle BS, i.e., do not have a user in their coverage region. On the other hand, in the full interference scenario, all BS are transmitting in a given RB. In this chapter, in order to have same density of interference with full interference scenario, in the given RB, we consider that in our model all BS transmit but in different allocated sub-channels. Using the same classification technique presented in chapter 4, we classify all users into $N$ classes and assume that BS in $\Phi_N$ are active and transmitting with the worse link quality. Still, they may have users in outage. Therefore, a cell is divided into $N$ classes, and a typical user belongs to a certain class depending on its SIR. Moreover, each class has its proper sub-band that may be used by the nearest interfering cell but only by the same user type in that interfering cell. By applying this modification in the model, the derivation of the type-$N$ user is not fixed point such as previous chapter and it depends on the other user type's probability. However, $p_k$, $k \in [\![1, N-1]\!]$, still has a fixed point equation form. In the following, we find the conditional coverage probability and spectral efficiency for type-$N$ user when all BS transmit in non-full interference scenario.

In the above full transmission assumption of non-full interference model, let us consider $X_i$ as the position of BS $i$, and $\mathrm{SIR}_i^k$ is the SIR experienced by a randomly selected user in cell $i$ over the subchannel $k$. The subset $\Phi_k$ is

$$\Phi_k \triangleq \begin{cases} \left\{X_i : \mathrm{SIR}_i^k \geq \theta_k \text{ and } \mathrm{SIR}_i^m < \theta_m, \forall m, 1 \leq m < k\right\}, & 1 \leq k \leq N-1 \\ \left\{X_i : \mathrm{SIR}_i^m < \theta_m, \forall m, 1 \leq m < k\right\}, & k = N \end{cases}, \tag{5.1}$$

where $\theta_k > 0$, $\forall k \in [\![1, N]\!]$, are the SIR classification thresholds. For the subset $\Phi_N$, the $\mathrm{SIR}_i^N$ can be higher or lower than the threshold $\theta_N$.

## 5.3 Our model with full transmission assumption

This section first derives the coverage probability of the typical user under a user-centric frequency reuse approach in the non-full interference network in the context of the model explained in subsection 5.2. Next, to fairly evaluate the proposed method, the SE of the network is studied.

### 5.3.1 Coverage probability

In the model presented in the previous chapter, the typical user was covered if it does not belong to the last type of users. However, in the model presented in section 5.2, we have a set of thresholds $\{\theta_k\}_{1\leq k\leq N}$ to successfully demodulate and decode the received signal. Then, the typical user located in the typical cell is covered on downlink if:

$$X_0 \in \Phi_1 \cup \cdots \cup \Phi_{N-1} \cup \{\Phi_N, \mathrm{SIR}_0^N \geq \theta_N\}. \tag{5.2}$$

The following corollary presents the downlink coverage probability of the typical user for a non-full interference network with $N$ classes.

**Corollary 3.** *Given $\{\theta_k\}_{1\leq k\leq N}$, the coverage probability of a randomly located typical user in a non-full interference network with N user types is given by*

$$p_c(\{\theta_k\}_{k=1}^N, \alpha, \lambda) = \sum_{k=1}^{N-1} p_k + p_N \cdot \mathscr{P}_N(\{\theta_k\}_{k=1}^N, \alpha, \lambda), \tag{5.3}$$

*where*

$$p_k = \int_0^\infty e^{-v(1+p_k\rho(\theta_k,\alpha))} \prod_{i=1}^{k-1} \left(1 - e^{-p_i\rho(\theta_i,\alpha)v}\right) \mathrm{d}v\,, \forall\, k \in [\![1, N-1]\!] \tag{5.4}$$

$$p_N = 1 - \sum_{k=1}^{N-1} p_k, \tag{5.5}$$

$$\mathscr{P}_N(\{\theta_k\}_{k=1}^N, \alpha, \lambda) = \frac{1}{p_N} \int_0^\infty e^{-v(1+p_N\rho(\theta_N,\alpha))} \prod_{i=1}^{N-1} \left(1 - e^{-p_i\rho(\theta_i,\alpha)v}\right) \mathrm{d}v, \tag{5.6}$$

*and*

$$\rho(\theta, \alpha) = \frac{2\theta}{\alpha - 2}\, {}_2F_1\left(1, 1 - \frac{2}{\alpha}; 2 - \frac{2}{\alpha}; -\theta\right). \tag{5.7}$$

*Proof.* The proof follows from the law of total probability and the fact that sets in (5.2) are disjoint. □

One important point is that (5.4) is a fixed point equation of $p_k$, which approximates the probability of a typical user being a type-$k$ user, $\mathscr{P}_N$ is the conditional coverage probability of type-$N$ user in the non-full interference network. Two other corollaries of importance are deduced from Corollary 3.

The expression in (5.4) can not be simplified further, except for the probability of the type-1 (cell center) user and is stated in the following corollary.

**Corollary 4.** *Given $\alpha$ and $\theta_1$, the probability of being the cell center user ($k=1$ in (5.4)) is given as*

$$p_c = p_1 = \frac{1}{2}\,{}_2F_1\left(\frac{1}{2},1;2;-4\rho(\theta_1,\alpha)\right). \tag{5.8}$$

*Proof.* The proof follows from (5.4) and using $\left(\frac{\sqrt{1+x}-1}{x}\right)^a = 2^{-a}\,{}_2F_1\left(\frac{a}{2},\frac{a+1}{2};a+1;-x\right)$. □

As the coverage does not consider the resource used, we investigate the impact of the proposed classification on SE as follows.

### 5.3.2 Spectral efficiency

In the model presented in subsection 5.2, a given RB is divided into $N$ subchannels, each assigned to its corresponding user type. Each type-$k$ user transmits over the $k$th subchannel. All derivation of spectral efficiency for different user types are same as the previous chapter and the only difference is for the SE of user type-$N$. In the following, the SE of type-$k$ user, $\forall k \in [\![1,N]\!]$ is expressed.

$$\mathscr{R}_k = \frac{1}{p_k}\left(p_k \ln(1+\theta_k) + \int_{\theta_k}^{\infty} g_k(z)\mathrm{d}z\right), \tag{5.9}$$

where

$$g_k(z) = \frac{1}{1+z}\int_0^{\infty} e^{-v(1+p_k\rho(z,\alpha))}\prod_{i=1}^{k-1}\left(1-e^{-p_i\rho(\theta_i,\alpha)v}\right)\mathrm{d}v, \tag{5.10}$$

and

$$\mathscr{R}_N = \int_0^{\infty}\int_0^{\infty}\frac{e^{-v(1+p_N\rho(e^u-1,\alpha))}}{p_N}\prod_{i=1}^{N-1}\left(1-e^{-p_i\rho(\theta_i,\alpha)v}\right)\mathrm{d}v\mathrm{d}u. \tag{5.11}$$

The next section explicitly studies the performance of BS cooperation in the non-full interference cellular networks. An OPS technique in a cooperation set of a type-$N$ user is applied to enhance the performance of the type-$N$ user.

## 5.4 Performance with cooperation

In this section, we investigate a BS cooperation scheme [155], an optimal point selection technique [125], to improve the performance of the typical type-$N$ user. Precisely, our proposed scheme exploits the fact that a BS that serves a type-$k$ user in another cell is only active on the $k$-th subchannel and remains idle for all the other subchannels and in particular for the $N$-th subchannel.

### 5.4.1 User classification

Recalling Fig. 4.8 and the fact that a type-$N$ user's cooperation set consists in the $N-1$ closest BS of class $k \in [\![1, N-1]\!]$ plus its BS on subchannel $N$, the tagged type-$N$ user selects the BS among the cooperation set with the best channel quality, while the remaining $N-1$ BS stay silent in the $N$th subchannel. Here, the channel quality is the product of the large-scale path loss and the small-scale fading. The user has the opportunity to change its firstly associated BS, with an association based on distance, to another BS with a better channel quality. To drive the related performance metrics, next we express the instantaneous received signal to interference ratio experienced by the type-$N$ user under the mentioned optimal point selection.

Let $\mathscr{C}_o = \{X^k \triangleq \arg\min_{X_i} \|X_i\| : X_i \in \Phi_k, 1 \le k \le N-1\}$ be the set of BS that are the nearest type-$k$ BS to the typical type-$N$ user. Hence, the SIR of the typical type-$N$ user is

$$\mathrm{SIR}_0^N = \frac{S_N}{I_N}, \tag{5.12}$$

where

$$I_N = \sum_{k=1}^{N} I_{N,k}, \tag{5.13}$$

and

$$S_N = \max_{X_i \in \mathscr{C}_0 \cup X_0} \{H_i^N R_i^{-\alpha}\}, \tag{5.14}$$

$$I_{N,k} = \sum_{X_i \in \Phi_k \setminus \mathscr{C}_0} H_i^N R_i^{-\alpha} \mathbf{1}_{\mathscr{A}_i^k}, \forall\, 1 \le k \le N, \tag{5.15}$$

while considering

$$\mathbf{1}_{\mathscr{A}_i^k} = \begin{cases} 1 & \text{if the type-}k\text{ BS } X_i \text{ is selected to serve a type-}N\text{ user} \\ 0 & \text{otherwise} \end{cases}. \tag{5.16}$$

The main intermediate stage in analyzing the proposed OPS's efficiency is to characterize the joint distribution of the distance between the typical user and the set of candidate BS to cooperate. Let $T_k$ be the distance of the typical type-$N$ user to the nearest BS serving a type-$k$ user and

$$T_k = \min_{X_i \in \Phi_k} R_i, \quad \forall 1 \le k \le N-1. \tag{5.17}$$

Moreover, let $G_k$, for $1 \le k \le N-1$, be the fading channel between the typical type-$N$ user and its nearest type-$k$ BS on the $N$-th subchannel of the RB.

### 5.4.2 The joint distances distribution

The following lemma gives the joint PDF of $\mathbf{T} = [T_1, \ldots, T_{N-1}, R_0]$.

**Lemma 1.** *Conditioning on the distance of a typical type-N user from its nearest BS $R_0$, the PDF of the distance between the typical user and the nearest helping BS which serves a type-k user $T_k$, $1 \leq k \leq N-1$, is*

$$f_{T_k|R_0}(t_k \mid r_0) = 2\pi\lambda p_k t_k \exp(-\pi\lambda p_k (t_k^2 - r_0^2)). \tag{5.18}$$

*Proof.* The void probability of a 2-D Poisson process $\Phi_k$ with density $\lambda_k = p_k\lambda$ in an area $A$ is $\exp(-\lambda_k A)$. The cumulative distribution function of the distance $T_k$ from the typical user to the nearest BS in $\Phi_k$ conditioning on $T_k > R_0$ is

$$F_{T_k|R_0}(t_k \mid r_0) = 1 - \exp(-\pi\lambda_k (t_k^2 - r_0^2)). \tag{5.19}$$

By tacking the derivative of (5.19) with respect to $t_k$ and knowing that in our model $\lambda_k = p_k\lambda$, we can derive (5.18). □

Using Lemma 1 and knowing that different types of BS come from disjoint sets, the joint conditional PDF of $\mathbf{T}$ given $R_0$ is

$$f_{\mathbf{T}|R_0}(t_1, \cdots, t_{N-1} \mid r_0) = \prod_{k=1}^{N-1} f_{T_k|R_0}(t_k \mid r_0) \tag{5.20}$$

Then, unconditioning it by the PDF of $R_0$, i.e., $f_{R_0}(r_0) = 2\pi\lambda r_0 e^{-\pi\lambda r_0^2}$, gives the joint distances distribution on $\{T_k > R_0, k \in [\![1, N-1]\!]\}$ as

$$f_{\mathbf{T}}(t_1, \cdots, r_0) = (2\pi\lambda)^N r_0 \left(\prod_{k=1}^{N-1} p_k t_k\right) \exp\left(-\pi\lambda \sum_{k=1}^{N-1} p_k t_k^2\right) \exp\left(-\pi\lambda \left(1 - \sum_{k=1}^{N-1} p_k\right) r_0^2\right). \tag{5.21}$$

### 5.4.3 The Laplace transform of the interference

According to (5.15), the Laplace transform of the interference is given by

$$\mathscr{L}_{I_N}(s) = \mathbb{E}_{I_{N,k}}\left[\exp\left(-s \sum_{k=1}^{N} I_{N,k}\right)\right] = \prod_{k=1}^{N} \mathscr{L}_{I_{N,k}}(s), \tag{5.22}$$

where

$$\mathscr{L}_{I_{N,k}}(s) = \mathbb{E}\left[\exp\left(-s \sum_{X_i \in \Phi_k \setminus \mathscr{C}_0} H_i^N R_i^{-\alpha} \mathbf{1}_{\mathscr{A}_i^k}\right)\right]$$

$$\stackrel{a}{=}\mathbb{E}_{\Phi,\{H_i^N\}}\Big[\prod_{X_i\in\Phi_k\setminus\mathscr{C}_0}\Big(\mathbb{E}[\mathbf{1}_{\mathscr{A}_i^k}]e^{-sH_i^N R_i^{-\alpha}}+(1-\mathbb{E}[\mathbf{1}_{\mathscr{A}_i^k}])\Big)\Big]$$

$$\stackrel{b}{=}\mathbb{E}_{\Phi}\Big[\prod_{X_i\in\Phi_k\setminus\mathscr{C}_0}1-\mathbb{E}[\mathbf{1}_{\mathscr{A}_i^k}]\left(1-\frac{1}{1+sR_i^{-\alpha}}\right)\Big] \tag{5.23}$$

where (a) follows from the law of total expectation, i.e., $\mathbb{E}_X[f(X)]=\mathbb{E}_Y[\mathbb{E}_X[f(X)|Y]]$, (b) comes from averaging over the i.i.d. exponential distribution of interfering fading channels $H_i^N$ with mean 1, as in [2], and factoring out the term $\mathbb{E}[\mathbf{1}_{\mathscr{A}_i^k}]$.

Finally by applying the probability generating function (PGFL) of a PPP [31], we have

$$\begin{aligned}\mathscr{L}_{I_{N,k}}(s)&=\exp\left(-2\pi\lambda_k p_{a_k}\int_{t_k}^{\infty}\frac{sr}{r^\alpha+s}\mathrm{d}r\right)\\&=\exp\left(-\pi\lambda p_k p_{a_k}\rho(st_k^{-\alpha},\alpha)t_k^2\right),\end{aligned} \tag{5.24}$$

where $p_{a_k}$ is the probability that a BS serving a type-$k$ user is selected by OPS to serve the typical type-$N$ user. Hence,

$$p_{a_k}=\mathbb{P}\Big(G_1T_1^{-\alpha}<G_kT_k^{-\alpha},\cdots,H_0^NR_0^{-\alpha}<G_kT_k^{-\alpha}\Big),\quad\forall\, k\in[\![1,N-1]\!]. \tag{5.25}$$

Similarly, for $k=N$,

$$\mathscr{L}_{I_{N,N}}(s)=\exp\left(-\pi\lambda\left(1-\sum_{k=1}^{N-1}p_k\right)p_{a_N}\rho(sr_0^{-\alpha},\alpha)r_0^2\right). \tag{5.26}$$

**Remark 1.** *Based on the cooperation set definition, it is possible to have the same BS in the cooperation set of different type-N users in the model. Moreover, in Section 5.2, we consider that each BS could serve only one user in the relative subchannel of the RB. Hence, if OPS scheme selects the same type-k BS for two or more type-N users, the selected BS can only serve one type-N user, and other type-N users must search for another BS in their cooperation set.*

According to the above remark, quantifying the probability that one cooperative BS be selected by two or more type-$N$ users is a complex problem. However, the density of type-$N$ users can be relatively lower than the other type of users based on the number of user classes and the classification threshold $\{\theta_k\}_{k=1}^{N-1}$ (see Fig. 4.1). Therefore, it is assumed that the common BS in the cooperation sets of different type-$N$ users can be neglected. The numerical results show that this assumption is reasonable and leads to tight approximations.

The probability that OPS technique selects the first associated type-$N$ BS is $p_{a_N}$, used in (5.26), and it is the complementary event of all cooperation events in (5.25).

Hence, we can write

$$p_{a_N} = 1 - \sum_{k=1}^{N-1} p_{a_k}. \tag{5.27}$$

The probabilities $p_{a_k}$ are given by the following theorem.

**Theorem 9.** *Given that OPS is applied to the cooperation set of a typical type-N user, the probability that a type-k BS is selected to serve the typical type-N user is*

$$p_{a_k} = \int_0^\infty \underbrace{\int_{B^c(0,r_0)}^\infty \cdots \int_{B^c(0,r_0)}^\infty}_{N-1} \int_0^\infty e^{-g} \left(1-e^{-\left(\frac{r_0}{t_k}\right)^\alpha g}\right) \prod_{\substack{m=1 \\ m\neq k}}^{N-1} \left(1-e^{-\left(\frac{t_m}{t_k}\right)^\alpha g}\right)$$
$$\times f_{T_1,\cdots,T_{N-1},R_0}(t_1,\cdots,t_{N-1},r_0)\mathrm{d}g\mathrm{d}t_1\cdots\mathrm{d}t_{N-1}\mathrm{d}r_0, \tag{5.28}$$

*where $B^c(0,r_0)$ denotes the complement of $B(0,r_0)$, which is a ball centered at the origin with radius $r_0$*

*Proof.* Referring (5.25) and knowing that $\{\{G_m\}_{m=1}^{N-1}, H_0^N\}$ are i.i.e.d., by conditioning on $G_k$ and on the distances distribution $\mathbf{T}$, we can write

$$\begin{aligned} p_{a_k} &= \mathbb{E}_{\mathbf{T}}\mathbb{E}_{G_k}\left[\mathbb{E}_{G_1}\left[\mathbf{1}\left(G_1 < G_k\left(\frac{T_1}{T_k}\right)^\alpha\right)\right] \times \cdots \times \mathbb{E}_{H_0^N}\left[\mathbf{1}\left(H_0^N < G_k\left(\frac{R_0}{T_k}\right)^\alpha\right)\right]\right] \\ &= \mathbb{E}_{\mathbf{T}}\mathbb{E}_{G_k}\left[\prod_{\substack{m=1 \\ m\neq k}}^{N-1} \mathbb{E}_{G_m}\left[\mathbf{1}\left(G_m < G_k\left(\frac{T_m}{T_k}\right)^\alpha\right)\right] \times \mathbb{E}_{H_0^N}\left[\mathbf{1}\left(H_0^N < G_k\left(\frac{R_0}{T_k}\right)^\alpha\right)\right]\right] \\ &= \mathbb{E}_{\mathbf{T}}\mathbb{E}_{G_k}\left[\prod_{\substack{m=1 \\ m\neq k}}^{N-1} \left(1-\exp\left(-\left(\frac{T_m}{T_k}\right)^\alpha G_k\right)\right) \times \left(1-\exp\left(-\left(\frac{R_0}{T_k}\right)^\alpha G_k\right)\right)\right]. \end{aligned} \tag{5.29}$$

the proof ends by averaging over $G_k$ and $\mathbf{T}$. □

### 5.4.4 Coverage probability

We derive the coverage probability of the typical type-$N$ user using the joint distribution of distances from its cooperation set BS, given in (5.21).

**Theorem 10.** *Given that OPS is applied to the cooperation set of a typical type-N user, the coverage probability of the typical type-N user is given by*

$$\mathscr{P}_N(\{\theta_k\}_{k=1}^N, \alpha, \lambda) = 1 - \frac{1}{p_N}\int_0^\infty \underbrace{\int_{B^c(0,r_0)}^\infty \cdots \int_{B^c(0,r_0)}^\infty}_{N-1} \left(1-\mathscr{L}_{I_N}(\theta_N r_0^\alpha)\right) \prod_{k=1}^{N-1}\left(1-\mathscr{L}_{I_N}(\theta_N t_k^\alpha)\right)$$

$$\times \left(1-\mathscr{L}_{I_{0,k}}(\theta_k r_0^{\alpha})\right) f_{T_1,\cdots,T_{N-1}R_0}(t_1,\cdots,t_{N-1},r_0)\,\mathrm{d}t_1\cdots\mathrm{d}t_{N-1}\mathrm{d}r_0, \tag{5.30}$$

*where* $\mathscr{L}_{I_N}(s)$ *is obtained by* (5.22) *and*

$$\mathscr{L}_{I_{0,k}}(s) = \exp\left(-\pi\lambda p_k \rho(s r_0^{-\alpha},\alpha) r_0^2\right). \tag{5.31}$$

*Proof.* See Appendix A.3. □

### 5.4.5 Spectral Efficiency

Using (2.36), the SE of the typical type-$N$ user under OPS scheme can be written as

$$\mathscr{R}_N = \int_0^{\infty} \mathscr{P}_N\left(\{\theta_k\}_{k=1}^{N-1}, \theta_N = e^u - 1, \alpha, \lambda\right) \mathrm{d}u. \tag{5.32}$$

Next, we give closed-form expressions of the type-2 (cell edge) user's performance metrics when OPS is applied in the non-full interference network with $N = 2$.

## 5.5 A special case: two user types classification

As a particular case, let us consider the non-full interference network with two user types in the network. In this case, type-1 and type-2, called cell center and cell edge users, are present in the network. The probability of a typical user be a cell center user is $p_c$ and its nearest BS fully covers it. Otherwise, the user will be a cell edge user with probability $1-p_c$. In the following, the closed-form expressions for the conditional coverage probability and the spectral efficiency of the typical cell edge user under OPS scheme are derived.

### 5.5.1 Cooperation probability

The probability that a BS serving a cell center user be selected by OPS to cooperate in the second (cell edge) subchannel of the scheduled resource is

$$p_a = \mathbb{P}(G_1 T_1^{-\alpha} > H_0^2 R_0^{-\alpha}), \tag{5.33}$$

where $G_1$ is the cooperation gain in the second subchannel, $H_0^2$ is the gain between the tagged BS and its cell-edge user, $T_1$ is the distance between the typical cell-edge user and the nearest cooperative BS, and $R_0$ is the distance between the tagged BS and the cell-edge user. The probability $p_a$ can be computed with the following lemma.

**Lemma 2.** *The probability that a typical BS serving a cell center user calls for a cooperation is*

$$p_a = 1 - \sum_{k=0}^{\infty} \frac{2\,p_c(-1)^k}{\alpha k + 2}\,{}_2F_1\left(2,1;\frac{\alpha k}{2}+2;1-p_c\right). \tag{5.34}$$

*Proof.* See Appendix A.4. □

### 5.5.2 Coverage probability

The coverage probability of a typical cell edge user when OPS is applied can be formalized as follows.

**Corollary 5.** *Based on theorem 10 and given two coverage thresholds $\theta_1$ and $\theta_2$, the coverage probability of a typical cell edge user when OPS is applied in the non-full interference network can be calculated as*

$$\mathscr{P}_2(\theta_1,\theta_2,\alpha) = \frac{1}{1-p_c}\sum_{i=1}^{3}\left(\mathscr{M}_i(\theta_1,\theta_2,\alpha) - \mathscr{Q}_i(\theta_1,\theta_2,\alpha)\right), \tag{5.35}$$

*where $\mathscr{M}_i$ and $\mathscr{Q}_i$, $i \in \{1,2,3\}$, are given in (5.36) as follow.*

$$\begin{aligned}
\mathscr{M}_1(\theta_1,\theta_2,\alpha) &= p_c\int_0^1 \frac{\mathrm{d}x}{\mathscr{K}^2(x,\rho(\theta_2 x^{\frac{\alpha}{2}},\alpha),\rho(\theta_2,\alpha))},\\
\mathscr{M}_2(\theta_1,\theta_2,\alpha) &= p_c\int_0^1 \frac{\mathrm{d}x}{\mathscr{K}^2(x,\rho(\theta_2,\alpha),\rho(\theta_2 x^{-\frac{\alpha}{2}},\alpha))},\\
\mathscr{M}_3(\theta_1,\theta_2,\alpha) &= -p_c\int_0^1 \frac{\mathrm{d}x}{\mathscr{K}^2(x,\rho(\theta_2(1+x^{\frac{\alpha}{2}}),\alpha),\rho(\theta_2(1+x^{-\frac{\alpha}{2}})),\alpha)},\\
\mathscr{Q}_1(\theta_1,\theta_2,\alpha) &= p_c\int_0^1 \frac{\mathrm{d}x}{\left(p_c\,\rho(\theta_1,\alpha)x+\mathscr{K}\left(x,\rho(\theta_2 x^{\frac{\alpha}{2}},\alpha),\rho(\theta_2,\alpha)\right)\right)^2},\\
\mathscr{Q}_2(\theta_1,\theta_2,\alpha) &= p_c\int_0^1 \frac{\mathrm{d}x}{\left(p_c\,\rho(\theta_1,\alpha)x+\mathscr{K}\left(x,\rho(\theta_2,\alpha),\rho(\theta_2 x^{-\frac{\alpha}{2}},\alpha)\right)\right)^2},\\
\mathscr{Q}_3(\theta_1,\theta_2,\alpha) &= -p_c\int_0^1 \frac{\mathrm{d}x}{\left(p_c\,\rho(\theta_1,\alpha)x+\mathscr{K}\left(x,\rho(\theta_2(1+x^{\frac{\alpha}{2}}),\alpha),\rho(\theta_2(1+x^{-\frac{\alpha}{2}}),\alpha)\right)\right)^2},\\
\mathscr{K}(x,\kappa_1,\kappa_2) &= p_c + (1-p_c)p_a\kappa_1 + (1-p_c)(1+(1-p_a)\kappa_2)x.
\end{aligned} \tag{5.36}$$

*Proof.* See Appendix A.5. □

### 5.5.3 Spectral efficiency

SE of a typical cell edge user in OPS scheme can be obtained similarly to the previous subsection as

$$\mathscr{R}_2 = \int_0^{\infty} \mathscr{P}_2(\theta_1, e^u - 1, \alpha) \mathrm{d}u. \tag{5.37}$$

In subsection 5.5, we obtained a semi-closed form solution for coverage probability when we have two user types in the context of the non-full interference model. Since SE of the type-$k$ user in (4.54) is a function of the assigned fraction of bandwidth to the user, the network's average spectral efficiency is strongly correlated to the bandwidth allocation among different types of users in the network. The next section studies different bandwidth allocation strategies to find the tradeoff between SE and fairness in the network.

## 5.6 Bandwidth allocation and fairness

From (4.54), the network's spectral efficiency $\boldsymbol{\eta} = [\eta_1, ..., \eta_N]$ is a function of individual BWP $\boldsymbol{\omega} = [\omega_1, ..., \omega_N]$. Hence, the bandwidth allocation strategy plays an important role in the performance achieved. In the literature, several rules for bandwidth allocation are proposed and each of them possesses specific properties which justify its use in order to find an appropriate solution to the sum rate maximization problem. We investigate different bandwidth allocation approaches. Max-mean BWP rule aims at maximizing the average SE subject to some constraints. Equal BWP rule allocates the same fraction of bandwidth regardless of the type of users. SIR-proportional BWP rule is a probabilistic allocation and has been introduced in chapter 4, and shares bandwidth considering the type of users. Max-min BWP rule allocates bandwidth such that the worse case user's SE be maximized. In order to find a tradeoff between the fairness and the average SE in the network, we study a mean–variance tradeoff-based BWP by applying a risk-sensitive model [151] to control the variance of the SE allocated to users in the network.

### 5.6.1 Max-mean BWP strategy

The first BWP strategy tries to maximize the mean SE and is expressed as

$$\begin{aligned} \mathscr{P}_1 : \quad & \max_{\boldsymbol{\omega}} \quad \sum_k p_k \eta_k(\omega_k) \\ \text{s.t.} \quad & C_1 : \quad \omega_k \geq 0, \quad \forall\ k \in [\![1, N]\!] \\ & C_2 : \quad \sum_k \omega_k = 1. \end{aligned} \tag{5.38}$$

The optimal solution is simply given by $\omega_k = 1$ for the index $k$ corresponding to the largest value of $\mathscr{R}_k$, which is a function of the set of the classification thresholds, and $\omega_k = 0$ otherwise. However, this allocation does not take into account fairness among different users; it only aims at maximizing the sum of SE of all users. It can be preferable to share the RB among all the covered users, i.e., $\omega_k > 0$ for all $k$.

### 5.6.2 Equal BWP strategy

As explained in chapter 4, the simplest partition policy, which does not need any other information from the system, is the equal partitioning method where the RB is equally divided into $N$ subchannels, i.e., $\omega_k = 1/N$, $\forall k$. In this case, the weighted SE of the typical user is

$$\overline{\eta} = \frac{1}{N}\left(\sum_{k=1}^{N-1}\left(p_k \ln(1+\theta_k) + \int_{\theta_k}^{\infty} g_k(z)\mathrm{d}z\right) + p_N \mathscr{R}_N\right). \tag{5.39}$$

### 5.6.3 SIR-proportional BWP strategy

The third strategy is adaptive bandwidth partitions that has been introduced in chapter 4. In this case, the available bandwidth is shared among the users according to the SIR distribution and traffic load [1]. In a regular grid network, the frequency reuse scheme relies on a geometry-based policy to allocate a set of contiguous bandwidth chunks among cell center and cell edge users, which is proportional to the square of the ratio of the interior and the cell radius. In PPP models, chunk allocation does not require geometric foreknowledge; instead, the allocation may be dependent on the SIR distribution [1]. Hence, in the SIR-proportional model, we have $\omega_k = p_k$, and the mean SE is

$$\overline{\eta} = \sum_{k=1}^{N-1}\left(p_k^2 \ln(1+\theta_k) + p_k \int_{\theta_k}^{\infty} g_k(z)\mathrm{d}z\right) + p_N^2 \mathscr{R}_N. \tag{5.40}$$

### 5.6.4 Max-min BWP strategy

The fourth used strategy is named max-min criterion proposed in [156]. It aims at gaining the worst-case performance by maximizing the lowest rate, or SE, among all user types as

$$\begin{aligned} \mathscr{P}_2: \quad & \max_{\boldsymbol{\omega}} \quad \min_{\eta_k} \quad \eta_k(\omega_k) \\ \text{s.t.} \quad & C_1, C_2. \end{aligned} \tag{5.41}$$

The solution is achieved when all SE are equal, i.e., $\eta_i = \eta_j, \forall i, j \in [\![1, N]\!]$. Hence,

the partition $\omega_k$ allocated to the $k$-th user is directly given by

$$\omega_k = \frac{1}{\mathscr{R}_k}\left(\sum_k \frac{1}{\mathscr{R}_k}\right)^{-1}. \tag{5.42}$$

The max-min criterion gives a kind of fairness since each user has the same spectral efficiency, but at the same time, this strategy leads to a poor global sum-rate. The tradeoff between the fairness and the maximum sum-rate in the network can be seen as an attempt to control the variance of the SE allocated to users in the network [151, 157]. In the following, we study a mean–variance tradeoff-based BWP with a given value of the tradeoff level. Fairness across all types of users in the network can be achieved in a variety of ways, one of which is variance [151, 157]. Thus, we reformulate the constrained optimization problem to maximize the mean of SE to its variance being bounded from above.

### 5.6.5 Mean–Variance tradeoff based BWP strategy

In this section, instead of maximizing the average SE, we introduce the concept of risk to ensure maximum average SE subject to a certain level of fairness among all user types in the network. Let's consider the discrete random variable $\boldsymbol{\eta}$ that takes values in the set $\{\eta_1, \eta_2, ..., \eta_N\}$ with probabilities $\{p_1, p_2, ..., p_N\}$, where $N$ is the number of classes. We use the expected exponential utility risk model [151, 152], which is defined as follows:

$$\begin{aligned}\mathscr{H}(\boldsymbol{\omega}) &= \frac{1}{\beta}\log\left[\mathbb{E}_{\boldsymbol{\eta}}\left[\exp(\beta\boldsymbol{\eta})\right]\right] \\ &= \frac{1}{\beta}\log\left[\sum_k p_k\, e^{\beta\eta_k(\omega_k)}\right].\end{aligned} \tag{5.43}$$

where $\beta$ is an appropriately chosen constant known as the risk sensitivity parameter. The above function is the aversion for the risk when $\beta < 0$ and risk-seeking if $\beta > 0$. Expanding the Maclaurin series of the log and exp functions indicates that (5.43) catches higher-order moments of BWP. Concretely, in small risks, the exponential utility function is expressed as [151]:

$$\mathscr{H}(\boldsymbol{\omega}) = \mathbb{E}_{\boldsymbol{\eta}}[\boldsymbol{\eta}] + \frac{\beta}{2}\mathrm{Var}_{\boldsymbol{\eta}}[\boldsymbol{\eta}] + \mathscr{O}(\beta^2). \tag{5.44}$$

where $\mathbb{E}_{\boldsymbol{\eta}}[\boldsymbol{\eta}] \triangleq \sum_{k=1}^{N} p_k\eta_k$, $\mathrm{Var}_{\boldsymbol{\eta}}[\boldsymbol{\eta}] \triangleq \sum_{k=1}^{N} p_k\left(\eta_k - \mathbb{E}_{\boldsymbol{\eta}}[\boldsymbol{\eta}]\right)^2$. The variance term controls the variability of the SE among user types and can be used to control the fairness among users. Therefore, the bandwidth partitioning problem based on a given level

of fairness can be formulated as the following optimization problem:

$$\begin{aligned} \mathscr{P}_4: \quad & \max_{\boldsymbol{\omega}} \quad \tfrac{1}{\beta}\log\left[\textstyle\sum_k p_k\, e^{\beta\eta_k(\omega_k)}\right] \\ \text{s.t.} \quad & C_1, C_2. \end{aligned} \tag{5.45}$$

The objective function in (5.45) has a positive Hessian w.r.t. $\boldsymbol{\omega}$ for $\beta > 0$ and a negative Hessian for $\beta < 0$ (See Appendix A.6). Hence, in the risk-averse setting, the utility function is concave w.r.t. $\boldsymbol{\omega}$. Moreover, the feasible region has the convexity property since the constraints $C_1$ and $C_2$ are linear constraints. Therefore, for some $\{\theta_k\}_{1\le k\le N}$ and $\alpha$, (5.45) is a convex optimization problem.

The problem in (5.45) is a standard convex optimization problem that can be solved using the Karush–Kuhn–Tucker (KKT) conditions [158]. The Lagrangian function is expressed as follows

$$L(\boldsymbol{\omega}, \mu, \xi) = \frac{1}{\beta}\log\left[\sum_k p_k\, e^{\beta\eta_k(\omega_k)}\right] + \mu(1 - \sum_k \omega_k) + \sum_k \xi_k \omega_k, \tag{5.46}$$

where $\mu$ and $\xi_k$ are the KKT multipliers. Subsequently, the KKT conditions gives

$$\begin{cases} \frac{\partial L}{\partial \omega_i} = \frac{p_i \mathscr{R}_i \exp(\beta\eta_i(\omega_i))}{\sum_k p_k \exp(\beta\eta_k(\omega_k))} - \mu + \xi_i = 0, \quad \forall\ i \in [\![1, N]\!] \\ 1 - \sum_k \omega_k = 0 \\ \xi_k \omega_k = 0, \quad \forall\ k \in [\![1, N]\!] \\ \sum_k p_k = 1. \end{cases} \tag{5.47}$$

Solving the system of equations in (5.47) yields the optimal BWP with adequate fairness. The system can be solved using the water-filling algorithm proposed in [159]. From the above results, we can write the water-filling value $\omega_i$ as a function of the Lagrange multiplier $\mu$, i.e., $\omega_i = f_i(\mu)$, where

$$f_i(\mu) = \frac{1}{\beta \mathscr{R}_i}\log\left[\frac{\mu \sum_{k=1, k\neq i}^{N} p_k \exp(\beta\eta_k(\omega_k))}{p_i \cdot (\mathscr{R}_i - \mu)}\right]. \tag{5.48}$$

Considering that $\omega_i$ must be nonnegative ($C_1$), the water-filling value can be represented as follows

$$\omega_i = \begin{cases} f_i(\mu) & \text{if } f_i(\mu) > 0 \\ 0 & \text{otherwise} \end{cases}. \tag{5.49}$$

Finally, the water-filling value $\mu$ can be obtained using the primal feasibility ($C_2$) as

$$\sum_i f_i(\mu)\mathbf{1}(f_i(\mu) > 0) = 1. \tag{5.50}$$

From (5.50), no closed-form expression for $\omega_i$ as a function of $\mu$ independent from $\{\omega_k, \forall\ k \in [\![1,N]\!] \backslash \{i\}\}$ can be obtained. However, for a given network realization, the solution can be iteratively estimated via a bisection search algorithm like in [159]. Bisection search is a simple method with very high performance that is easy to implement. However, the starting points of the algorithm have to be chosen carefully. The following corollary bounds the possible value of the Lagrangian multiplier $\mu$.

**Corollary 6.** *Given $p_k$ and $\eta_k$ for all $k \in [\![1,N]\!]$, the water-filling value $\mu$ should satisfy:*

$$\underbrace{0}_{\mu_{min}} \leq \mu \leq \underbrace{\min_i \left(\frac{p_i \mathscr{R}_i}{p_i + \sum_{k=1,k\neq i}^{N} p_k \exp(\beta \eta_k(\omega_k))}\right)}_{\mu_{max}}. \tag{5.51}$$

*Proof.* Since $\mu$ is a Lagrangian multiplier, the minimum value is zero. In the case of maximum value of $\mu$, the proof follows from (5.49) and the point that $\beta$ takes a negative value in the risk-averse model. It limits the inner expression of the logarithm function to be positive and less than 1, i.e.,

$$\frac{\mu \sum_{k=1,k\neq i}^{N} p_k \exp(\beta \eta_k(\omega_k))}{p_i \cdot (\mathscr{R}_i - \mu)} \leq 1. \tag{5.52}$$

By solving (5.52) for $\mu$, we can obtain the upper bound. □

The bisection search approach in Algorithm 1 is proposed in [159], and we use it to approximate the solution values of the optimization problem $\mathscr{P}_5$.

**The data:** $\mu_{min}, \mu_{max}, \beta, \theta, \alpha$
**The result:** $\omega_k$ for $k = 1, \cdots, \mathscr{K}$
Initialize $\omega_k = 0$ for $k = 1, \cdots, \mathscr{K}$ ;
Set $\mu = (\mu_{max} + \mu_{min})/2$ ;
**repeat**
  **if** $\sum_k \omega_k < 1$ **then**
    Set $\mu_{max} = (\mu_{max} + \mu_{min})/2$;
  **else**
    Set $\mu_{min} = (\mu_{max} + \mu_{min})/2$;
  **end**
  Update $\mu = (\mu_{max} + \mu_{min})/2$ ;
  Compute $f_k$ 's using (5.48);
  Calculate $\omega_k$ 's using (5.49);
**until** (5.50) *converges*;

**Algorithm 1:** The bisection search algorithm to solve (5.50).

At each iteration of Algorithm 1, subchannels whose $f_k$ are equal or less than zero are eliminated from the iteration and their bandwidth values are forced to be zero. Moreover, since the utility function is concave, then its derivative is a decreasing function. Therefore, the subchannels with larger bandwidth allocated have less increasing rate than others which have lower allocated bandwidth. For instance, at each iteration, Algorithm 1 assigns a larger fraction of the bandwidth to the subchannel whose related SE has the maximum increasing rate to maximize the total SE. This idea replicates until all available resources have fairly been allocated.

In order to compare the fairness of the different BWP strategies, we use the Jain's index, since it is a widely used metric in literature [59, 160]. The definition of Jain's index is formulated as follows.

### 5.6.6 Quantitative fairness measure

The fairness measure attempts to quantify how much fairly the resources are allocated with a given strategy. There are many quantitative criteria for fairness in literature, as variance and entropy-based index [60]. As presented in 2.4.3, Jain's index has some properties that a good fairness measure are expected to have, i.e., population independent, scale independent, normalization and continuity. Jain's index is a widely used fairness measure in literature [149].

**Definition 7.** *Given a set of achievable SE $\eta_k : k = 1, ..., N$, the corresponding Jain's index is*

$$\mathscr{F}(\boldsymbol{\omega}) = \frac{\left[\sum_k p_k \eta_k(\omega_k)\right]^2}{\sum_k p_k \eta_k^2(\omega_k)}. \tag{5.53}$$

*where $\mathscr{F}(\boldsymbol{\omega})$ is continuous in the range* $\left[\min_k\{p_k\}, 1\right]$.

## 5.7 Numerical results

Simulations are conducted in a PPP network. The coverage probability and SE are evaluated at the typical user for 100,000 network realizations. We consider an interference-limited scenario with $\alpha = 4$, i.e., without thermal noise at the receiver. At each realization, the BS locations are generated as a PPP of unit intensity in an area of $[-30, 30] \times [-30, 30]$, and user density is considered large enough to have at least one user per cell.

Fig. 5.1 shows the simulation and analytical results of the cell edge coverage probability in the case of two user types (5.35) with/without OPS in the non-full interference

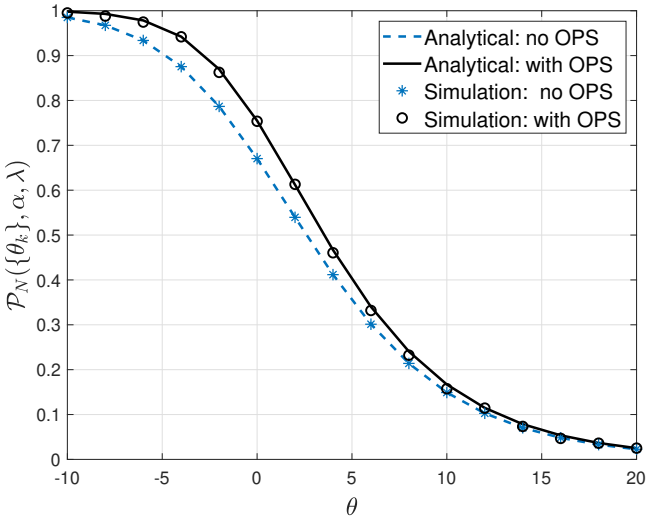


Figure 5.1 – Cell-edge user coverage probability using OPS with $N = 2$ partitions.

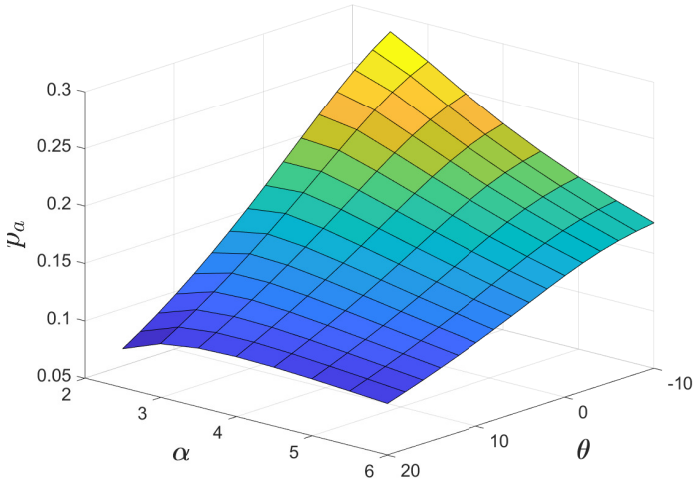


Figure 5.2 – OPS cooperation probability in $N = 2$ users case.

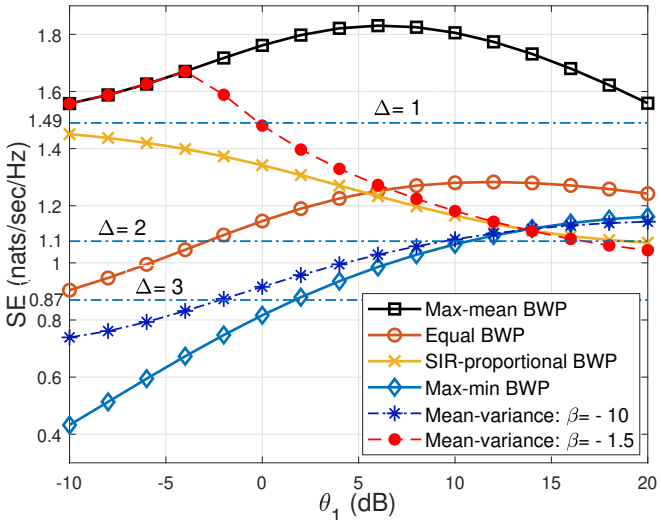


Figure 5.3 – SE under different BWP strategies.

network with a unique classification threshold. From the figure, the coverage probability of the cell edge user is enhanced under OPS compared to the non-cooperative scenario. When the unique threshold increases, both techniques converge, because the number of BS serving a type-1 user in the network decreases and goes to zero. Moreover, simulation and analytical results match, which validates the theoretical findings of Section 5.4.

Fig. 5.2 represents the cooperation probability (5.34) in case of cell center/edge user classification. We can see that when the path loss exponent increases and the unique threshold increases, the cooperation probability decreases.

Fig. 5.3 compares analytical results of the average SE for the cell center/edge user classification in the non-full interference scenario versus the type-1 user target threshold $\theta_1$ under different BWP strategies. Moreover, the achieved average SE is compared with the conventional frequency reuse technique with reuse factor $\Delta$ presented in [2]. The figure depicts that the max-mean BWP outperforms other strategies, since giving all the bandwidth to the best user is optimal regarding the network SE performance. Moreover, the curve corresponding to the max-mean SE first increases and then decreases after almost 8 dB, because for small values of $\theta_1$, almost all users are in the cell center. On the other hand, large values of $\theta_1$ make all users be cell edge users, and it tends to the full interference case, i.e., frequency reuse with $\Delta = 1$. Moreover, it can clearly be observed that when $\theta_1$ increases, the average SE under SIR-proportional policy (5.40) decreases while SE increases under equal partitioning (5.39). It can be seen that equal BWP eventually outperforms SIR-proportional BWP by increasing $\theta_1$ above 5 dB. This is because, contrary to equal BWP, SIR-proportional BWP gives more bandwidth to cell edge users when $\theta_1$ increase, that

is less efficient for the global SE. Indeed, in SIR-proportional policy, the typical user benefits from a fraction of resources that depends on the SIR and suffers from the same fraction of the interference. However, SIR-proportional policy still has a higher SE than static frequency reuse with $\Delta = 2$. Besides, the figure shows the mean-variance BWP (5.45) according to the risk sensitivity level $\beta$. For $\beta = -1.5$, the mean-variance BWP is a weak risk-averse policy and attempts to maximize the network SE by giving more bandwidth to the cell center users. Hence, the SE achieved by mean-variance BWP is identical to the max-mean strategy for small $\theta_1$ and then decreases when $\theta_1$ increases. This is because the number of cell center users decreasing by increasing the threshold value, and the policy tends to limit the increase of the variance in the SE allocation. On the other hand, if $\beta = -10$, the policy is even more risk-averse and tends to ensure fairness among users in the Jain's index sense. It also means that by negatively increasing the risk level, the SE achieved by the mean-variance strategy tends to the one obtained with the max-min BWP (5.41). Max-min BWP consists in giving the same amount of SE among user types and hence minimizing the variance of the allocation and SE increases by increasing $\theta$.

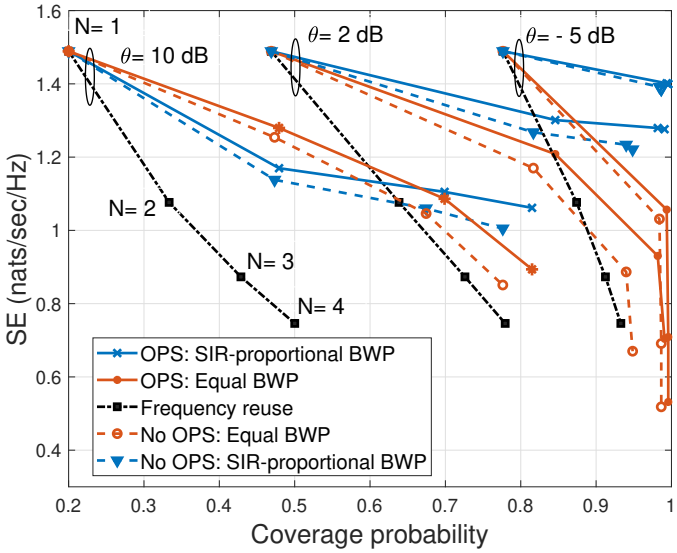


Figure 5.4 – SE-Coverage tradeoff for different BWP strategies with several number of user classes.

Fig. 5.4 compares the network average SE-coverage probability tradeoff for SIR-proportional BWP, equal BWP and frequency reuse (with $\Delta = N$) with/without BS cooperation technique, i.e., OPS scheme, and for an unique threshold value $\theta$ ranging in $\{-5, 2, 10\}$ dB. Whatever the BWP scheme considered, the coverage probability increases whereas the average SE decreases when $N$ increases, but with different

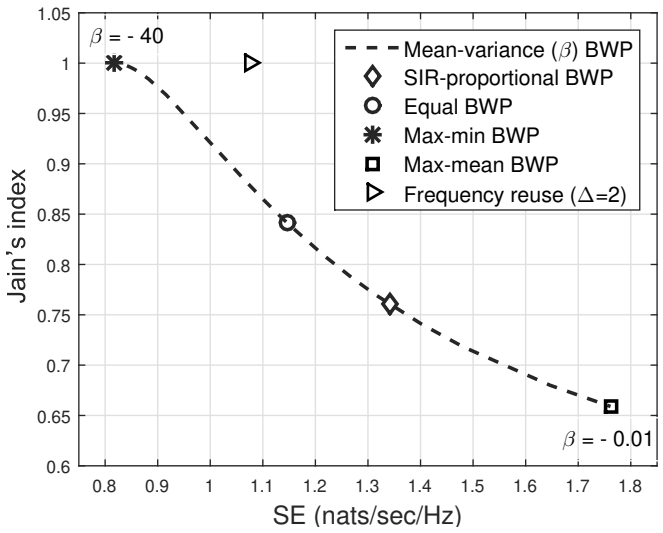


Figure 5.5 – Fairness-SE tradeoff under different BWP strategies for $N = 2$ and $\theta = 0$ dB.

trends according to the threshold $\theta$. However, the curves corresponding to the SIR-proportional and equal BWP policies are above the conventional frequency reuse. Furthermore, for $\theta \in \{-5, 2\}$ dB, the average SE achieved with SIR-proportional BWP is higher because it allocates more bandwidth to the type-1 user, which has a higher achievable spectral efficiency than other user types in the network. In contrast, equal BWP equally allocates bandwidth regardless of the density of the different user types in the network. On the other hand, for $\theta = 10$ dB, under two user types (cell center/edge), i.e., $N = 2$, equal BWP has a higher SE than SIR-proportional BWP. This is due to the fact that a high threshold value shrinks the cell center region, and the SIR-proportional approach allocates more bandwidth to the cell edge user, which has a lower SE than the cell center user. But, when $N$ increases, SIR-proportional achieves again higher SE than equal BWP. This is because the negative effect of equally dividing the available bandwidth is greater than the density-dependent allocation based on the user type. Finally, OPS strategy improves the tradeoff front by increasing the SE of the type-$N$ user using a BS selection diversity scheme.

Fig. 5.5 illustrates the Jain's index-average SE tradeoff for different strategies investigated in this work. The mean-variance BWP characterizes the tradeoff between the network SE and the fairness among user types, when $\beta$ value decreases from $-0.01$ to $-40$. As the network SE decreases, the fairness measured with the Jain's index increases and this index decreases when SE increases. The max-mean BWP has the maximum SE but with the lowest fairness in bandwidth partitioning. By sacrificing SE, SIR-proportional and equal BWPs achieve higher fairness regarding the max-mean strategy. The max-min BWP offers the fairest bandwidth sharing, in the Jain's index sense, while having the lowest SE. One can remark that the frequency reuse technique

allows to achieve a larger network SE than the one obtained with the max-min policy with a Jain's index equal to 1. This is because the allocated bandwidth does not depend on the position of the typical user in the cell so the user-type fairness is one. The fairness measured is among user-types and it does not mean that the fairness among users would be one with the frequency reuse technique since users do not experience the same SE. The mean-variance fairness criterion with a given risk level $\beta$ allows exploring the feasible operational point based on the desired SE and level of fairness among different user types in the cellular network.

## 5.8 Conclusion

This chapter has presented a complete characterization of a typical user's downlink coverage probability and spectral efficiency in a non-full interference homogeneous PPP network, i.e., when the statistic of the interference depends on the classification of the users. To help cell edge users in the network, an optimal point selection cooperation scheme was applied and semi-closed-form expressions of performance metrics based on the typical user's received SIR level have been derived. Then, to maximize the network average spectral efficiency, different bandwidth allocation schemes among user types have been expressed and evaluated. Finally, using the Jain's index, the fairness of the bandwidth allocation schemes has been quantified. Numerical results demonstrated that the user-centric resource allocation approach outperforms the conventional frequency reuse approach.

# Chapter 6

# Conclusions and future works

This chapter highlights the thesis's key contributions. Furthermore, we propose future research paths where our contributions might be helpful to apply.

## 6.1 Conclusions

This thesis has addressed the cell-edge user problem in wireless networks. The ever-increasing demand for mobile broadband communications has led to dense cellular networks. Network densification causes a lot of interference. Interference occurs when two or more BS use the same resources and leads to QoS degradation on the cell edge area. Hence, controlling interference is a critical issue in wireless networks. The utilization of interference mitigation techniques such as soft frequency reuse, optimal resource allocation, cooperative transmission scheme is a necessity for nowadays and future cellular networks. Stochastic geometry provides a natural approach to characterize the wireless network performance like the outage probability and the throughput. The objective of the thesis was to provide a way to manage the interference from the user point of view in order to alleviate the interference seen by the cell-edge user. By doing so, we developed a framework dealing with the non-full interference context resulting in correlation between the coverage probability and the activation probability of a BS.

We started this document by providing a brief history of SG as an important analytical tool for evaluating wireless network's system-level performance. We presented the mathematical tools and theorems from stochastic geometry used in this thesis to solve the problem. Moreover, we give mathematical features of PPP that is used as a baseline model in wireless networks. To provide an idea about performance metrics investigated in this thesis, we conducted a brief survey on the most commonly used KPIs in wireless networks such as coverage probability and spectral efficiency; and their mathematical definitions have been presented.

We then performed an exhaustive overview of the existing SG-based approaches to achieve the coverage probability in random wireless networks. These practical techniques, namely: standard approach, RDP approach, factorial moment approach, Gil-Pelaez inversion approach, Laplace transform inversion approach, Interference approximation approach, have been revisited when a PPP is considered. As the main challenge of the thesis, we reviewed the concept of the non-full interference networks in the literature and gave a new definition for it based on the coverage region. In this model, locating close to the cell edges does not necessarily lead to significant performance degradation because all BS are not active in the same resource. We reviewed the different interference mitigation techniques, that we classified into two categories: cell-centric and user-centric. The resource management in cell-centric is handled by a pre-designed fixed frequency reuse scheme. These methods are simple and require low signaling overhead. Nevertheless, they are not suited for dense environments with user mobility and dynamic channels which are challenging to address in cell-centric. In contrast, in user-centric, resource management is coordinated based on known user locations via multi-cell interaction. This is more sophisticated and requires more signaling overhead than cell-centric, but it is appropriate for the future generation of networks since it can handle the dynamism of user locations effectively, and there are many initiatives ongoing to eliminate signaling overhead in 5G networks.

After this analysis, we formulated a user-centric non-full interference problem. The existing state-of-the-art considers full interference and do not capture the correlation in SIR induced by the fact that the user's interference set is a function of its coverage probability. Besides, these analyses do not explicitly classify users with distinct signal qualities, which is crucial to detect user performance degradation accurately. The non-full interference model presented in this thesis overcame the above limitations while enabling the tractable system-level study of the typical user performance in downlink using SG. We classified users with distinct link qualities into CCU and CEU. We mathematically defined the cell center region and cell edge region for any stationary PPP in $\mathbb{R}^2$ of BS deployment, based on the received SIR by users. We proved that the interfering BS set is a thinned version of the original PPP and is related to the coverage probability of the cell center region. Results show that the scheme increases the network's global coverage probability compared to conventional cell-centric frequency reuse approach.

In addition, if the SIR requirement remains the same in the conventional frequency reuse approach, splitting the bandwidth into $N$ subchannels increases the coverage probability but at the cost in an $N$-fold reduction in spectral efficiency. To examine this challenge, we extended the user classification from two classes to $N+1$ classes. In our extended non-full interference model, a cell is divided into $N+1$ classes, and a typical user belongs to a particular class depending on its SIR. A user type-$N+1$ has the weakest SIR and is in outage from the network. An accurate approximation of

the user classification probability is derived. The expression is obtained in the form of a fixed-point equation that models the existing correlation between the desired signal and the interference set of each user type. In this model, the average number of interfering BS that lie within a given distance from each user type is a function of its coverage probability.

On the other hand, it was shown that the correlated interfering scenario can be estimated as a thinning process: the original PPP is split into $N+1$ thinned complementary processes, and the thinning factor for each class is quantified. The interference is mathematically modeled, and semi-tractable expressions for the coverage probability and SE are obtained. The results showed that if the SIR requirement remains the same, by splitting the bandwidth into $N$ subchannels, SE under our proposed user-centric frequency reuse approach decreases and converges.

We also addressed a BS cooperation technique based on an optimal point selection approach to improve the cell-edge user's performance under our non-full interference model. The relevant state-of-the-art methods applied the BS cooperation at the typical link, representing all links' average performance in a snapshot of the network under a full interference scenario. The main disadvantage of these works is that all BS participating in cooperation should sacrify their scheduled user in their cells by postponing them to the next round of transmissions that may increase traffic load in the network. In contrast, in the non-full interference network presented in this work, each BS is allowed to transmit a signal to its served user in the assigned fraction of the scheduled RB, and it is off in the remaining subchannels of the RB. In this scenario, an edge user can send its cooperation request to BS who serve different user types. The results showed that our model improved the performance of the cell-edge user without jeopardizing other scheduled users in the same RB and without raising the interference level in the network.

Furthermore, since the SE of the user is a function of the assigned fraction of bandwidth to the user, the network's average spectral efficiency is strongly correlated to the bandwidth allocation among different types of users in the network. We studied different bandwidth allocation strategies, namely max-mean BWP strategy, uniform BWP strategy, SIR-proportional BWP strategy, max-min BWP strategy. We have also addressed the tradeoff between network's SE and fairness using mean-variance tradeoff-based BWP strategy. In the mean-variance tradeoff approach, instead of maximizing the average SE, we introduced the concept of risk to ensure maximum network SE subject to a certain level of fairness among all user types in the network. In particular, we used the expected exponential utility risk model. The variance term controls the variability of the SE among user types and can be used to control the fairness among users. We formulated the bandwidth partitioning problem based on a given level of fairness as a convex optimization problem. We solved the problem using the bisection search algorithm that yields the optimal BWP with adequate fairness. Each of the BWP

strategies addressed in this thesis has its merit in fairness. To compare the fairness gain of the different BWP strategies, we used the Jain's index.

Finally, The results illustrated that the proposed mean-variance fairness criterion with a given risk level parameter allows the exploration of the feasible operational point based on the desired SE and the fairness level among different user types in the cellular network.

## 6.2 Future works

The ideas provided throughout this thesis provide viable methods for interference mitigation in both current and future cellular networks. However, the exponentially rising demand for mobile broadband data is posing new research challenges.

- One of these problems is managing interference-aware heterogeneous cellular networks. In reality, heterogeneous networks offer an effective method to meet the growing needs for mobile data traffic. Several radio access technologies (RATs) may span the same geographic region to maximize network capacity and user throughput. In the multi-tier network, in addition to the co-tier interference, we need to manage cross-tier interference problem. Co-tier interference occurs between network components of the same kind, such as nearby femtocells. In contrast, cross-tier interference occurs between network elements of different tiers, such as macrocells and femtocells. Numerous goal functions can be established, such as increasing system throughput, spectral and energy efficiency, throughput fairness, while ensuring the minimum needed QoS in the network.

- The uplink scenario can be studied in terms of coverage probability and average SE by utilizing the same system model as the downlink. Inter-cell interference occurs in the uplink due to all users in other cells using the same sub-band. The cells establish an uplink link using distance-based proportional power control technique. The diversity of the received power in this power control scheme is determined by Rayleigh fading, and all users have the same averaged received power. This direction of study has the potential to give analytical findings for the uplink system in a dense multi-cell situation. Because of the tractability of the PPP model, all results can be obtained in either closed or pseudo-closed form.

- In this thesis, we have considered the OFDMA scheme in our system model. Deriving the theoretical expressions under the NOMA scheme, a promising candidate technique in a 5G wireless system, can be very challenging. Unlike OFDMA, NOMA enables multiple users to access the same frequency/time

resource simultaneously. It has numerous advantages such as enhanced spectral efficiency, improved connectivity, higher cell-edge throughput, and lower transmission delay.

- Another relevant subject for future research is the tradeoff between spectral efficiency and energy efficiency maximization. The tradeoff between spectral efficiency and energy efficiency maximization may be controlled by the radio resource allocation and power allocation techniques. Because energy consumption has become a key concern for mobile network operators, optimizing spectrum utilization should consider power considerations. This SE and energy efficiency tradeoff might be addressed by updating the optimization problem's objective function in this thesis.

# Appendix A

# Proofs

## A.1 Proof of Theorem 3

For coverage probability of the typical cell center user in (4.5), we can write

$$\begin{aligned} p_c(\theta_c, \lambda, \alpha) &= \mathbb{P}(\Gamma_c \geq \theta_c) \\ &= \mathbb{P}\left(\frac{H_{0,0}^c R_0^{-\alpha}}{\sigma^2 + I_c} \geq \theta_c\right). \end{aligned} \tag{A.1}$$

By conditioning on $R_0$, we have

$$p_c(\theta_c, \lambda, \alpha) = \int_0^\infty \mathbb{P}\left(\frac{H_{0,0}^c R_0^{-\alpha}}{\sigma^2 + I_c} \geq \theta_c \middle| R_0 = r_0\right) f_{R_0}(r_0) \mathrm{d}r_0, \tag{A.2}$$

where

$$I_c = \sum_{i>0} H_{0,i}^c R_i^{-\alpha} 1(\Gamma_{c,i} \geq \theta_c). \tag{A.3}$$

Conditioned on $r_0$, others BS follow a Palm distribution described by the point process $\Phi \cap b^c(0, r_0)$, where $b(0, r_0)$ is the ball centered at the origin and of radius $r_0$.

The PDF of the distance to the nearest BS is

$$f_{R_0}(r_0) = 2\pi\lambda r_0 \exp(-\pi\lambda {r_0}^2). \tag{A.4}$$

Then, using (A.4), we can rewrite (A.2) as

$$p_c(\theta_c, \lambda, \alpha) = 2\pi\lambda \int_0^\infty \exp(-\pi\lambda {r_0}^2) \mathbb{P}\left(H_{0,0}^c \geq \theta_c r_0^\alpha (\sigma^2 + I_c) \middle| r_0\right) r_0 \mathrm{d}r_0. \tag{A.5}$$

Similar to [2] and using the fact that $H_{0,0}^c$ has exponential distribution with mean 1, the coverage probability can be expressed as

$$\begin{aligned}\mathbb{P}\left(H_{0,0}^c \geq \theta_c r_0^\alpha \left(\sigma^2 + I_c\right) | r_0\right) &= \mathbb{E}_{I_c}\left[\mathbb{P}\left(H_{0,0}^c \geq \theta_c r_0^\alpha \left(\sigma^2 + I_c\right) | r_0, I_c\right)\right] \\ &= \mathbb{E}_{I_c}\left[\exp(-\theta_c r_0^\alpha \left(\sigma^2 + I_c\right)) | r_0, I_c\right] \\ &= e^{-s\sigma^2} \mathscr{L}_{I_c}(s), \end{aligned} \tag{A.6}$$

where $s = \theta_c r_0^\alpha$ and $\mathscr{L}_{I_c}(s)$ is the Laplace transform of random variable $I_c$ evaluated at $s$ conditioned on the distance to the closest BS from the origin. This gives a coverage expression

$$p_c(\theta_c, \lambda, \alpha) = 2\pi\lambda \int_0^\infty \exp(-\pi\lambda {r_0}^2) e^{-s\sigma^2} \mathscr{L}_{I_c}(s) r_0 \mathrm{d}r_0. \tag{A.7}$$

Using the definition of the Laplace transform yields

$$\begin{aligned}\mathscr{L}_{I_c}(s) &= \mathbb{E}_{\Phi,\{H_{0,i}^c\}}\left[\exp\left(\sum_{i>0} -sH_{0,i}^c R_i^{-\alpha} 1(\Gamma_{c,i} \geq \theta_c)\right)\right] \\ &\overset{a}{=} \mathbb{E}_{\Phi,\{H_{0,i}^c\}}\left[1(\Gamma_{c,i} \geq \theta_c) \exp\left(\sum_{i>0} -sH_{0,i}^c R_i^{-\alpha}\right) + 1 - 1(\Gamma_{c,i} \geq \theta_c)\right] \\ &\overset{b}{\approx} \mathbb{E}_{\Phi,\{H_{0,i}^c\}}\left[\prod_{i>0}\left(1 - \mathbb{E}[1(\Gamma_{c,i} \geq \theta_c)](1 - e^{-sH_{0,i}^c R_i^{-\alpha}})\right)\right] \\ &\overset{c}{=} \exp\left(-2\pi\lambda \int_{r_0}^\infty \mathbb{E}\left[1(\Gamma_{c,i} \geq \theta_c)\right]\left(1 - \frac{1}{1+sr^{-\alpha}}\right) r\mathrm{d}r\right) \\ &\overset{d}{=} \exp\left(-2\pi\lambda p_c(\theta_c, \lambda, \alpha) \int_{r_0}^\infty \left(1 - \frac{1}{1+sr^{-\alpha}}\right) r\mathrm{d}r\right) \\ &= \exp\left(-2\pi\lambda p_c(\theta_c, \lambda, \alpha) \int_{r_0}^\infty \left(\frac{s}{r^\alpha + s}\right) r\mathrm{d}r\right) \\ &= \exp\left(-2\pi\lambda p_c(\theta_c, \lambda, \alpha) r_0^2 \theta_c^{2/\alpha} \int_{\frac{1}{\theta_c^{1/\alpha}}}^\infty \left(\frac{x}{x^\alpha + 1}\right) \mathrm{d}x\right) \\ &= \exp\left(-2\pi\lambda p_c(\theta_c, \lambda, \alpha) \frac{\theta_c r_0^2}{\alpha - 2} {}_2F_1\left(1, 1 - \frac{2}{\alpha}; 2 - \frac{2}{\alpha}; -\theta_c\right)\right), \end{aligned} \tag{A.8}$$

where: (a) follows rewriting of the exponential term considering indicator function; (b) comes from the law of total expectation, $\mathbb{E}_X[f(X)] = \mathbb{E}_Y[\mathbb{E}_X[f(X)|Y]]$, the independence of $\{\Gamma_{c,i}\}_i$, which is a reasonable assumption whose accuracy has been verified by simulations, and finally by factoring out $\mathbb{E}[1(\Gamma_{c,i} > \theta_c)]$; (c) follows from the PGFL [31] of the PPP and identically distributed $\{\Gamma_{c,i}\}_i$, and (d) refers to the definition of the central coverage probability in (4.5).

## A.2 Proof of Theorem 4

Starting with (4.6) and using the Bayes rule, we have

$$p_e(\theta_e,\theta_c,\lambda,\alpha)=\frac{\mathbb{P}\left[\frac{H^e_{0,0}R_0^{-\alpha}}{\sigma^2+I_e}\geq\theta_e,\frac{H^c_{0,0}R_0^{-\alpha}}{\sigma^2+I_c}<\theta_c\right]}{\mathbb{P}\left[\frac{H^c_{0,0}R_0^{-\alpha}}{\sigma^2+I_c}<\theta_c\right]} \tag{A.9}$$

where $I_e=\sum_{i>0}H^e_{0,i}R_i^{-\alpha}1(\Gamma_{c,i}<\theta_c)$.

Conditioned on $R_0$, the joint coverage probability in numerator of (A.9) becomes

$$\mathbb{P}\left[\frac{H^c_{0,0}R_0^{-\alpha}}{\sigma^2+I_c}<\theta_c\right]=\int_0^\infty\mathbb{P}\left[\frac{H^e_{0,0}R_0^{-\alpha}}{\sigma^2+I_e}\geq\theta_e,\frac{H^c_{0,0}R_0^{-\alpha}}{\sigma^2+I_c}<\theta_c\middle|R_0=r_0\right]f_{R_0}(r_0)\mathrm{d}r_0. \tag{A.10}$$

Since $H^c_{0,0},H^e_{0,0}\sim\exp(1)$ it comes

$$\begin{aligned}
&\mathbb{P}\Big(H^e_{0,0}\geq s_1(\sigma^2+I_e),H^c_{0,0}<s_2(\sigma^2+I_c)|r_0\Big)\\
&\overset{a}{=}\mathbb{E}_{I_c,I_e}\Big[\mathbb{P}\left(H^e_{0,0}\geq s_1(\sigma^2+I_e)|r_0,I_e\right)\\
&\qquad\qquad\times\mathbb{P}\left(H^c_{0,0}<s_2(\sigma^2+I_c)|r_0,I_c\right)\Big]\\
&\overset{b}{=}\mathbb{E}_{I_e}\Big[\mathbb{P}\left(H^e_{0,0}\geq s_1(\sigma^2+I_e)|r_0,I_e\right)\Big]\\
&\qquad-\mathbb{E}_{I_c,I_e}\Big[\mathbb{P}\left(H^e_{0,0}\geq s_1(\sigma^2+I_e)|r_0,I_e\right)\\
&\qquad\qquad\times\mathbb{P}\Big(H^c_{0,0}\geq s_2(\sigma^2+I_c)|r_0,I_c\Big)\Big]\\
&=e^{-s_1\sigma^2}\mathscr{L}_{I_e}(s_1)-e^{-(s_1+s_2)\sigma^2}\mathscr{L}_{I_e,I_c}(s_1,s_2),
\end{aligned} \tag{A.11}$$

where $s_1=\theta_e r_0^\alpha$, $s_2=\theta_c r_0^\alpha$, (a) comes from that conditioned on the interference, the two r.v. are independent, and (b) follows from the probability of a complementary event.

Following the same derivation as in (A.8), $\mathscr{L}_{I_e}(s_1)$ can be expressed as $\mathscr{L}_{I_e}(s_1)=\exp(-\pi\lambda\rho(\theta_e,\lambda,\alpha)r_0^2)$. Also, $\mathscr{L}_{I_e,I_c}(s_1,s_2)$ captures the joint LT between $\Gamma_c$ and $\Gamma_e$ and can be derived as

$$\begin{aligned}
&\mathscr{L}_{I_e,I_c}(s_1,s_2)=\mathbb{E}_{I_c,I_e}[e^{-s_1I_e}e^{-s_2I_c}] \qquad\qquad (A.12)\\
&=\mathbb{E}_{\Phi,\{H^c_{0,i}\},\{H^e_{0,i}\}}\Bigg[\exp\Big(-s_1\sum_{i>0}H^e_{0,i}R_i^{-\alpha}1(\Gamma_{c,i}<\theta_c)\Big)\\
&\qquad\times\exp\Big(-s_2\sum_{i>0}H^c_{0,i}R_i^{-\alpha}1(\Gamma_{c,i}\geq\theta_c)\Big)\Bigg]\\
&\overset{a}{\approx}\mathbb{E}_{\Phi,\{H^c_{0,i}\},\{H^e_{0,i}\}}\Bigg[\prod_{i>0}\Big(\mathbb{E}\big[1(\Gamma_{c,i}\geq\theta_c)\big]e^{-s_2H^c_{0,i}R_i^{-\alpha}}
\end{aligned}$$

$$
\begin{aligned}
&\quad + \left(1 - \mathbb{E}\left[1(\Gamma_{c,i} \geq \theta_c)\right]\right) e^{-s_1 H_{0,i}^e R_i^{-\alpha}} \Big) \Big] \\
&= \mathbb{E}_\Phi \left[ \prod_{i>0} \left( \frac{\mathbb{E}[1(\Gamma_{c,i} \geq \theta_c)]}{1 + s_2 R_i^{-\alpha}} + \frac{1 - \mathbb{E}[1(\Gamma_{c,i} \geq \theta_c)]}{1 + s_1 R_i^{-\alpha}} \right) \right] \\
&\overset{b}{=} \exp\left( -2\pi\lambda \int_{r_0}^{\infty} \left( 1 - \frac{\mathbb{E}[1(\Gamma_{c,i} \geq \theta_c)]}{1 + s_2 r^{-\alpha}} - \frac{1 - \mathbb{E}[1(\Gamma_{c,i} \geq \theta_c)]}{1 + s_1 r^{-\alpha}} \right) r \mathrm{d}r \right) \\
&= \exp\left( -2\pi\lambda \int_{r_0}^{\infty} \left( \mathbb{E}[1(\Gamma_{c,i} \geq \theta_c)] - \frac{\mathbb{E}[1(\Gamma_{c,i} \geq \theta_c)]}{1 + s_2 r^{-\alpha}} \right.\right. \\
&\qquad \left.\left. + 1 - \mathbb{E}[1(\Gamma_{c,i} \geq \theta_c)] - \frac{1 - \mathbb{E}[1(\Gamma_{c,i} \geq \theta_c)]}{1 + s_1 r^{-\alpha}} \right) r \mathrm{d}r \right) \\
&= \exp\left( -2\pi\lambda p_c(\theta_c, \lambda, \alpha) \int_{r_0}^{\infty} \left( 1 - \frac{1}{1 + s_2 r^{-\alpha}} \right) r \mathrm{d}r \right. \\
&\qquad \left. - 2\pi\lambda \left(1 - p_c(\theta_c, \lambda, \alpha)\right) \int_{r_0}^{\infty} \left( 1 - \frac{1}{1 + s_1 r^{-\alpha}} \right) r \mathrm{d}r \right).
\end{aligned}
$$

where (a) follows from the same hypothesis used in the proof of Theorem 3 and the independence assumption of $\{\Gamma_{c,i}\}_i$. (b) uses PGFL such as the step (c) in appendix A.1.

## A.3 Proof of Theorem 10

By using the Bayes rule and recalling (5.14) and (5.15), we get

$$\begin{aligned}\mathscr{P}_N(\{\theta_k\}_{k=1}^N,\alpha,\lambda) &= \frac{\mathbb{P}(S_N \geq \theta_N I_N, X_N \in \Phi_N)}{\mathbb{P}(X_N \in \Phi_N)} \\ &= 1 - \frac{\mathbb{P}(S_N < \theta_N I_N, X_N \in \Phi_N)}{\mathbb{P}(X_N \in \Phi_N)}. \end{aligned} \tag{A.13}$$

Next, we expand the term $\Xi = \mathbb{P}(S_N < \theta_N I_N, X_N \in \Phi_N)$ as

$$\begin{aligned}\Xi &= \mathbb{P}\Big(\max_{X_i \in \mathscr{C}_0 \cup X_0} \{H_i^N R_i^{-\alpha}\} < \theta_N I_N, X_N \in \Phi_N\Big) \\ &= \mathbb{P}(G_1 T_1^{-\alpha} < \theta_N I_N, \cdots, H_0^N R_0^{-\alpha} < \theta_N I_N, X_N \in \Phi_N) \\ &= \mathbb{E}_{\mathbf{T}}\Big[\prod_{k=1}^{N-1} \mathbb{P}(G_k T_k^{-\alpha} < \theta_N I_N \mid T_k)\mathbb{P}(H_0^N R_0^{-\alpha} < \theta_N I_N \mid R_0)\mathbb{P}(X_N \in \Phi_N \mid R_0)\Big], \end{aligned} \tag{A.14}$$

where

$$\mathbb{P}(G_k T_k^{-\alpha} < \theta_N I_N \mid T_k) = 1 - \mathscr{L}_{I_N}(\theta_N T_k^{\alpha}), \tag{A.15}$$

and

$$\begin{aligned}\mathbb{P}(X_N \in \Phi_N \mid R_0) &= \prod_{k=1}^{N-1} \mathbb{P}(\mathrm{SIR}_0^k < \theta_k | R_0) \\ &= \prod_{k=1}^{N-1} \Big(1 - \mathbb{P}(\mathrm{SIR}_0^k \geq \theta_k | R_0)\Big) \\ &= \prod_{k=1}^{N-1} 1 - \mathscr{L}_{I_{0,k}}(\theta_k R_0^{\alpha}). \end{aligned} \tag{A.16}$$

## A.4 Proof of Lemma 2

Using the definition of $p_a$ in (5.33) and by conditioning on the joint distance distribution of $T_1$ and $R_0$

$$\begin{aligned} p_a &= 1 - \mathbb{E}_{T_1,R_0}\mathbb{E}_{G_1}\left[\mathbb{P}\left(H_0^2 > G_1\left(\frac{R_0}{T_1}\right)^{\alpha}\right)\right] \\ &= 1 - \mathbb{E}_{T_1,R_0}\left[\frac{1}{1+\left(\frac{R_0}{T_1}\right)^{\alpha}}\right] \\ &\overset{a}{=} 1 - \sum_{k=0}^{\infty}(-1)^k \mathbb{E}_{T_1,R_0}\left[\left(\frac{R_0}{T_1}\right)^{\alpha k}\right], \end{aligned}$$

where (a) comes from $(1+x)^{-1} = \sum_{k=0}^{\infty}(-1)^k x^k$. From the joint distances distribution in (5.21), the joint PDF of $T_1$ and $R_0$ is

$$f_{T_1,R_0}(t_1,r_0) = p_c(2\pi\lambda)^2 t_1 r_0 e^{-p_c\lambda\pi t_1^2} e^{-(1-p_c)\lambda\pi r_0^2}, \tag{A.17}$$

where $r_0 \in [0,\infty)$ and $t_1 \in [r_0,\infty)$. Hence, we have

$$\mathbb{E}_{T_1,R_0}\left[\left(\frac{R_0}{T_1}\right)^{\alpha k}\right] = p_c(2\pi\lambda)^2 \int_0^{\infty}\int_{r_0}^{\infty}\left(\frac{r_0}{t_1}\right)^{\alpha k} t_1 r_0 e^{-\lambda\pi\left(p_c t_1^2 + (1-p_c)r_0^2\right)} \mathrm{d}t_1 \mathrm{d}r_0$$

$$\begin{aligned} &\overset{a}{=} p_c(2\pi\lambda)^2 \int_0^{\infty}\int_0^1 u^{\alpha k-3} v^3 e^{-\lambda\pi\left(p_c u^{-2} + (1-p_c)\right)v^2} \mathrm{d}u\mathrm{d}v \\ &\overset{b}{=} p_c(2\pi\lambda)^2 \int_0^1 u^{\alpha k-3} \int_0^{\infty} \frac{y e^{-y}\mathrm{d}y}{2(\pi\lambda)^2\left(p_c u^{-2} + (1-p_c)\right)^2}\mathrm{d}u \\ &= 2p_c \int_0^1 \frac{u^{\alpha k-3}}{\left(p_c u^{-2} + (1-p_c)\right)^2}\mathrm{d}u \\ &= \frac{p_c^{-1}}{\frac{\alpha k}{2}+1} {}_2F_1\left(2, \frac{\alpha k}{2}+1; \frac{\alpha k}{2}+2; \frac{p_c-1}{p_c}\right), \end{aligned} \tag{A.18}$$

where (a) is change of variables $\frac{r_0}{t_1} = u$ and $v = r_0$, (b) is change of variables $y = \lambda\pi\left(1 - p_c\left(1 - \frac{1}{u^2}\right)\right)v^2$. Finally, by applying

$${}_2F_1(a,b;c;z) = (1-z)^{-a}\,{}_2F_1\left(a, c-b; c; \frac{z}{z-1}\right), \tag{A.19}$$

and substituting (A.18) in (A.17), we can derive (5.34).

## A.5 Proof of Theorem 5

Applying Theorem 10 for $N=2$ leads to (A.20) as

$$\begin{aligned}\mathscr{P}_2(\theta_1,\theta_2,\alpha,\lambda)&=1-\frac{1}{1-p_c}\int_0^\infty\int_{r_0}^\infty\left(1-\mathscr{L}_{I_2}(\theta_2 r_0^\alpha)\right)\left(1-\mathscr{L}_{I_2}(\theta_2 t_1)\right)\left(1-\mathscr{L}_{I_{0,1}}(\theta_1 r_0^\alpha)\right)\times\\ &\qquad f_{T_1,R_0}(t_1,r_0)\mathrm{d}t_1\mathrm{d}r_0\\ &=\frac{1}{1-p_c}\sum_{i=1}^{3}\left(\mathscr{M}_i(\theta_1,\theta_2,\alpha)-\mathscr{Q}_i(\theta_1,\theta_2,\alpha)\right).\end{aligned}\tag{A.20}$$

We can derive $\mathscr{M}_1$ as follow

$$\begin{aligned}\mathscr{M}_1&=\mathbb{E}_{T_1,R_0}\left[\mathscr{L}_{I_2}(\theta_2 R_0^\alpha)\right]\\ &=\int_0^\infty\int_{r_0}^\infty\mathscr{L}_{I_2}(\theta_2 r_0^\alpha)f_{T_1,R_0}(t_1,r_0)\ \mathrm{d}t_1\mathrm{d}r_0\\ &=\int_0^\infty\int_{r_0}^\infty\mathscr{L}_{I_{2,1}}(\theta_2 r_0^\alpha)\mathscr{L}_{I_{2,2}}(\theta_2 r_0^\alpha)f_{T_1,R_0}(t_1,r_0)\ \mathrm{d}t_1\mathrm{d}r_0,\end{aligned}\tag{A.21}$$

where by substituting $\mathscr{L}_{I_{2,1}}(\theta_2 r_0^\alpha)$ and $\mathscr{L}_{I_{2,2}}(\theta_2 r_0^\alpha)$ from (5.24) and (5.26) into (A.21), we have (A.22) as

$$\begin{aligned}\mathscr{M}_1&=p_c(2\pi\lambda)^2\int_0^\infty\int_{r_0}^\infty e^{-\lambda\pi p_c p_a\rho(\theta_2(\frac{r_0}{t_1})^\alpha,\alpha)t_1^2}e^{-\lambda\pi(1-p_c)(1-p_a)\rho(\theta_2,\alpha)r_0^2}e^{-\lambda\pi p_c t_1^2}e^{-\lambda\pi(1-p_c)r_0^2}\\ &\qquad\times t_1 r_0\mathrm{d}t_1\mathrm{d}r_0\\ &=p_c(2\pi\lambda)^2\int_0^\infty\int_{r_0}^\infty e^{-\pi\lambda p_c(1+p_a\rho(\theta_2(\frac{r_0}{t_1})^\alpha,\alpha))t_1^2}e^{-\pi\lambda(1-p_c)(1+(1-p_a)\rho(\theta_2,\alpha))r_0^2}t_1 r_0\mathrm{d}t_1\mathrm{d}r_0\\ &=p_c(2\pi\lambda)^2\int_0^\infty\int_0^1 e^{-\lambda\pi p_c(1+p_a\rho(\theta_2 u^\alpha,\alpha))u^{-2}r_0^2}e^{-\lambda\pi(1-p_c)(1+(1-p_a)\rho(\theta_2,\alpha))r_0^2}r_0^3u^{-3}\mathrm{d}u\mathrm{d}r_0\\ &=p_c(2\pi\lambda)^2\int_0^1\int_0^\infty e^{-\lambda\pi\left[p_c(1+p_a\rho(\theta_2 u^\alpha,\alpha))u^{-2}+(1-p_c)(1+(1-p_a)\rho(\theta_2,\alpha))\right]r_0^2}r_0^3\mathrm{d}r_0u^{-3}\mathrm{d}u\\ &=p_c(2\pi\lambda)^2\int_0^1\frac{u^{-3}}{2(\pi\lambda)^2(p_c(1+p_a\rho(\theta_2 u^\alpha,\alpha))u^{-2}+(1-p_c)(1+(1-p_a)\rho(\theta_2,\alpha)))^2}\mathrm{d}u\\ &=p_c\int_0^1\frac{1}{\left(p_c(1+p_a\rho(\theta_2 x^{\frac{\alpha}{2}},\alpha))+(1-p_c)(1+(1-p_a)\rho(\theta_2,\alpha))x\right)^2}\mathrm{d}x.\end{aligned}\tag{A.22}$$

With the same approach as we used to find $\mathscr{M}_1$ starting from (A.21), the expressions of $\mathscr{M}_i, i=2,3$ and $\mathscr{Q}_j, j=1,2,3$ can be obtained as follows.

$$\mathscr{M}_2=\mathbb{E}_{T_1,R_0}\left[\mathscr{L}_{I_2}(\theta_2 T_1^\alpha)\right]$$

$$
\begin{aligned}
&= \int_0^\infty \int_{r_0}^\infty \mathscr{L}_{I_2}(\theta_2 t_1^\alpha) f_{T_1,R_0}(t_1, r_0)\ \mathrm{d}t_1 \mathrm{d}r_0 \\
&= \int_0^\infty \int_{r_0}^\infty \mathscr{L}_{I_{2,1}}(\theta_2 t_1^\alpha) \mathscr{L}_{I_{2,2}}(\theta_2 t_1^\alpha) f_{T_1,R_0}(t_1, r_0)\ \mathrm{d}t_1 \mathrm{d}r_0 \\
&= p_c (2\pi\lambda)^2 \int_0^\infty \int_{r_0}^\infty e^{-\lambda\pi p_c p_a \rho(\theta_2,\alpha) t_1^2} e^{-\lambda\pi(1-p_c)(1-p_a)\rho(\theta_2(\frac{t_1}{r_0})^\alpha,\alpha) r_0^2} e^{-\lambda\pi p_c t_1^2} e^{-\lambda\pi(1-p_c) r_0^2} \\
&\qquad\qquad \times t_1 r_0 \mathrm{d}t_1 \mathrm{d}r_0 \\
&= p_c (2\pi\lambda)^2 \int_0^\infty \int_{r_0}^\infty e^{-\pi\lambda p_c (1+p_a \rho(\theta_2,\alpha)) t_1^2} e^{-\pi\lambda(1-p_c)(1+(1-p_a)\rho(\theta_2(\frac{t_1}{r_0})^\alpha,\alpha)) r_0^2} t_1 r_0 \mathrm{d}t_1 \mathrm{d}r_0 \\
&= p_c (2\pi\lambda)^2 \int_0^\infty \int_0^1 e^{-\lambda\pi p_c (1+p_a \rho(\theta_2,\alpha)) u^{-2} r_0^2} e^{-\lambda\pi(1-p_c)(1+(1-p_a)\rho(\theta_2 u^{-\alpha},\alpha)) r_0^2} r_0^3 u^{-3} \mathrm{d}u \mathrm{d}r_0 \\
&= p_c (2\pi\lambda)^2 \int_0^1 \int_0^\infty e^{-\lambda\pi \left[ p_c (1+p_a \rho(\theta_2,\alpha)) u^{-2} + (1-p_c)(1+(1-p_a)\rho(\theta_2 u^{-\alpha},\alpha)) \right] r_0^2} r_0^3 u^{-3} \mathrm{d}r_0 \mathrm{d}u \\
&= p_c (2\pi\lambda)^2 \int_0^1 \frac{u^{-3}\mathrm{d}u}{2(\pi\lambda)^2 (p_c(1+p_a\rho(\theta_2,\alpha)) u^{-2} + (1-p_c)(1+(1-p_a)\rho(\theta_2 u^{-\alpha},\alpha)))^2} \\
&= p_c \int_0^1 \frac{\mathrm{d}x}{\left( p_c(1+p_a\rho(\theta_2,\alpha)) + (1-p_c)(1+(1-p_a)\rho(\theta_2 x^{-\frac{\alpha}{2}},\alpha)) x \right)^2}.
\end{aligned} \tag{A.23}
$$

$$
\begin{aligned}
\mathscr{M}_3 &= -\mathbb{E}_{T_1,R_0}\left[\mathscr{L}_{I_2}(\theta_2 R_0^\alpha)\mathscr{L}_{I_2}(\theta_2 T_1^\alpha)\right] \\
&= -\int_0^\infty\int_{r_0}^\infty \mathscr{L}_{I_2}(\theta_2 r_0^\alpha)\mathscr{L}_{I_2}(\theta_2 t_1^\alpha) f_{T_1,R_0}(t_1,r_0)\,\mathrm{d}t_1\mathrm{d}r_0 \\
&= -\int_0^\infty\int_{r_0}^\infty \mathscr{L}_{I_{2,1}}(\theta_2 r_0^\alpha)\mathscr{L}_{I_{2,1}}(\theta_2 t_1^\alpha)\mathscr{L}_{I_{2,2}}(\theta_2 r_0^\alpha)\mathscr{L}_{I_{2,2}}(\theta_2 t_1^\alpha) f_{T_1,R_0}(t_1,r_0)\,\mathrm{d}t_1\mathrm{d}r_0 \\
&= p_c(2\pi\lambda)^2\int_0^\infty\int_{r_0}^\infty e^{-\lambda\pi p_c p_a \rho(\theta_2(\frac{r_0}{t_1})^\alpha,\alpha)t_1^2} e^{-\lambda\pi p_c p_a\rho(\theta_2,\alpha)t_1^2} e^{-\lambda\pi(1-p_c)(1-p_a)\rho(\theta_2,\alpha)r_0^2} \\
&\qquad\qquad \times e^{-\lambda\pi(1-p_c)(1-p_a)\rho(\theta_2(\frac{t_1}{r_0})^\alpha,\alpha)r_0^2} e^{-\lambda\pi p_c t_1^2} e^{-\lambda\pi(1-p_c)r_0^2} t_1 r_0 \mathrm{d}t_1\mathrm{d}r_0 \\
&= p_c(2\pi\lambda)^2\int_0^\infty\int_{r_0}^\infty e^{-\pi\lambda p_c(1+p_a(\rho(\theta_2,\alpha)+\rho(\theta_2(\frac{r_0}{t_1})^\alpha,\alpha)))t_1^2} \\
&\qquad\qquad \times e^{-\pi\lambda(1-p_c)(1+(1-p_a)(\rho(\theta_2,\alpha)+\rho(\theta_2(\frac{t_1}{r_0})^\alpha,\alpha)))r_0^2} t_1 r_0 \mathrm{d}t_1\mathrm{d}r_0 \\
&= p_c(2\pi\lambda)^2\int_0^\infty\int_1^\infty e^{-\pi\lambda p_c(1+p_a(\rho(\theta_2,\alpha)+\rho(\theta_2 u^\alpha,\alpha)))u^{-2}r_0^2} \\
&\qquad\qquad \times e^{-\pi\lambda(1-p_c)(1+(1-p_a)(\rho(\theta_2,\alpha)+\rho(\theta_2 u^{-\alpha},\alpha)))r_0^2} u^{-3} r_0^3 \mathrm{d}r_0\mathrm{d}u \\
&= p_c(2\pi\lambda)^2\int_0^1\int_0^\infty e^{-\lambda\pi\left[p_c(1+p_a(\rho(\theta_2,\alpha)+\rho(\theta_2 u^\alpha,\alpha)))u^{-2}+(1-p_c)(1+(1-p_a)(\rho(\theta_2,\alpha)+\rho(\theta_2 u^{-\alpha},\alpha)))\right]r_0^2} \\
&\qquad\qquad \times r_0^3 u^{-3}\mathrm{d}r_0\mathrm{d}u \\
&= \int_0^1 \frac{p_c(2\pi\lambda)^2 u^{-3}\mathrm{d}u}{2(\pi\lambda)^2(p_c(1+p_a(\rho(\theta_2,\alpha)+\rho(\theta_2 u^\alpha,\alpha)))u^{-2}+(1-p_c)(1+(1-p_a)(\rho(\theta_2,\alpha)+\rho(\theta_2 u^{-\alpha},\alpha))))^2} \\
&= \int_0^1 \frac{p_c\mathrm{d}x}{\left(p_c(1+p_a(\rho(\theta_2,\alpha)+\rho(\theta_2 x^{\frac{\alpha}{2}},\alpha)))+(1-p_c)(1+(1-p_a)(\rho(\theta_2,\alpha)+\rho(\theta_2 x^{-\frac{\alpha}{2}},\alpha)))x\right)^2}.
\end{aligned}
\tag{A.24}
$$

$$
\begin{aligned}
\mathcal{Q}_1 &= \mathbb{E}_{T_1,R_0}\left[\mathscr{L}_{I_2}(\theta_2 R_0^\alpha)\mathscr{L}_{I_{0,1}}(\theta_1 R_0^\alpha)\right] \\
&= \int_0^\infty \int_{r_0}^\infty \mathscr{L}_{I_2}(\theta_2 r_0^\alpha)\mathscr{L}_{I_{0,1}}(\theta_1 r_0^\alpha) f_{T_1,R_0}(t_1,r_0)\ \mathrm{d}t_1\mathrm{d}r_0 \\
&= \int_0^\infty \int_{r_0}^\infty \mathscr{L}_{I_{2,1}}(\theta_2 r_0^\alpha)\mathscr{L}_{I_{2,2}}(\theta_2 r_0^\alpha)\mathscr{L}_{I_{0,1}}(\theta_1 r_0^\alpha) f_{T_1,R_0}(t_1,r_0)\ \mathrm{d}t_1\mathrm{d}r_0 \\
&= p_c(2\pi\lambda)^2 \int_0^\infty \int_{r_0}^\infty e^{-\lambda\pi p_c p_a \rho(\theta_2(\frac{r_0}{t_1})^\alpha,\alpha)t_1^2} e^{-\lambda\pi(1-p_c)(1-p_a)\rho(\theta_2,\alpha)r_0^2} \\
&\qquad\qquad \times e^{-\lambda\pi p_c\rho(\theta_1,\alpha)r_0^2} e^{-\lambda\pi p_c t_1^2} e^{-\lambda\pi(1-p_c)r_0^2} t_1 r_0 \mathrm{d}t_1\mathrm{d}r_0 \\
&= p_c(2\pi\lambda)^2 \int_0^\infty \int_{r_0}^\infty e^{-\pi\lambda p_c(1+p_a\rho(\theta_2(\frac{r_0}{t_1})^\alpha,\alpha))t_1^2} e^{-\pi\lambda(1-p_c)(1+(1-p_a)\rho(\theta_2,\alpha))r_0^2} e^{-\lambda\pi p_c\rho(\theta_1,\alpha)r_0^2} \\
&\qquad\qquad \times t_1 r_0 \mathrm{d}t_1\mathrm{d}r_0 \\
&= p_c(2\pi\lambda)^2 \int_0^\infty \int_0^1 e^{-\lambda\pi p_c(1+p_a\rho(\theta_2 u^\alpha,\alpha))u^{-2}r_0^2} e^{-\lambda\pi(1-p_c)(1+(1-p_a)\rho(\theta_2,\alpha))r_0^2} e^{-\lambda\pi p_c\rho(\theta_1,\alpha)r_0^2} \\
&\qquad\qquad \times r_0^3 u^{-3}\mathrm{d}u\mathrm{d}r_0 \\
&= p_c(2\pi\lambda)^2 \int_0^1 \int_0^\infty e^{-\lambda\pi\left[p_c\rho(\theta_2,\alpha)+p_c(1+p_a\rho(\theta_2 u^\alpha,\alpha))u^{-2}+(1-p_c)(1+(1-p_a)\rho(\theta_2,\alpha))\right]r_0^2} \\
&\qquad\qquad \times r_0^3 \mathrm{d}r_0 u^{-3}\mathrm{d}u \\
&= p_c(2\pi\lambda)^2 \int_0^1 \\
&\qquad \frac{u^{-3}\mathrm{d}u}{2(\pi\lambda)^2(p_c\rho(\theta_1,\alpha)+p_c(1+p_a\rho(\theta_2 u^\alpha,\alpha))u^{-2}+(1-p_c)(1+(1-p_a)\rho(\theta_2,\alpha)))^2} \\
&= p_c\int_0^1 \frac{1}{\left(p_c\rho(\theta_1,\alpha)x + p_c(1+p_a\rho(\theta_2 x^{\frac{\alpha}{2}},\alpha)) + (1-p_c)(1+(1-p_a)\rho(\theta_2,\alpha))x\right)^2}\mathrm{d}x.
\end{aligned}
\tag{A.25}
$$

$$
\begin{aligned}
\mathcal{Q}_2 &= \mathbb{E}_{T_1,R_0}\left[\mathscr{L}_{I_2}(\theta_2 T_1)\mathscr{L}_{I_{0,1}}(\theta_1 R_0^\alpha)\right] \\
&= \int_0^\infty \int_{r_0}^\infty \mathscr{L}_{I_2}(\theta_2 t_1^\alpha)\mathscr{L}_{I_{0,1}}(\theta_1 r_0^\alpha)\mathscr{L}_{I_{0,1}}(\theta_1 r_0^\alpha) f_{T_1,R_0}(t_1,r_0)\,\mathrm{d}t_1\mathrm{d}r_0 \\
&= \int_0^\infty \int_{r_0}^\infty \mathscr{L}_{I_{2,1}}(\theta_2 t_1^\alpha)\mathscr{L}_{I_{2,2}}(\theta_2 t_1^\alpha)\mathscr{L}_{I_{0,1}}(\theta_1 r_0^\alpha)\mathscr{L}_{I_{0,1}}(\theta_1 r_0^\alpha) f_{T_1,R_0}(t_1,r_0)\,\mathrm{d}t_1\mathrm{d}r_0 \\
&= p_c(2\pi\lambda)^2 \int_0^\infty \int_{r_0}^\infty e^{-\lambda\pi p_c p_a \rho(\theta_2,\alpha) t_1^2} e^{-\lambda\pi(1-p_c)(1-p_a)\rho(\theta_2(\frac{t_1}{r_0})^\alpha,\alpha) r_0^2} \\
&\qquad \times e^{-\lambda\pi p_c \rho(\theta_1,\alpha) r_0^2} e^{-\lambda\pi p_c t_1^2} e^{-\lambda\pi(1-p_c) r_0^2} t_1 r_0 \mathrm{d}t_1\mathrm{d}r_0 \\
&= p_c(2\pi\lambda)^2 \int_0^\infty \int_{r_0}^\infty e^{-\pi\lambda p_c(1+p_a\rho(\theta_2,\alpha)) t_1^2} e^{-\pi\lambda(1-p_c)(1+(1-p_a)\rho(\theta_2(\frac{t_1}{r_0})^\alpha,\alpha)) r_0^2} \\
&\qquad \times e^{-\lambda\pi p_c \rho(\theta_1,\alpha) r_0^2} t_1 r_0 \mathrm{d}t_1\mathrm{d}r_0 \\
&= p_c(2\pi\lambda)^2 \int_0^\infty \int_0^1 e^{-\lambda\pi p_c(1+p_a\rho(\theta_2,\alpha)) u^{-2} r_0^2} e^{-\lambda\pi(1-p_c)(1+(1-p_a)\rho(\theta_2 u^{-\alpha},\alpha)) r_0^2} \\
&\qquad \times e^{-\lambda\pi p_c \rho(\theta_1,\alpha) r_0^2} r_0^3 u^{-3} \mathrm{d}u\mathrm{d}r_0 \\
&= p_c(2\pi\lambda)^2 \int_0^1 \int_0^\infty e^{-\lambda\pi\left[p_c\rho(\theta_1,\alpha)+p_c(1+p_a\rho(\theta_2,\alpha))u^{-2}+(1-p_c)(1+(1-p_a)\rho(\theta_2 u^{-\alpha},\alpha))\right] r_0^2} \\
&\qquad \times r_0^3 u^{-3} \mathrm{d}r_0\mathrm{d}u \\
&= p_c(2\pi\lambda)^2 \int_0^1 \\
&\qquad \frac{u^{-3}\mathrm{d}u}{2(\pi\lambda)^2(p_c\rho(\theta_1,\alpha)+p_c(1+p_a\rho(\theta_2,\alpha))u^{-2}+(1-p_c)(1+(1-p_a)\rho(\theta_2 u^{-\alpha},\alpha)))^2} \\
&= p_c \int_0^1 \frac{\mathrm{d}x}{\left(p_c\rho(\theta_1,\alpha)x + p_c(1+p_a\rho(\theta_2,\alpha)) + (1-p_c)(1+(1-p_a)\rho(\theta_2 x^{-\frac{\alpha}{2}},\alpha))x\right)^2}.
\end{aligned}
\tag{A.26}
$$

$$
\begin{aligned}
\mathcal{Q}_3 &= -\mathbb{E}_{T_1,R_0}\left[\mathscr{L}_{I_2}(\theta_2 R_0^\alpha)\mathscr{L}_{I_2}(\theta_2 T_1^\alpha)\mathscr{L}_{I_{0,1}}(\theta_1 R_0^\alpha)\right] \\
&= -\int_0^\infty\int_{r_0}^\infty \mathscr{L}_{I_2}(\theta_2 r_0^\alpha)\mathscr{L}_{I_2}(\theta_2 t_1^\alpha)\mathscr{L}_{I_{0,1}}(\theta_1 r_0^\alpha) f_{T_1,R_0}(t_1,r_0)\ \mathrm{d}t_1\mathrm{d}r_0 \\
&= -\int_0^\infty\int_{r_0}^\infty \mathscr{L}_{I_{2,1}}(\theta_2 r_0^\alpha)\mathscr{L}_{I_{2,1}}(\theta_2 t_1^\alpha)\mathscr{L}_{I_{2,2}}(\theta_2 r_0^\alpha)\mathscr{L}_{I_{2,2}}(\theta_2 t_1^\alpha)\mathscr{L}_{I_{0,1}}(\theta_1 r_0^\alpha) f_{T_1,R_0}(t_1,r_0)\ \mathrm{d}t_1\mathrm{d}r_0 \\
&= p_c(2\pi\lambda)^2\int_0^\infty\int_{r_0}^\infty e^{-\lambda\pi p_c p_a \rho(\theta_2(\frac{r_0}{t_1})^\alpha,\alpha)t_1^2} e^{-\lambda\pi p_c p_a\rho(\theta_2,\alpha)t_1^2} e^{-\lambda\pi(1-p_c)(1-p_a)\rho(\theta_2,\alpha)r_0^2} \\
&\quad\times e^{-\lambda\pi(1-p_c)(1-p_a)\rho(\theta_2(\frac{t_1}{r_0})^\alpha,\alpha)r_0^2} e^{-\lambda\pi p_c\rho(\theta_1,\alpha)r_0^2} e^{-\lambda\pi p_c t_1^2} e^{-\lambda\pi(1-p_c)r_0^2} t_1 r_0 \mathrm{d}t_1\mathrm{d}r_0 \\
&= p_c(2\pi\lambda)^2\int_0^\infty\int_{r_0}^\infty e^{-\pi\lambda p_c(1+p_a(\rho(\theta_2,\alpha)+\rho(\theta_2(\frac{r_0}{t_1})^\alpha,\alpha)))t_1^2} e^{-\pi\lambda(1-p_c)(1+(1-p_a)(\rho(\theta_2,\alpha)+\rho(\theta_2(\frac{t_1}{r_0})^\alpha,\alpha)))r_0^2} \\
&\qquad\qquad\times e^{-\lambda\pi p_c\rho(\theta_1,\alpha)r_0^2} t_1 r_0 \mathrm{d}t_1\mathrm{d}r_0 \\
&= p_c(2\pi\lambda)^2\int_0^\infty\int_1^\infty e^{-\pi\lambda p_c(1+p_a(\rho(\theta_2,\alpha)+\rho(\theta_2 u^\alpha,\alpha)))u^{-2}r_0^2} e^{-\pi\lambda(1-p_c)(1+(1-p_a)(\rho(\theta_2,\alpha)+\rho(\theta_2 u^{-\alpha},\alpha)))r_0^2} \\
&\qquad\qquad\times e^{-\lambda\pi p_c\rho(\theta_1,\alpha)r_0^2} u^{-3} r_0^3 \mathrm{d}r_0\mathrm{d}u \\
&= p_c(2\pi\lambda)^2\int_0^1\int_0^\infty \\
&\quad e^{-\lambda\pi\left[p_c\rho(\theta_1,\alpha)+p_c(1+p_a(\rho(\theta_2,\alpha)+\rho(\theta_2 u^\alpha,\alpha)))u^{-2}+(1-p_c)(1+(1-p_a)(\rho(\theta_2,\alpha)+\rho(\theta_2 u^{-\alpha},\alpha)))\right]r_0^2} r_0^3 u^{-3}\mathrm{d}r_0\mathrm{d}u \\
&= \frac{1}{2(\pi\lambda)^2}\int_0^1 \\
&\qquad\qquad\qquad\qquad p_c(2\pi\lambda)^2 u^{-3}\mathrm{d}u \\
&\overline{(p_c\rho(\theta_1,\alpha)+p_c(1+p_a(\rho(\theta_2,\alpha)+\rho(\theta_2 u^\alpha,\alpha)))u^{-2}+(1-p_c)(1+(1-p_a)(\rho(\theta_2,\alpha)+\rho(\theta_2 u^{-\alpha},\alpha))))^2} \\
&= \int_0^1 \\
&\qquad\qquad\qquad\qquad p_c\mathrm{d}x \\
&\overline{\left(p_c\rho(\theta_1,\alpha)x+p_c(1+p_a(\rho(\theta_2,\alpha)+\rho(\theta_2 x^{\frac{\alpha}{2}},\alpha)))+(1-p_c)(1+(1-p_a)(\rho(\theta_2,\alpha)+\rho(\theta_2 x^{-\frac{\alpha}{2}},\alpha)))x\right)^2}.
\end{aligned}
\tag{A.27}
$$

## A.6 Proof of Concavity (§ 5.6.5)

The objective function is

$$\mathscr{H}(\boldsymbol{\omega},\beta) = \frac{1}{\beta}\log\left[\sum_k p_k\, e^{\beta\omega_k\mathscr{R}_k}\right]. \tag{A.28}$$

Considering $\left(z_k = p_k \exp(\beta\mathscr{R}_k w_k)\right)$

$$\frac{\partial}{\partial w_j} f(\boldsymbol{\omega}) = \frac{1}{\beta}\cdot\frac{\partial}{\partial z_j}\log \mathbf{1}^T\mathbf{z}\cdot\frac{\partial z_j}{\partial \omega_j} = \frac{1}{\mathbf{1}^T\mathbf{z}}\cdot\mathscr{R}_j z_j. \tag{A.29}$$

$$\begin{aligned}
\frac{\partial^2 f(\boldsymbol{\omega})}{\partial\omega_i\partial\omega_j} &= \frac{\partial}{\partial z_i}\left(\frac{\mathscr{R}_j z_j}{\mathbf{1}^T\mathbf{z}}\right)\cdot\frac{\partial z_i}{\partial\omega_i} \\
&= \frac{\mathscr{R}_j\delta_{ij}\mathbf{1}^T\mathbf{z} - \mathscr{R}_j z_j}{\left(\mathbf{1}^T\mathbf{z}\right)^2}\cdot\beta\mathscr{R}_i z_i \\
&= \beta\cdot\frac{\mathscr{R}_i\mathscr{R}_j\delta_{ij}z_i\cdot\mathbf{1}^T\mathbf{z} - (\mathscr{R}_i z_i)(\mathscr{R}_j z_j)}{\left(\mathbf{1}^T\mathbf{z}\right)^2} \\
&= \beta\cdot\left(\frac{\delta_{ij}(\mathscr{R}_i^2 z_i)}{\mathbf{1}^T\mathbf{z}} - \frac{(\mathscr{R}_i z_i)(\mathscr{R}_j z_j)}{\left(\mathbf{1}^T\mathbf{z}\right)^2}\right) \\
&= \beta\cdot\left(\frac{\mathscr{R}^T\odot\operatorname{diag}(\mathbf{x})}{\mathbf{1}^T\mathbf{z}} - \frac{1}{\left(\mathbf{1}^T\mathbf{z}\right)^2}\mathbf{x}\mathbf{x}^T\right)_{i,j}
\end{aligned} \tag{A.30}$$

$$\nabla^2 f(\boldsymbol{\omega}) = \beta\cdot\left(\frac{\mathscr{R}^T\odot\operatorname{diag}(\mathbf{x})}{\mathbf{1}^T\mathbf{z}} - \frac{1}{\left(\mathbf{1}^T\mathbf{z}\right)^2}\mathbf{x}\mathbf{x}^T\right). \tag{A.31}$$

To show $\nabla^2 f(\boldsymbol{\omega}) \le 0$, we must verify that $v^T\nabla^2 f(\boldsymbol{\omega})v \le 0$ for all $v$ :

$$v^T\nabla^2 f(\boldsymbol{\omega})v = \beta\cdot\frac{\left(\sum_k \mathscr{R}_k^2 z_k v_k^2\right)\left(\sum_k z_k\right) - \left(\sum_k v_k\mathscr{R}_k z_k\right)^2}{\left(\sum_k z_k\right)^2} \le 0, \tag{A.32}$$

which is correct when $\beta \le 0$, since $\left(\sum_k \mathscr{R}_k v_k z_k\right)^2 \le \left(\sum_k z_k\mathscr{R}_k v_k^2\right)\left(\sum_k z_k\right)$ ( from Cauchy-Schwarz inequality $\left(a^T a\right)\left(b^T b\right) \ge \left(a^T b\right)^2$ by considering $a_i = \mathscr{R}_i v_i\sqrt{z_i}$ and $b_i = \sqrt{z_i}$).

# Bibliography


[1] T. D. Novlan, R. K. Ganti, A. Ghosh, and J. G. Andrews, "Analytical evaluation of fractional frequency reuse for ofdma cellular networks," *IEEE Transactions on wireless communications*, vol. 10, pp. 4294–4305, Dec. 2011.

[2] J. G. Andrews, F. Baccelli, and R. K. Ganti, "A tractable approach to coverage and rate in cellular networks," *IEEE Transactions on communications*, vol. 59, pp. 3122–3134, Nov. 2011.

[3] G. Nigam, P. Minero, and M. Haenggi, "Coordinated multipoint joint transmission in heterogeneous networkss," *IEEE Transactions on Communications*, vol. 62, pp. 4134–4146, Nov. 2014.

[4] A. H. Sakr and E. Hossain, "Location-aware cross-tier coordinated multipoint transmission in two-tier cellular networks," *IEEE Transactions on Wireless Communications*, vol. 13, pp. 6311–6325, Nov. 2017.

[5] R. Tanbourgi, S. Singh, J. G. Andrews, and F. K. Jondral, "A tractable model for noncoherent joint-transmission base station cooperation," *IEEE Transactions on Wireless Communications*, vol. 13, pp. 4959–4973, Sep. 2014.

[6] S. Bassoy, H. Farooq, M. A. Imran, and A. Imran, "Coordinated multi-point clustering schemes: A survey," *IEEE Communications Surveys & Tutorials*, vol. 19, pp. 743–764, Feb. 2017.

[7] I. Lahsen-Cherif, *Spectral and Energy Efficiency in 5G Wireless Networks*, 1st ed. Université Paris-Saclay (ComUE), 2016.

[8] M. Yassin, M. A. AboulHassan, S. Lahoud, M. Ibrahim, D. Mezher, B. Cousin, and E. A. Sourour, "Survey of icic techniques in lte networks under various mobile environment parameters," *Wireless Networks*, vol. 23, pp. 403–418, Sep. 2017.

[9] R. Ghaffar and R. Knopp, "Fractional frequency reuse and interference suppression for ofdma networks," *8th International Symposium on Modeling and Optimization in Mobile, Ad Hoc, and Wireless Networks*, pp. 273–277, Oct. 2010.

[10] W. Mohr, "The 5g infrastructure public-private partnership," *Proc. Presentation ITU GSC Meeting*, p. 35, 2015.

[11] J. Yoon and G. Hwang, "Distance-based inter-cell interference coordination in small cell networks: stochastic geometry modeling and analysis," *IEEE Transactions on Wireless Communications*, vol. 17, pp. 4089–4103, Apr. 2018.

[12] S. Lee and K. Huang, "Coverage and economy of cellular networks with many base stations," *IEEE Communications Letters*, vol. 16, pp. 1038–1040, Jul. 2012.

[13] M. Kamel, W. Hamouda, and A. Youssef, "Ultra-dense networks: A survey," *IEEE Communications Surveys & Tutorials*, vol. 16, pp. 2522–2545, May 2018.

[14] J. Park, S.-L. Kim, and J. Zander, "Tractable resource management with uplink decoupled millimeter-wave overlay in ultra-dense cellular networks," *IEEE Transactions on Wireless Communications*, vol. 15, pp. 4362–4379, Jun. 2016.

[15] S. S. Kalamkar, "Reliability and local delay in wireless networks: Does bandwidth partitioning help?" *IEEE Global Communications Conference (GLOBECOM)*, pp. 1–6, Dec. 2019.

[16] K. Feng and M. Haenggi, "A location-dependent base station cooperation scheme for cellular networks," *IEEE Transactions on Communications*, vol. 67, pp. 6415–6426, Sep. 2019.

[17] A. D. Wyner, "Shannon-theoretic approach to a gaussian cellular multiple-access channel," *IEEE Transactions on Information Theory*, vol. 40, pp. 1713–1727, Nov. 1994.

[18] H. ElSawy, E. Hossain, and M. Haenggi, "Stochastic geometry for modeling, analysis, and design of multi-tier and cognitive cellular wireless networks: A survey," *IEEE Communications Surveys & Tutorials*, vol. 15, pp. 996–1019, Jun. 2013.

[19] A. S. Hamza, S. S. Khalifa, H. S. Hamza, and K. Elsayed, "A survey on inter-cell interference coordination techniques in ofdma-based cellular networks," *IEEE Communications Surveys & Tutorials*, vol. 15, pp. 1642–1670, Mar. 2013.

[20] M. Hasan, A. Ismail, A. H. Abdalla, K. Abdullah, H. Ramli, S. Islam, and R. A. Saeed, "Inter-cell interference coordination in lte-a hetnets: A survey on self organizing approaches," *International Conference on Computing, Electrical And Electronic Engineering (ICCEEE)*, pp. 196–201, Aug. 2013.

[21] S. A. R. Zaidi, D. C. McLernon, M. Ghogho, and M. A. Imran, "Cloud empowered cognitive inter-cell interference coordination for small cellular networks," *IEEE International Conference on Communication Workshop (ICCW)*, pp. 2218–2224, Jun. 2015.

[22] X. Zhang and M. Haenggi, "A stochastic geometry analysis of inter-cell interference coordination and intra-cell diversity," *IEEE Transactions on Wireless Communications*, vol. 13, pp. 6655–6669, Dec. 2014.

[23] B. U. Kazi, M. Etemad, G. Wainer, and G. Boudreau, "Signaling overhead and feedback delay reduction in heterogeneous multicell cooperative networks," *International Symposium on Performance Evaluation of Computer and Telecommunication Systems (SPECTS)*, pp. 1–8, Jul. 2016.

[24] M. Afshang, Z. Yazdanshenasan, S. Mukherjee, and P. H. J. Chong, "Hybrid division duplex for hetnets: Coordinated interference management with uplink power control," *IEEE International Conference on Communication Workshop (ICCW)*, pp. 106–112, Jun. 2015.

[25] H. ElSawy and E. Hossain, "Two-tier hetnets with cognitive femtocells: Downlink performance modeling and analysis in a multichannel environment," *IEEE Transactions on Mobile Computing*, vol. 13, pp. 649–663, Mar. 2013.

[26] J. Lee, J. G. Andrews, and D. Hong, "Spectrum-sharing transmission capacity with interference cancellation," *IEEE Transactions on Communications*, vol. 61, pp. 76–86, Jan. 2012.

[27] S. Y. Jung, H.-k. Lee, and S.-L. Kim, "Worst-case user analysis in poisson voronoi cells," *IEEE communications letters*, vol. 17, pp. 1580–1583, Aug. 2013.

[28] M. Mardani, P. Mary, and J.-Y. Baudais, "A user-centric non-full interference cellular networks: Bs cooperation and bandwidth partitioning," *IEEE Transactions on Communications*, submitted on nov. 2021.

[29] ——, "A tractable model for coverage in non-full interference cellular networks with cell center/edge users," in *IEEE International Workshop on Signal Processing Advances in Wireless Communications*, Atlanta, Georgie, USA (virtual), May 2020, pp. 1–5.

[30] ——, "A user-centric frequency reuse in non-full interference cellular networks," in *IEEE Global Communications Conference*, Taipei, Taiwan (virtual), Dec. 2020, pp. 1–6.

[31] S. N. Chiu, D. Stoyan, W. S. Kendall, and J. Mecke, *Stochastic geometry and its applications*. John Wiley & Sons, 2013.

[32] F. Baccelli and S. Zuyev, "Stochastic geometry models of mobile communication networks," *Frontiers in queueing, CRC Press*, pp. 227–243, 1996.

[33] F. Baccelli, M. Klein, M. Lebourges, and S. Zuyev, "Stochastic geometry and architecture of communication networks," *Telecommunication Systems*, vol. 7, pp. 209–227, Jun. 1997.

[34] F. Baccelli, B. Blaszczyszyn, and P. Muhlethaler, "Stochastic analysis of spatial and opportunistic aloha," *IEEE journal on selected areas in communications*, vol. 27, pp. 1105–1119, Sep. 2009.

[35] E. N. Gilbert, "Random plane networks," *Journal of the society for industrial and applied mathematics*, vol. 9, pp. 533–543, 1961.

[36] M. Haenggi, "A geometric interpretation of fading in wireless networks: Theory and applications," *IEEE Transactions on Information Theory*, vol. 54, pp. 5500–5510, Dec. 2008.

[37] S. Zuyev, *Stochastic geometry and telecommunications networks*. Oxford University Press, 2009.

[38] J. G. Andrews, A. K. Gupta, and H. S. Dhillon, "A primer on cellular network analysis using stochastic geometry," *arXiv preprint arXiv:1604.03183*, 2016.

[39] D. Moltchanov, "Distance distributions in random networks," *Ad Hoc Networks*, vol. 10, pp. 1146–1166, Aug. 2012.

[40] M. Haenggi and R. K. Ganti, "Interference in large wireless networks," *Now Publishers Inc*, vol. 3, pp. 127–248, 2009.

[41] P. Cardieri, "Modeling interference in wireless ad hoc networks," *IEEE Communications Surveys & Tutorials*, vol. 12, pp. 551–572, Nov. 2010.

[42] H. ElSawy, A. Sultan-Salem, M.-S. Alouini, and M. Z. Win, "Modeling and analysis of cellular networks using stochastic geometry: A tutorial," *IEEE Communications Surveys & Tutorials*, vol. 19, pp. 167–203, Nov. 2016.

[43] M. Haenggi, *Stochastic geometry for wireless networks*. Cambridge University Press, 2012.

[44] J. Illian, A. Penttinen, H. Stoyan, and D. Stoyan, *Statistical analysis and modelling of spatial point patterns*. John Wiley & Sons, 2008.

[45] J.-F. Coeurjolly, J. Møller, and R. Waagepetersen, "A tutorial on palm distributions for spatial point processes," *International Statistical Review*, vol. 85, pp. 404–420, Dec. 2017.

[46] S. Srinivasa and M. Haenggi, "Distance distributions in finite uniformly random networks: Theory and applications," *IEEE Transactions on Vehicular Technology*, vol. 59, pp. 940–949, Feb. 2009.

[47] D. J. Daley and D. Vere-Jones, *An introduction to the theory of point processes: volume I: elementary theory and methods*, 2nd ed. Springer, 2003, traduction française de J. André, B. Belet, J.-C. Charpentier, J.-M. Hufflen et Y. Soulet.

[48] H. S. Dhillon, R. K. Ganti, F. Baccelli, and J. G. Andrews, "Modeling and analysis of k-tier downlink heterogeneous cellular networks," *IEEE Journal on Selected Areas in Communications*, vol. 30, pp. 550–560, Apr. 2012.

[49] T. Bai and R. W. Heath, "Coverage and rate analysis for millimeter-wave cellular networks," *IEEE Transactions on Wireless Communications*, vol. 14, pp. 1100–1114, Feb. 2014.

[50] T. Sanguanpuak, S. Guruacharya, E. Hossain, N. Rajatheva, and M. Latva-aho, "Infrastructure sharing for mobile network operators: Analysis of trade-offs and market," *IEEE Transactions on Mobile Computing*, vol. 17, pp. 2804–2817, Dec. 2018.

[51] J. Kibiłda, N. J. Kaminski, and L. A. DaSilva, "Radio access network and spectrum sharing in mobile networks: A stochastic geometry perspective," *IEEE Transactions on Wireless Communications*, vol. 16, pp. 2562–2575, Apr. 2017.

[52] V. V. Chetlur and H. S. Dhillon, "Coverage analysis of a vehicular network modeled as cox process driven by poisson line process," *IEEE Transactions on Wireless Communications*, vol. 17, pp. 4401–4416, Jul. 2018.

[53] A. Munari, P. Mähönen, and M. Petrova, "A stochastic geometry approach to asynchronous aloha full-duplex networks," *IEEE/ACM Transactions on Networking*, vol. 25, pp. 3695–3708, Dec. 2017.

[54] A. H. Sakr and E. Hossain, "Cognitive and energy harvesting-based d2d communication in cellular networks: Stochastic geometry modeling and analysis," *IEEE Transactions on Communications*, vol. 63, pp. 1867–1880, May 2015.

[55] P. Madhusudhanan, J. G. Restrepo, Y. E. Liu, T. X. Brown, and K. Baker, "Stochastic ordering based carrier-to-interference ratio analysis for the shotgun cellular systems," *IEEE Wireless Communications Letters*, vol. 1, pp. 565–568, Dec. 2012.

[56] R. K. Ganti, F. Baccelli, and J. G. Andrews, "Series expansion for interference in wireless networks," *IEEE Transactions on Information Theory*, vol. 58, pp. 2194–2205, Apr. 2012.

[57] H.-S. Jo, Y. J. Sang, P. Xia, and J. G. Andrews, "Heterogeneous cellular networks with flexible cell association: A comprehensive downlink sinr analysis," *IEEE Transactions on Wireless Communications*, vol. 10, pp. 3484–3495, Oct. 2012.

[58] S. Huaizhou, R. V. Prasad, E. Onur, and I. Niemegeers, "Fairness in wireless networks: Issues, measures and challenges," *IEEE Communications Surveys & Tutorials*, vol. 16, pp. 5–24, May 2013.

[59] R. K. Jain, D.-M. W. Chiu, W. R. Hawe *et al.*, *A quantitative measure of fairness and discrimination*. Eastern Research Laboratory, Digital Equipment Corporation, Hudson, MA, 1984.

[60] M. Uchida and J. Kurose, "An information-theoretic characterization of weighted alpha-proportional fairness," *IEEE INFOCOM 2009*, pp. 1053–1061, Apr. 2009.

[61] B. Radunovic and J.-Y. Le Boudec, "A unified framework for max-min and min-max fairness with applications," *IEEE/ACM Transactions on networking*, vol. 15, pp. 1073–1083, Oct. 2007.

[62] F. Kelly, "Charging and rate control for elastic traffic," *European transactions on Telecommunications, Wiley Online Library*, vol. 8, pp. 33–37, Sep. 1997.

[63] M. Haenggi, "The meta distribution of the sir in poisson bipolar and cellular networks," *IEEE Transactions on Wireless Communications*, vol. 15, pp. 2577–2589, Apr. 2015.

[64] Y. Hmamouche, M. Benjillali, S. Saoudi, H. Yanikomeroglu, and M. Di Renzo, "New trends in stochastic geometry for wireless networks: A tutorial and survey," *Proceedings of the IEEE*, vol. 109, pp. 1200 – 1252, Mar. 2021.

[65] D. Kedar and S. Arnon, "Urban optical wireless communication networks: the main challenges and possible solutions," *IEEE Communications Magazine*, vol. 42, pp. S2–S7, May 2004.

[66] J. Wildman, P. H. J. Nardelli, M. Latva-aho, and S. Weber, "On the joint impact of beamwidth and orientation error on throughput in directional wireless poisson networks," *IEEE Transactions on Wireless Communications*, vol. 13, pp. 7072–7085, Dec. 2014.

[67] A. K. Gupta, X. Zhang, and J. G. Andrews, "Sinr and throughput scaling in ultradense urban cellular networks," *IEEE Wireless Communications Letters*, vol. 4, pp. 605–608, Dec. 2015.

[68] I. Atzeni, J. Arnau, and M. Kountouris, "Downlink cellular network analysis with los/nlos propagation and elevated base stations," *IEEE Transactions on Wireless Communications*, vol. 17, pp. 142–156, Jan. 2017.

[69] M. Di Renzo, A. Guidotti, and G. E. Corazza, "Average rate of downlink heterogeneous cellular networks over generalized fading channels: A stochastic geometry approach," *IEEE Transactions on Communications*, vol. 61, pp. 3050–3071, Jul. 2013.

[70] Y. Hmamouche, M. Benjillali, and S. Saoudi, "A stochastic geometry based approach to tractable 5g rnpo with a new *h*-los model," *IEEE Wireless Communications and Networking Conference (WCNC)*, pp. 1–8, Apr. 2019.

[71] S. Guruacharya, H. Tabassum, and E. Hossain, "Integral approximations for coverage probability," *IEEE Wireless Communications Letters*, vol. 5, pp. 24–27, Feb. 2015.

[72] R. K. Ganti and M. Haenggi, "Asymptotics and approximation of the sir distribution in general cellular networks," *IEEE Transactions on Wireless Communications*, vol. 15, pp. 2130–2143, Mar. 2015.

[73] S. Guruacharya and E. Hossain, "Approximation of meta distribution and its moments for poisson cellular networks," *IEEE Wireless Communications Letters*, vol. 7, pp. 1074–1077, Dec. 2018.

[74] H. P. Keeler, B. Błaszczyszyn, and M. K. Karray, "Sinr-based k-coverage probability in cellular networks with arbitrary shadowing," *IEEE International Symposium on Information Theory*, pp. 1167–1171, Jul. 2013.

[75] S. Mukherjee, "Downlink sinr distribution in a heterogeneous cellular wireless network with max-sinr connectivity," *Annual Allerton Conference on Communication, Control, and Computing (Allerton)*, pp. 1649–1656, Sep. 2011.

[76] B. Błaszczyszyn and H. P. Keeler, "Studying the sinr process of the typical user in poisson networks using its factorial moment measures," *IEEE Transactions on Information Theory*, vol. 16, pp. 6774–6794, Dec. 2015.

[77] J. Gil-Pelaez, "Note on the inversion theorem," *Biometrikas*, 1951.

[78] M. Di Renzo, W. Lu, and P. Guan, "The intensity matching approach: A tractable stochastic geometry approximation to system-level analysis of cellular networks," *IEEE Transactions on Wireless Communications*, vol. 15, pp. 5963–5983, Sep. 2016.

[79] M. Di Renzo, "Stochastic geometry modeling and analysis of multi-tier millimeter wave cellular networks," *IEEE Transactions on Wireless Communications*, vol. 14, pp. 5038–5057, Sep. 2015.

[80] Y. Zhong, T. Q. Quek, and X. Ge, "Heterogeneous cellular networks with spatio-temporal traffic: Delay analysis and scheduling," *IEEE Journal on Selected Areas in Communications*, vol. 35, pp. 1373–1386, Jun. 2017.

[81] M. Salehi, A. Mohammadi, and M. Haenggi, "Analysis of d2d underlaid cellular networks: Sir meta distribution and mean local delay," *IEEE Transactions on Communications*, vol. 65, pp. 2904–2916, Jul. 2017.

[82] B. Błaszczyszyn, M. K. Karray, and H. P. Keeler, "Using poisson processes to model lattice cellular networks," *Proceedings IEEE INFOCOM*, pp. 773–781, Apr. 2013.

[83] P. Madhusudhanan, J. G. Restrepo, Y. Liu, T. X. Brown, and K. R. Baker, "Downlink performance analysis for a generalized shotgun cellular system," *IEEE Transactions on Wireless Communications*, vol. 13, pp. 6684–6696, Dec. 2014.

[84] O. Georgiou, "Polarized rician fading models for performance analysis in cellular networks," *IEEE Communications Letters*, vol. 20, pp. 1255–1258, Jun. 2016.

[85] Z. Zhang and R. Q. Hu, "Dense cellular network analysis with los/nlos propagation and bounded path loss model," *IEEE Communications Letters*, vol. 22, pp. 2386–2389, Nov. 2018.

[86] V. V. Chetlur and H. S. Dhillon, "Downlink coverage analysis for a finite 3-d wireless network of unmanned aerial vehicles," *IEEE Transactions on Communications*, vol. 65, pp. 4543–4558, Oct. 2017.

[87] M. Z. Win, P. C. Pinto, and L. A. Shepp, "A mathematical theory of network interference and its applications," *Proceedings of the IEEE*, vol. 97, pp. 205–230, Feb. 2009.

[88] R. W. Heath, M. Kountouris, and T. Bai, "Modeling heterogeneous network interference using poisson point processes," *IEEE Transactions on Signal Processing*, vol. 61, pp. 4114–4126, Aug. 2013.

[89] H. Ghazzai, E. Yaacoub, M.-S. Alouini, Z. Dawy, and A. Abu-Dayya, "Optimized lte cell planning with varying spatial and temporal user densities," *IEEE Transactions on vehicular technology*, vol. 65, pp. 1575–1589, Mar. 2015.

[90] A. Achtzehn, J. Riihijärvi, and P. Mähönen, "Large-scale cellular network modeling from population data: An empirical analysis," *IEEE Communications Letters*, vol. 20, pp. 2292–2295, Nov. 2016.

[91] M. Di Renzo, S. Wang, and X. Xi, "Inhomogeneous double thinning—modeling and analysis of cellular networks by using inhomogeneous poisson point processes," *IEEE Transactions on Wireless Communications*, vol. 20, pp. 5162–5182, Aug. 2017.

[92] M. Michalopoulou, J. Riihijärvi, and P. Mähönen, "Studying the relationships between spatial structures of wireless networks and population densities," *IEEE Global Telecommunications Conference (GLOBECOM)*, pp. 1–6, Dec. 2010.

[93] Y. Zhou, Z. Zhao, Y. Louët, Q. Ying, R. Li, X. Zhou, X. Chen, and H. Zhang, "Large-scale spatial distribution identification of base stations in cellular networks," *IEEE access*, vol. 3, pp. 2987–2999, 2015.

[94] L. Chiaraviglio, F. Cuomo, M. Maisto, A. Gigli, J. Lorincz, Y. Zhou, Z. Zhao, C. Qi, and H. Zhang, "What is the best spatial distribution to model base station density? a deep dive into two european mobile networks," *IEEE Access*, vol. 4, pp. 1434–1443, 2016.

[95] A. Guo and M. Haenggi, "Spatial stochastic models and metrics for the structure of base stations in cellular networks," *IEEE Transactions on Wireless Communications*, vol. 12, pp. 5800–5812, Nov. 2013.

[96] Y. Li, F. Baccelli, H. S. Dhillon, and J. G. Andrews, "Fitting determinantal point processes to macro base station deployments," *IEEE Global Communications Conference*, pp. 3641–3646, Dec. 2014.

[97] R. Nasri and A. Jaziri, "Analytical tractability of hexagonal network model with random user location," *IEEE Transactions on Wireless Communications*, vol. 15, pp. 3768–3780, May 2016.

[98] J. Kibiłda, B. Galkin, and L. A. DaSilva, "Modelling multi-operator base station deployment patterns in cellular networks," *IEEE Transactions on Mobile Computing*, vol. 15, pp. 3087–3099, Dec. 2015.

[99] F. J. Martin-Vega, B. Soret, M. C. Aguayo-Torres, I. Z. Kovacs, and G. Gomez, "Geolocation-based access for vehicular communications: Analysis and optimization via stochastic geometry," *IEEE Transactions on Vehicular Technology*, vol. 67, pp. 3069–3084, Apr. 2018.

[100] B. Matérn, *Spatial variation*, 2nd ed. Springer Science & Business Media, 1986.

[101] F. Lavancier, J. Møller, and E. Rubak, "Statistical aspects of determinantal point processes," *https://hal.archives-ouvertes.fr/hal-00698958/document*, pp. 1–62, 2012.

[102] N. Miyoshi and T. Shirai, "A cellular network model with ginibre configured base stations," *Advances in Applied Probability*, vol. 46, pp. 832–845, Oct. 2014.

[103] C.-S. Choi, J. O. Woo, and J. G. Andrews, "An analytical framework for modeling a spatially repulsive cellular network," *IEEE Transactions on Communications*, vol. 66, pp. 862–874, Feb. 2018.

[104] M. Haenggi, "User point processes in cellular networks," *IEEE Wireless Communications Letters*, vol. 6, pp. 258–261, Feb. 2017.

[105] J.-S. Ferenc and Z. Néda, "On the size distribution of poisson voronoi cells," *Physica A: Statistical Mechanics and its Applications*, pp. 518–526, 2007.

[106] S. M. Yu and S.-L. Kim, "Downlink capacity and base station density in cellular networks," *11th international symposium and workshops on modeling and optimization in mobile, ad hoc and wireless networks (WiOpt)*, pp. 119–124, May 2013.

[107] S. Singh, H. S. Dhillon, and J. G. Andrews, "Offloading in heterogeneous networks: Modeling, analysis, and design insights," *IEEE transactions on wireless communications*, vol. 15, pp. 2484–2497, May 2012.

[108] S. Singh, M. N. Kulkarni, A. Ghosh, and J. G. Andrews, "Tractable model for rate in self-backhauled millimeter wave cellular networks," *IEEE Journal on Selected Areas in Communications*, vol. 13, pp. 2196–2211, Oct. 2015.

[109] M. Haenggi, "On distances in uniformly random networks," *IEEE Transactions on Information Theory*, vol. 51, pp. 3584–3586, Oct. 2005.

[110] M. Afshang and H. S. Dhillon, "Fundamentals of modeling finite wireless networks using binomial point process," *IEEE Transactions on Wireless Communications*, vol. 16, pp. 3355–3370, May 2017.

[111] H. S. Dhillon, R. K. Ganti, and J. G. Andrews, "Load-aware modeling and analysis of heterogeneous cellular networks," *IEEE Transactions on Wireless Communications*, vol. 12, pp. 1666–1677, Apr. 2013.

[112] A. Mahmud and K. A. Hamdi, "A unified framework for the analysis of fractional frequency reuse techniques," *IEEE Transactions on Communications*, vol. 62, pp. 3692–3705, Oct. 2014.

[113] B. Xie, Z. Zhang, R. Q. Hu, G. Wu, and A. Papathanassiou, "Joint spectral efficiency and energy efficiency in ffr-based wireless heterogeneous networks," *IEEE Transactions on Vehicular technology*, vol. 67, pp. 8154–8168, Sep. 2018.

[114] P. D. Mankar, G. Das, and S. S. Pathak, "Load-aware performance analysis of cell center/edge users in random hetnets," *IEEE Transactions on Vehicular Technology*, vol. 67, pp. 2476–2490, Mar. 2017.

[115] C. Skouroumounis, C. Psomas, and I. Krikidis, "Heterogeneous fd-mm-wave cellular networks with cell center/edge users," *IEEE Transactions on Communications*, vol. 67, pp. 791–806, Sep. 2018.

[116] P. D. Mankar and H. S. Dhillon, "Downlink analysis of noma-enabled cellular networks with 3gpp-inspired user ranking," *IEEE Transactions on Wireless Communications*, vol. 19, pp. 3796–3811, Mar. 2020.

[117] H. Wang, K. Huang, and T. A. Tsiftsis, "Base station cooperation in millimeter wave cellular networks: Performance enhancement of cell-edge users," *IEEE Transactions on Wireless Communications*, vol. 66, pp. 5124–5139, Nov. 2018.

[118] H. Zhuang and T. Ohtsuki, "A model based on poisson point process for analyzing mimo heterogeneous networks utilizing fractional frequency reuse," *IEEE Transactions on Communications*, vol. 13, pp. 6839–6850, Oct. 2018.

[119] F. Dominique, C. G. Gerlach, N. Gopalakrishnan, A. Rao, J. P. Seymour, R. Soni, A. Stolyar, H. Viswanathan, C. Weaver, and A. Weber, "Self-organizing interference management for lte," *Bell Labs Technical Journal*, vol. 15, pp. 19–42, Dec. 2010.

[120] C. Skouroumounis, C. Psomas, and I. Krikidis, "A hybrid cooperation scheme for sub-6 ghz/mmwave cellular networks," *IEEE Communications Letters*, vol. 24, pp. 1539–1543, Oct. 2020.

[121] G. Nigam and P. Minero, "Spatiotemporal base station cooperation in a cellular network: The worst-case user," *IEEE Global Communications Conference (GLOBECOM)*, pp. 1–6, Dec. 2015.

[122] W. Bao and B. Liang, "Optimizing cluster size through handoff analysis in user-centric cooperative wireless networks," *IEEE Transactions on Wireless Communications*, vol. 17, pp. 766–778, Nov. 2017.

[123] X. Yu, Q. Cui, and M. Haenggi, "Coherent joint transmission in downlink heterogeneous cellular networks," *IEEE Wireless Communications Letters*, vol. 7, pp. 274–277, Nov. 2018.

[124] S. Chen, X. Liu, T. Zhao, H.-H. Chen, and W. Meng, "Performance analysis of joint transmission schemes in ultra-dense networks–a unified approach," *IEEE/ACM Transactions on Networking*, vol. 28, pp. 154–167, Dec. 2019.

[125] Y. Li, M. Xia, and S. Aïssa, "Coordinated multi-point transmission: A poisson-delaunay triangulation based approach," *IEEE Transactions on Wireless Communications*, vol. 19, pp. 2946–2959, May 2020.

[126] S. Akoum and R. W. Heath, "Multi-cell coordination: A stochastic geometry approach," *IEEE 13th International Workshop on Signal Processing Advances in Wireless Communications (SPAWC)*, pp. 16–20, Jun. 2012.

[127] K. Huang and J. G. Andrews, "An analytical framework for multicell cooperation via stochastic geometry and large deviations," *IEEE transactions on information theory*, vol. 59, pp. 2501–2516, Dec. 2012.

[128] X. Zhang and M. Haenggi, "A stochastic geometry analysis of inter-cell interference coordination and intra-cell diversity," *IEEE Transactions on Wireless Communications*, vol. 13, pp. 6655–6669, Jul. 2014.

[129] F. Baccelli and A. Giovanidis, "A stochastic geometry framework for analyzing pairwise-cooperative cellular networks," *IEEE Transactions on Wireless Communications*, vol. 14, pp. 794–808, Sep. 2015.

[130] N. Lee, D. Morales-Jimenez, A. Lozano, and R. W. Heath, "Spectral efficiency of dynamic coordinated beamforming: A stochastic geometry approach," *IEEE Transactions on Wireless Communications*, vol. 14, pp. 230–241, Jul. 2014.

[131] V. Garcia, Y. Zhou, and J. Shi, "Coordinated multipoint transmission in dense cellular networks with user-centric adaptive clustering," *IEEE Transactions on Wireless Communications*, vol. 13, pp. 4297–4308, Apr. 2014.

[132] J. He, Z. Tang, Z. Ding, and D. Wu, "Successive interference cancellation and fractional frequency reuse for lte uplink communications," *IEEE Transactions on Vehicular Technology*, vol. 67, pp. 10 528–10 542, Aug. 2018.

[133] A. Papazafeiropoulos, P. Kourtessis, M. Di Renzo, S. Chatzinotas, and J. M. Senior, "Performance analysis of cell-free massive mimo systems: A stochastic geometry approach," *IEEE Transactions on Vehicular Technology*, vol. 69, pp. 3523–3537, Jan. 2020.

[134] M. Ding and H. Luo, *Multi-point cooperative communication systems: Theory and applications*. Springer, 2013.

[135] H. Wang, X. Tao, and P. Zhang, "Adaptive modulation for dynamic point selection/dynamic point blanking," *IEEE Communications Letters*, vol. 19, pp. 343–346, Jan. 2015.

[136] Q. Cui, X. Yu, Y. Wang, and M. Haenggi, "The sir meta distribution in poisson cellular networks with base station cooperation," *IEEE Transactions on Communications*, vol. 66, pp. 1234–1249, Nov. 2017.

[137] A. Jahid, A. S. Ahmad, and M. F. Hossain, "Energy efficient bs cooperation in dps comp based cellular networks with hybrid power supply," *19th International Conference on Computer and Information Technology (ICCIT)*, pp. 93–98, Dec. 2016.

[138] M. F. Hossain, M. J. Huque, A. S. Ahmad, K. S. Munasinghe, and A. Jamalipour, "Energy efficiency of combined dps and jt comp technique in downlink lte-a cellular networks," *IEEE International Conference on Communications (ICC)*, pp. 1–6, Jul. 2016.

[139] F. Baccelli and A. Giovanidis, "Coverage by pairwise base station cooperation under adaptive geometric policies," *Asilomar Conference on Signals, Systems and Computers*, pp. 748–753, Nov. 2013.

[140] X. Yu, Q. Cui, and M. Haenggi, "Coherent joint transmission in downlink heterogeneous cellular networks," *IEEE Wireless Communications Letters*, vol. 7, pp. 274–277, Nov. 2017.

[141] Q. Cui, H. Wang, P. Hu, X. Tao, P. Zhang, J. Hamalainen, and L. Xia, "Evolution of limited-feedback comp systems from 4g to 5g: Comp features and limited-feedback approaches," *IEEE Vehicular Technology Magazine*, vol. 9, pp. 94–103, Aug. 2014.

[142] K. Manolakis, C. Oberli, L. Herrera, and V. Jungnickel, "Analytical models for channel aging and synchronization errors for base station cooperation," *European Signal Processing Conference (EUSIPCO 2013)*, pp. 1–5, May 2013.

[143] P. Marsch and G. Fettweis, "Uplink comp under a constrained backhaul and imperfect channel knowledge," *IEEE Transactions on Wireless Communications*, pp. 1730–1742, Apr. 2011.

[144] D. López-Pérez, A. Ladányi, A. Jüttner, H. Rivano, and J. Zhang, "Optimization method for the joint allocation of modulation schemes, coding rates, resource blocks and power in self-organizing lte networks," *Proceedings IEEE INFOCOM*, pp. 111–115, Apr. 2011.

[145] Y. L. Lee, T. C. Chuah, J. Loo, and A. Vinel, "Recent advances in radio resource management for heterogeneous lte/lte-a networks," *IEEE Communications Surveys & Tutorials*, vol. 16, pp. 2142–2180, Jun. 2014.

[146] V. Chandrasekhar and J. G. Andrews, "Spectrum allocation in tiered cellular networks," *IEEE transactions on communications*, vol. 57, pp. 3059–3068, Oct. 2009.

[147] R. Jain, *The art of computer systems performance analysis: techniques for experimental design, measurement, simulation, and modeling*. John Wiley & Sons, 1990.

[148] F. Baccelli and S. S. Kalamkar, "Bandwidth allocation and service differentiation in d2d wireless networks," *IEEE INFOCOM 2020-IEEE Conference on Computer Communications*, pp. 2116–2125, Jul. 2020.

[149] S. Timotheou and I. Krikidis, "Fairness for non-orthogonal multiple access in 5g systems," *IEEE Signal Processing Letters*, vol. 22, pp. 1647–1651, Mar. 2015.

[150] Y. Sun, D. W. K. Ng, Z. Ding, and R. Schober, "Optimal joint power and subcarrier allocation for full-duplex multicarrier non-orthogonal multiple access systems," *IEEE Transactions on Communications*, vol. 65, pp. 1077–1091, Jan. 2017.

[151] O. Mihatsch and R. Neuneier, "Risk-sensitive reinforcement learning," *Machine learning, Springer*, vol. 49, pp. 267–290, Nov. 2002.

[152] M. Alsenwi, N. H. Tran, M. Bennis, S. R. Pandey, A. K. Bairagi, and C. S. Hong, "Intelligent resource slicing for embb and urllc coexistence in 5g and beyond: A deep reinforcement learning based approach," *IEEE Transactions on Wireless Communications*, vol. 20, pp. 4585 – 4600, Feb. 2021.

[153] K. S. Ali, M. Haenggi, H. ElSawy, A. Chaaban, and M.-S. Alouini, "Downlink non-orthogonal multiple access (noma) in poisson networks," *IEEE Transactions on Communications*, vol. 19, pp. 1613–1628, Oct. 2018.

[154] W. C. Cheung, T. Q. Quek, and M. Kountouris, "Throughput optimization, spectrum allocation, and access control in two-tier femtocell networks," *IEEE Journal on Selected Areas in Communications*, vol. 30, pp. 561–574, Mar. 2012.

[155] M. Sawahashi, Y. Kishiyama, A. Morimoto, D. Nishikawa, and M. Tanno, "Coordinated multipoint transmission/reception techniques for lte-advanced [coordinated and distributed mimo]," *IEEE Wireless Communications*, vol. 17, pp. 26–34, Jun. 2010.

[156] J.-Y. Huang and H.-F. Lu, "Achieving large sum rate and good fairness in miso broadcast communication," *IEEE Transactions on Vehicular Technology*, vol. 68, pp. 5684–5695, Mar. 2019.

[157] H. M. Markowitz and G. P. Todd, *Mean-variance analysis in portfolio choice and capital markets*. John Wiley & Sons, 2000.

[158] D. Bertsekas, *Nonlinear Programming*, 2nd ed. Athena Scientific, 1999.

[159] C. Xing, Y. Jing, S. Wang, S. Ma, and H. V. Poor, "New viewpoint and algorithms for water-filling solutions in wireless communications," *IEEE Transactions on Signal Processing*, vol. 68, pp. 1618–1634, Feb. 2020.

[160] T. Lan, D. Kao, M. Chiang, and A. Sabharwal, *An axiomatic theory of fairness in network resource allocation*. IEEE, 2010.

DOCTORAT BRETAGNE LOIRE / MATHSTIC

INSA RENNES

**Titre :** **Contributions à l'analyse des réseaux sans fil aléatoires avec interférence partielle**

**Mots clés :** Processus ponctuel de Poisson, probabilité de couverture, classification utilisateur, partitionnement de la bande passante, équation à point fixe, interférence partielle.

**Résumé :** La géométrie stochastique est très utilisée pour l'analyse de performance des réseaux à grande échelle. Le processus ponctuel de Poisson est le processus le plus utilisé de part sa simplicité mathématique et sa capacité à fournir des régles générales de conception radio. La plupart des travaux considèrent que toutes les stations de base du réseau, ou bien une fraction d'entre elles aléatoirement choisie, et de manière indépendante, transmettent en même temps sur le même bloc de resources. C'est ce que l'on appelle un réseau à interférence totale ou à amincissement indépendant. Ces approches ne prennent pas en compte la corrélation qu'il peut exister entre l'activité d'une station de base et la probabilité de couverture de ces utilisateurs. D'autre part, une réutilisation agressive des fréquences est préjudiciable aux utilisateurs en bord de cellule. Dans cette thèse, nous considérons le principe de réutilisation de f'réquence d'un point de vue utilisateur plutôt que d'un point de vue cellule. Selon ce point de vue, si un utilisateur n'est pas couvert sur un bloc de resources, alors la station de base ne transmet pas sur cette resource et donc ne cause pas d'interférence sur l'utilisateur typique d'une autre cellule utilisant cette resource. Cela engendre une corrélation entre l'activité d'une station de base et sa région de couverture et a pour but notamment d'améliorer la couverture de l'utilisateur de bord de cellule. Dans ce cadre théorique, les probabilités de couverture et d'activité d'une station de base sont obtenues et nous montrons qu'elles sont les solutions d'équations du point fixe. De plus, nous étudions les performances moyennes de plusieurs stratégies de partitionnement de bande et le compromis entre l'équité des différents type d'utilisateurs et leur efficacité spectrale. Finalement le compromis probabilité de couverture, efficacité spectrale d'une technique de coopération sont étudiées dans le cadre théorique proposé.

**Title :** **Contributions to the analysis of random wireless networks in non-full interference**

**Keywords :** Poisson point process, Coverage probability, User classification, Bandwidth Partitioning, Fixed-point equation, Non-full interference

**Abstract :** Stochastic geometry is widely used to evaluate large scale wireless networks. The Poisson point process is the most used point process for modeling the spatial location of base stations, because of its mathematical tractability and network design insights it provides. Most of the works in literature assume that either all base stations are transmitting all the time or a fraction of them but randomly chosen. This model is called full interference or independent thinning and does not take into account the correlation that may exist between the activity of a base station and the coverage probability of their users. Moreover, an aggressive frequency reuse scheme is generally not beneficial to cell edge users. In this thesis, we advance the state of art in network performance analysis a step further, by considering the frequency reuse as user centric instead of cell centric. The change of point of view implies that if a user is not covered in a given resource block, its base station does not transmit on this resource and hence does not cause interference on the typical user. This change of paradigm correlates the activity of a base station to its coverage region and aims at helping cell edge users. Under this theoretical framework, the coverage and the base station activity probabilities are derived and are shown to be the solutions of fixed point equations. Moreover, under this framework, the average performance of different bandwidth allocation is investigated and the tradeoff between the fairness and the spectral efficiency of different user types is presented. Finally, the performance of a cooperation technique is evaluated under the proposed framework of non-full interference.